



**Boundary Element Analysis of Time-Dependent
Material Non-Linearity**

by

Chatrchai Chandenduang

B.Eng., M.Eng.

**Thesis submitted to the University of Nottingham
for the Degree of Doctor of Philosophy**

December 1999

Contents

Abstract	v
Acknowledgements	vii
Nomenclature	viii
Chapter 1: Review of the Boundary Element Method in Inelastic Application	1
1.1 Inelastic BE Analysis	1
1.2 Continuum Damage Mechanics	8
1.3 Contact Problems	10
1.4 Summary	12
Chapter 2: Creep Behaviour	14
2.1 Uniaxial Tensile Creep Curve	14
2.2 Mathematical Model of Uniaxial Creep.....	15
2.3 Variable Stress Creep Behaviour	17
2.4 Stress Relaxation.....	18
2.5 Multiaxial Creep Model	20
Chapter 3: Boundary Element Method for Two-Dimensional Creep Problems	27
3.1 Analytical Formulation	28
3.1.1 The Displacement Differential Equations.....	28
3.1.2 Kelvin Solution	32
3.1.3 Reciprocal Work Theorem.....	34
3.1.4 The BEM for Two-Dimensional Creep Problem.....	39

3.2 Numerical Implementation.....	42
3.2.1 Division of the Boundary into Elements and the Domain into Cells	43
3.2.2 Numerical Integration of the Kernels.....	45
3.2.3 Singularity Treatment.....	48
3.2.4 Application of the Boundary Conditions	52
3.2.5 Calculation of the Boundary Stresses	55
3.2.6 Calculation of the Interior Variables.....	57
3.3 BE-Creep Algorithm	61
3.4 Convergence Criteria	65
3.5 The Creep Computer Program	67
Chapter 4: Creep Examples Using the Boundary Element Method	75
4.1 Square Plate Tests	75
4.2 Plate With a Circular Hole Test	78
4.3 Plate With a Semicircular Notch Test.....	79
Chapter 5: The Effects of Gaussian Integration Points, Initial Time Steps and Tolerances	85
5.1 Comparison of Convergence Criteria.....	85
5.2 The Effect of the Integration Points	86
5.3 The Effect of the Initial Time Steps.....	86
5.4 The Effect of the Tolerances.....	87

Chapter 6: Boundary Element Method for Creep Damage Problems	94
6.1 Creep Damage Constitutive Equations	94
6.2 BE Creep Damage Algorithm	96
6.3 BE Creep Damage Examples	97
6.3.1 A Rectangular Plate.....	98
6.3.2 A Square Plate With a Circular Hole	100
Chapter 7: Boundary Element Method for Combined Plasticity and Creep	
Problems	106
7.1 The Constitutive Equations	106
7.2 BE Combined Plasticity and Creep Algorithm	107
7.3 BE Combined Plasticity and Creep Examples	108
7.3.1 Square Plate.....	109
7.3.2 Plate With a Circular Hole	110
7.3.3 Plate With a Semicircular Notch.....	112
Chapter 8: Boundary Element Method for Creep Contact Problems	116
8.1 Contact Conditions.....	116
8.2 BE Creep Contact Algorithm	117
8.3 BE Creep Contact Examples	118
8.3.1 A Punch on a Foundation.....	119
8.3.2 A Cylindrical Punch on a Flat Foundation.....	120

Chapter 9: Conclusions and Further Studies	127
9.1 Conclusions	127
9.2 Further Studies	129
References	130
Appendix A: Differentials of the Linear Shape Functions	140
Appendix B: Differentials of the Quadratic Shape Functions	141
Appendix C: Analytical Solutions of Plasticity of a Plate under Uniaxial Load in Plane Stress Problems	142

Abstract

A two dimensional boundary element method (BEM) formulation and computer program for creep problems based on an initial strain approach has been successfully implemented using Fortran code. Two creep laws which can be used in this program are time hardening and strain hardening. The details of the numerical algorithm are presented using isoparametric quadratic elements to model the boundary with 3-node boundary elements, and to model the interior domain with 8-node quadrilateral cells. The BEM program also covers the variable stress load problems. The creep problems of a square plate, a plate with a circular hole and a plate with a semicircular notch are investigated.

The boundary element formulation for creep problems has also been applied to creep damage mechanics problems. These types of problems have not been done by using the boundary element method before. A single damage variable is used in the program. The details of the numerical algorithm are presented. The two dimensional problems of creep damage in a rectangular plate and a square plate with a circular hole are tested and compared with the finite element solutions using ABAQUS UMAT.

A BEM program for combined plasticity and creep problems has also been established. It is assumed that the plasticity and creep processes are separable. The details of the numerical algorithm are presented. The problems of a square plate, a plate with a circular hole and a plate with a semicircular notch are investigated.

A BEM program for frictionless creep contact problems has been created. Similar to plasticity and creep problems, it is assumed that contact and creep processes are separable. In this program, it is assumed that the actual contact area is fixed during the creep procedure. The problems of a punch and a cylindrical punch on foundations are investigated.

The results of all problems above are compared with the finite element solutions using ABAQUS and the analytical solutions where available and shown to be in good agreement.

Acknowledgements

I wish to express my profound gratitude to my supervisor, Dr. A. A. Becker, for his invaluable guardian. My thanks are also due to Dr. H. Gun for his explanation on his plasticity computer program and to Dr. W. Sun for his support on ABAQUS UMAT Damage Code. I would like to thank my wife, Thanawadee, for encouraging me to study for PhD. Finally, I would like to thank the Royal Thai Government for their financial support.

Notation

Some of the key variables used in this work are listed below. All other symbols are defined when first introduced. Some symbols may have more than one meaning.

ϵ_{eff}^c	= Effective creep strain
ϵ_{ij}^c	= Creep strains
$\dot{\epsilon}_{ij}^c$	= Creep strain rates
$\dot{\sigma}_{ij}$	= Stress rates
$\dot{\epsilon}_{ij}$	= Total strain rates
\dot{t}_i	= Traction rates
\dot{u}_i	= Displacement rates
$\dot{\epsilon}_{ij}^e$	= Elastic strain rates
$\dot{\omega}$	= Damage rate
$\hat{\sigma}$	= Maximum principal stress
$\dot{\epsilon}_{ij}^p$	= Plastic strain rates
λ	= Proportionality factor
ν	= Poisson's ratio
μ	= Shear modulus
ω	= Damage parameter
σ_{eff}	= Effective or equivalent stress
δ_{ij}	= Kronecker delta

δ_t	= Slip displacement in the tangential direction
σ_y	= Yield stress
$[A^*]$	= Solution matrix multiply the unknown vector $[x]$
$[A]$	= Matrix containing the traction kernels
$[B^*]$	= Modified form of $[B]$ after application of the boundary conditions
$[B]$	= Matrix containing the displacement kernels
$[C^*]$	= Modified form of $[B]$ after application of the effect of creep strain rates
$[W]$	= Matrix containing the third-order stress tensor
D_{kij}	= Third-order displacement tensor for stress
E	= Young's modulus
G_i	= Galerkin vectors
H	= Plastic hardening modulus
$J(\xi)$	= Jacobian of transformation for boundary
$J(\xi_1, \xi_2)$	= Jacobian of transformation for domain
m	= Unit tangential vector at the boundary
n	= Unit outward normal at the boundary
$N_c(\xi)$	= Quadratic shape functions for the boundary
$N_c(\xi_1, \xi_2)$	= Quadratic shape functions for the domain
s	= Scaling factor
S_{ij}	= Deviatoric stresses
S_{kij}	= Third-order traction tensor for strain
t_{eff}	= Effective time
t_i	= Traction vectors
T_{ij}	= Traction kernels

u_i = Displacement vectors

U_{ij} = Displacement kernels

W_{kij} = Third-order stress tensor

Chapter 1

Review of the Boundary Element Method in Inelastic Applications

1.1 Inelastic Boundary Element Analysis

The boundary element method (BEM) has been widely used to analyse both elastic and time-dependent inelastic engineering problems. Swedlow and Cruse [1971] proposed the first direct boundary element formulation in rate form for three-dimensional elastoplastic flow based on an initial strain approach. In the early stages of solving time-dependent inelastic deformation problems, time-independent plasticity and time-dependent creep were treated separately and constitutive relationships of material behaviour were not realistic. After Hart [1976] has modelled realistic constitutive relations of material behaviour which combined time-independent plasticity and time-dependent creep together, many researchers used Hart's constitutive model to analyse engineering problems. Hart's constitutive model represents material behaviour more realistically than the power law creep and needs many material parameters which are obtained from load relaxation and constant strain rate tension experiments. Creep power law is simpler and needs fewer material parameters which can be easily determined from a uniaxial creep test.

Kumar and Mukherjee [1977] presented the direct BEM formulation in terms of rates based on an initial strain approach for analysing time-dependent inelastic deformation problems of arbitrary shaped three-dimensional metallic bodies. The BEM formulation included the effects of the thermal strain. The boundary element formulation for two-

dimensional problems (plane stress and plane strain) was also shown. The closed form solutions of the problem of a thick spherical shell and a thick cylinder under internal and external pressures and a rotating disc were derived. The problem of a thick-walled spherical shell subjected to internal pressure increasing at a constant rate was solved using Hart's constitutive model. The surface elements were discretized into plane triangular elements. The surface and volume elements were denoted by their centroids. A modified Euler predictor-corrector scheme and a Simpson's rule were implemented for time integration.

Mukherjee et al. [1978] used the same procedure as Kumar and Mukherjee [1977] and solved the same problems with a different material and different types of loading such as constant internal pressure, interrupted load, load change, and cyclic internal displacement.

Mukherjee and Kumar [1978] introduced the boundary element formulation for 2-D planar problems based on an initial strain approach and solved the problems of uniform plates and plates with circular holes subjected to constant stress and constant stress rate uniaxial and biaxial loading. Two types of constitutive equations, power law creep and Hart's constitutive model, were implemented. A modified Euler predictor-corrector scheme was applied for integration in time. Constant elements were used on both boundary and internal elements and referred to by their centroids. The results were compared and agreed well with analytical solutions.

Morjaria et al. [1980] compared the boundary element method based on an initial strain approach with the finite element method by analysing the same planar problems of a uniform plate under uniaxial load, a circular plate with a concentric cutout under internal pressure increasing at a constant rate, and a square plate with a circular cutout under uniaxial load. Hart's constitutive model was employed in both the BEM and the FEM. The BEM and FEM elements were represented by linear elements and linear strain triangular elements, respectively. An Euler type strategy with automatic time-step control was used for time integration. The results of the BEM agreed well with the FEM and direct numerical integral solutions. Morjaria et al. [1980] also showed that the BEM had two advantages over the FEM. One advantage was the number of the BEM unknowns was proportional to the number of boundary nodes. The ease of discretisation and input data preparation was another advantage of the BEM.

Morjaria and Mukherjee [1980] used the same BEM formulation as that of Morjaria et al. [1980] to solve the planar problems of a uniform plate under uniaxial load, a circular plate with a concentric circular cutout under internal pressure and a plate with an elliptic cutout under uniaxial load. The results agreed very well with direct numerical integral solutions.

Mukherjee [1980, 1982a] presented the 2-D boundary element formulation for thin plate bending and torsion problems as well as planar deformations. The boundary and domain were discretized into straight boundary elements and triangular internal elements, respectively. The discontinuities at the corners were taken care of by placing a zero length element between two boundary nodes. Hart's constitutive model was applied to

solve a plate bending problem and the time-hardening creep law was used to analyse a torsion problem. An Euler type strategy with automatic time-step control was implemented for time integration. The solution algorithm was also shown and the results were compared with the FEM solutions.

Telles and Brebbia [1981] presented the BEM formulation based on an initial strain approach for 2-D elastoplastic problems. Linear interpolation functions were employed for the boundary elements and the internal triangular cells. The von Mises yield criterion and the Prandtl-Reuss flow rule were applied for the plastic strain increment. The problems of a perforated aluminium strip under uniaxial tension, a polystyrene crazing problem under uniaxial and biaxial tension and plate strain punch were analysed. The results were compared and agreed well with the FEM and experimental results.

Mukherjee and Morjaria [1981], Morjaria and Mukherjee [1981, 1982], Mukherjee and Banthia [1984], and Banthia and Mukherjee [1985] presented the boundary element formulations for solving plates with cracks in mode I, mode II, and mode III. These formulations were modified from the boundary element formulation for a plate with an elliptical cutout. The crack was modelled as a very thin ellipse. The crack problems of square plates with elliptical cutouts of large axis ratio were analysed in mode I, mode II and mode III with varying loading. Power law creep and Hart's constitutive model were used. The boundary element and the interior were represented by straight boundary elements and triangular internal elements, respectively. An Euler type strategy with

automatic time-step control was employed for time integration. The results were compared and agreed well with asymptotic analytical solutions.

Sarihan and Mukherjee [1982] introduced the 3-D boundary element formulation for axisymmetric viscoplastic bodies subjected to axisymmetric mechanical loads. A uniform cylinder subjected to increasing and constant axial loads was analysed using Hart's constitutive model. The piecewise linear elements were used on the boundary and internal cells. A march forward time integration scheme was used for time integration. The results agreed well with the FEM and analytical solutions.

Mukherjee [1982b] presented the 3-D boundary element formulation based on an initial strain approach for time-independent plastic and time-dependent viscoplastic deformation. He showed that the governing differential equations of time-independent plasticity and time-dependent viscoplasticity were of the same form with two important differences. The first was that the plastic strain rates in the plasticity equations were replaced by nonelastic strain rates, e.g. creep strain rates. The second was that the rate was with respect to real time. He also showed that there were two methods of calculating the internal stress rates. The first method was the numerical differentiation of the internal displacement rate equation by finite difference or finite element techniques to obtain the strain rates and then applying Hooke's law to obtain the stress rates. The second method was the analytical differentiation of the internal displacement rate equation to obtain the strain rates and subsequently applying Hooke's law to get the stress rates.

Cathie and Banerjee [1982] have presented the 3-D boundary element method for inelastic (plasticity and creep) problems. Two approaches, initial stress and initial strain, as well as the solution algorithm were introduced. A combined creep law which included both time hardening and strain hardening creep laws has been presented. The problems of square plates with and without holes under constant uniaxial and biaxial tension and a thick cylinder under internal pressure were analysed using a power law creep function. The boundary geometry and unknowns were represented by quadratic elements. The forward difference approximation (Euler) was implemented for time integration. The results agreed well with the exact solutions.

Telles and Brebbia [1983] have presented the boundary element formulation based on an initial stress approach for 2-D (plane stress and plane strain) and 3-D viscoplasticity and creep problems. Euler's formula was used for time integration. The problems of a deep beam under uniform load, a thin disc under constant external edge load and a plate under thermal shrinkage were solved and compared with the FEM and the analytical solutions showing good agreement.

Banerjee and Davies [1984] have introduced the direct boundary element formulation based on both initial stress and initial strain approach for 3-D elastoplastic and viscoplastic problems. The geometry and the variations were represented by quadratic isoparametric elements. The initial stress elastoplastic, viscoplastic and creep solution algorithms has been provided. The forward difference approximation (Euler) was applied for time integration. The time step size had to be sufficiently small for the error introduced by this approximation to be negligible. The stress at interior points were

carried out by differentiating the interior displacement equations and then using the elastoplastic stress-strain relationships.

Banerjee and Raveendra [1986] have proposed the boundary element formulation based on an initial stress approach for 2-D and 3-D elastoplastic problems. The quadratic isoparametric representation was used to model the boundary elements and the volume cells. An iterative algorithm has been presented. The problems of 2-D and 3-D thick cylinder and 3-D thick sphere under internal pressure, 2-D and 3-D perforated strip under tension and 2-D notched plate under axial tension were analysed. The results agreed well with the FEM and experimental results. The computational time of 3-D problem was about 5 times of that of 2-D problem.

Lee and Fenner [1986] have presented the isoparametric quadratic boundary element formulation for two-dimensional elastoplastic analysis based on an initial strain approach. The boundary element formulation based on an initial stress approach was also provided. Two methods of calculating the internal stress and strain rates were proposed. The first method obtained the strain rates by analytically differentiating the internal displacement rate equations and the stress rates were obtained by applying the stress-strain relations. The second method obtained the strain rates by numerically differentiating the internal displacement rate equations via the shape functions and the stress-strain relations were applied to obtain the stress rates. An iteration solution algorithm has been shown for both methods. It has been shown that the computational time of the first method took at most one and a half times of that of the second method but the accuracy of the first method is better than that of the second method. The

problems of uniaxial tensile behaviour, bending behaviour, internally pressurised cylinder, perforated plate in tension, and uniaxial behaviour in cyclic plasticity were analysed. The results were compared to and agreed well with the analytical solutions, experimental results and the FEM.

The constitutive equations for non-elastic deformation were modelled with step-wise integration in time and an iterative method. Early work (see, for examples, Kumar and Mukherjee [1977], Mukherjee et al. [1978] and Mukherjee and Kumar [1978]) used the Euler predictor-corrector scheme for step-wise integration in time. Later work (see, for examples, Mukherjee [1980,1982a] and Mukherjee and Morjaria [1981]) used Euler type strategy with automatic time-step control which controlled the incremental time with prescribed limits of error. This method has been found to be relatively simple to use and very efficient.

In most of above works on creep the boundary geometries and unknowns were represented by linear elements and some (see, for examples, Cathie and Banerjee [1982] and Banerjee and Davies [1984]) represented by quadratic elements which gave more accurate results.

1.2 Continuum Damage Mechanics

In creep rupture the constitutive equations must be modified to increase the strain rates rapidly at tertiary stage. Hayhurst [1973] has presented multiaxial creep damage relationships which were based on Norton's law and Rabotnov's damage parameter.

The damage parameter has been introduced and defined as the ratio of the void area to the original cross-sectional area. Leckie and Hayhurst [1977] have generalized uniaxial constitutive equations of Rabotnov-Kachanov to multiaxial constitutive equations in an FE formulation. The FE solution has shown a good agreement with experimental data.

The finite element method has been used as a tool to solve the creep damage problems. Chen and Hsu [1987] have used the constitutive equations of Leckie and Hayhurst [1977] to analyse a problem of a thin center-notched plate subjected to uniaxial stress by finite element method.

Murakami et al. [1988] have applied the finite element method based on a local approach to analyse creep crack growth of a plate subjected to biaxial tensile loads. The creep law of the McVetty type based on a von Mises flow rule and the strain hardening hypothesis was used. The effects of the mesh discretization and mesh size have also been investigated.

Othman et al. [1993] have used the finite element method to analyse creep rupture lifetime of single and double notched tensile bars. The sinh law and two damage variables were used to characterise material behaviour.

Since the constitutive equations with damage involved many material constants, Dunne et al. [1990] have shown how to determine such constants from experimental data.

1.3 Contact Problems

The boundary element method has been applied to contact problems which are non-linear in nature since the contact area is not known in advance. Andersson et al. [1980] have presented the BEM for two-dimensional contact problems without friction based on an iteration technique. The problems of an elastic roller on an elastic foundation, an elastic roller in an infinite plate with a hole, and linkage assemblage have been analysed using constant elements. The results agreed well with analytical and finite element solutions.

Andersson [1981] has also presented the BEM for two-dimensional contact problems with friction based on an incremental and iterative procedure. The same types of the above problems have been solved using constant elements. The results agreed well with the analytical solutions. The work has been extended to linear and parabolic elements in Andersson [1982].

Karami and Fenner [1987] have presented the BEM for two-dimensional contact problems with and without friction using isoparametric quadratic representations for both geometry and unknowns. The problems of Hertzian and non-Hertzian contact have been analysed. The results were in good agreement with analytical solutions.

Paris and Garrido [1990] have presented the BEM for 2-D frictional contact problems based on an incremental procedure. The problems of an elastic punch on an elastic foundation subjected to normal and lateral loads, an elastic roller on an elastic

foundation and a rigid curved punch pressed on an elastic foundation have been analysed using discontinuous and linear elements. The results were compared with analytical and finite element solutions and showed good agreement. Dandekar and Conant [1992a,b] and Man et al. [1993] used linear and quadratic elements to solve different contact problems. The results agreed well with analytical solutions.

Paris et al. [1992] and Kamiya and Nishiki [1996] have presented the BEM for three-dimensional elastic contact problems without friction based on an iterative procedure. The different contact problems were solved using triangular and constant elements. The results agreed well with analytical and finite element solutions. Garrido et al. [1994] have presented the BEM for three-dimensional contact problems with friction. The similar problems were analysed using triangular and constant elements.

Kamimura et al. [1996] have presented the BEM of two-dimensional elasto-plastic contact in rolling based on Tresca yield criterion and initial strain approach. The results of rolling analysis was shown.

Xiao et al. [1996] have presented the BEM for three-dimensional elasto-plastic contact for rolling using von Mises yield criterion and Prandtl-Ruess flow rule and based on initial stress approach. The results of rolling analysis agreed with the classical rolling theory.

Leahy and Becker [1999a] have presented a 3-D isoparametric quadratic BEM formulation with friction. Details of the 3-D automatic iteration scheme have been presented in Leahy and Becker [1999b].

Tsuta and Yamaji [1983] have presented the BEM for contact thermo-elastoplastic problems with creep based on von Mises yield criterion and initial strain approach. Three types of problems, contact plasticity, elastoplastic creep and contact creep, have been analysed with different problems.

1.4 Summary

The 2-D and 3-D boundary element method (BEM) for time-independent (plasticity) and time-dependent (creep) inelastic deformation problems based on an initial stress and an initial strain approach have been published by many researchers since the first introduction by Swedlow and Cruse in 1971. The boundary element has been developed from constant element to linear element and quadratic element. The domain element has been developed from triangular to quadrilateral element. Two constitutive models used in publications were Hart and creep power laws. Euler, modified Euler predictor-corrector, and Euler with automatic time-step control scheme were used for time integration. Many types of problems such as planar problems and crack in mode I, II and III have been analysed.

The previous work of BEM on creep problems has been limited to constant and linear elements. Furthermore, vital details of the creep numerical algorithm have not been

published. The BE formulation for continuum damage mechanics problems has never been presented. The objectives of this work are (a) to establish a reliable and accurate two dimensional BEM program for creep, creep damage, elastoplasticity and creep, and creep contact problems using a Fortran code, (b) to create numerical algorithms for such problems, (c) to implement the BEM program to analyse the problems, and (d) to investigate the effects of the convergence criteria, the Gaussian integration points, the initial time steps, and the tolerances. The results are compared with the analytical solutions where available and the finite element solutions using ABAQUS [1997].

Chapter 2

Creep Behaviour

Creep is the time dependent deformation and failure of materials. Creep deformation is caused by thermally activated movement of voids and dislocations, under load, usually at high temperature. When a metallic material is subjected to a constant load under a constant temperature for a period of time, creep behaviour usually occurs at $T/T_m > 0.4$, where T and T_m are the absolute operating temperature and absolute melting temperature of that material, respectively. The analysis of creep behaviour has an important role in high-temperature engineering applications such as gas turbines, power plants and engines. Further details on creep theory can be found in Kraus [1980].

2.1 Uniaxial Tensile Creep Curve

When a uniaxial tensile specimen is loaded at a constant load for a period of time under a constant temperature which is high enough to cause creep, a typical uniaxial curve of strain versus time is shown in Figure 2.1. At $t = 0$, the instantaneous strain (ϵ_0) is elastic or elastoplastic depending on the magnitude of the applied stress. If the experiment is repeated with different loads, the different curves will result as shown in Figure 2.2. Conventionally, the creep curve is divided into three parts. The first part is called *primary or transient creep* in which the creep strain rate decreases rapidly. This part is usually recoverable with time after unloading. The second part is called *secondary or steady creep* in which the creep strain rate is constant or nearly constant. In this part permanent strains occur. The third part is called *tertiary creep* in which the

creep strain rates increases rapidly and leads to rupture. In tertiary creep, the strain rate increases rapidly because of the change of the cross-sectional area of the specimen at large strain. The creep strain rate against time is shown in Figure 2.3.

The information of the basic curves can be represented in different forms such as the *isochronous* (constant time) and the *isostrain* (constant strain) creep curves, shown in Figure 2.4. The isochronous and the isostrain creep curves are plotted on log-log plots of strain rate versus stress, and stress versus time, respectively.

The isochronous creep curve is useful in determining the stress-strain behaviour of the material. The isostrain creep curves can determine the time when a given strain was reached for a given stress level.

2.2 Mathematical Model of Uniaxial Creep

In general, the stress-strain relationship of a uniaxial creep curve can be modelled by an expression of the form (see, for example, Kraus [1980] and Boyle and Spence [1983])

$$\varepsilon^c = f(\sigma, T, t) \quad (2.1)$$

where ε^c is the creep strain and f is a function of stress σ , temperature T , and time t . This equation is usually assumed to be separable for simplification. Thus the equation can be written as follows:

$$\varepsilon^c = f_1(\sigma) f_2(t) f_3(T) \quad (2.2)$$

For the stress dependence, many mathematical models have been presented, for example:

$$\begin{aligned}
f_1(\sigma) &= B\sigma^n && \text{(Norton)} \\
f_2(\sigma) &= C\sinh(\beta\sigma) && \text{(Prandtl)} \\
f_3(\sigma) &= D\exp(\alpha\sigma) && \text{(Dorn)} \\
f_4(\sigma) &= E[\sinh(\gamma\sigma)]^n && \text{(Garofalo)}
\end{aligned} \tag{2.3}$$

where symbols other than σ are material constants.

The time dependence is assumed as follows:

$$\begin{aligned}
f_2(t) &= t && \text{(secondary creep)} \\
f_2(t) &= bt^m && \text{(Bailey)} \\
f_2(t) &= (1+bt^{\frac{1}{3}})e^{kt} && \text{(Andrade)} \\
f_2(t) &= \sum_j a_j t^{m_j} && \text{(Graham and Walles)}
\end{aligned} \tag{2.4}$$

From the theoretical considerations and experimental evidence, the temperature dependence is

$$f_3(T) = \exp\left(\frac{-Q}{RT}\right) \tag{2.5}$$

where Q is the activation energy, R is Boltzmann's constant and T is the absolute temperature. Since the primary creep occurs in a short duration and the tertiary creep leads quickly to rupture, the secondary creep is used in design in many engineering applications; though the primary creep cannot be neglected.

The Norton equation is often used to model secondary creep because of its ease in mathematical analysis. For isothermal conditions the equation is

$$\varepsilon^c = B\sigma^n t \tag{2.6}$$

where B and n are material constants. This equation is used for secondary creep behaviour.

A combination between Norton and Bailey equations is used to model primary and secondary creep in the isothermal conditions as follows (see, for example, Becker and Hyde [1993]):

$$\varepsilon^c = B \sigma^n t^m \quad (2.7)$$

where m is a material constant and $m < 1$ is used for primary creep stage. This equation is called 'Norton-Bailey' equation.

A combination of the secondary creep (equation(2.6)) and Bailey (equation (2.7)) equations can be used to model combined primary and secondary creep behaviour as follows:

$$\varepsilon^c = B_1 \sigma^{n_1} t + B_2 \sigma^{n_2} t^m \quad (2.8)$$

where the first and second terms on the right hand side are secondary creep and primary creep ($m < 1$), respectively.

2.3 Variable Stress Creep Behaviour

For a variable stress problem, the strain rate is of interest. Two approximations can be used for the creep strain; *time hardening and strain hardening*. For time hardening, the creep strain rate equation is obtained by differentiating equation (2.7) with time as follows:

$$\dot{\varepsilon}^c = m B \sigma^n t^{(m-1)} \quad (2.9)$$

where the dot above the strain indicates the rate of change with time. The creep strain rate is assumed to depend on the current stress and the time from the beginning of the test. This equation is not realistic when the step changes in stress are of short duration because

the stress variation with time has been ignored and the time is measured from an arbitrary origin. In the case of constant or approximately constant stress, this equation is widely used and gives reasonable results.

For strain hardening, the creep strain rate is assumed to depend on the current stress and the accumulated creep strain. The creep strain rate equation is obtained by substituting the time from the Norton-Bailey equation into equation (2.9) as follows:

$$\dot{\varepsilon}^c = mB^{\frac{1}{m}} \sigma^{\frac{n}{m}} (\varepsilon^c)^{\frac{m-1}{m}} \quad (2.10)$$

Note that when $m = 1$ (the secondary creep stage), the time hardening is equivalent with the strain hardening. The response of creep strain versus time for time and strain hardening is shown in solid line in Figure 2.5.

The time hardening assumption is easier to use in calculations but the strain hardening assumption is more accurate and agrees well with experimental tests. These two assumptions are not suitable for the case of changing sign of stress or covering all three stages of creep.

2.4 Stress Relaxation

When a uniaxial specimen is loaded up to a stress level of σ_0 and then held at a constant strain ε_0 , stress relaxation occurs. The strain at any time consists of an elastic strain and a creep strain, as follows:

$$\varepsilon_0 = \varepsilon^e + \varepsilon^c = \text{constant} \quad (2.11)$$

By differentiating this equation with respect to time, the rate form is obtained, as follows:

$$\frac{d\varepsilon_0}{dt} = 0 = \dot{\varepsilon}^e + \dot{\varepsilon}^c \quad (2.12)$$

Using the assumptions of the Norton-Bailey creep equation and time hardening (i.e. equation (2.9)), this equation becomes

$$0 = \frac{1}{E} \frac{d\sigma}{dt} + m B \sigma^n t^{(m-1)} \quad (2.13)$$

By integration this equation, the stress change with time is given by:

$$\sigma = \left[\frac{1}{\sigma_0^{(n-1)}} + (n-1) B E t^m \right]^{\frac{-1}{(n-1)}} \quad (2.14)$$

If strain hardening is used instead of the time hardening, equation (2.13) can be written as

$$0 = \frac{1}{E} \frac{d\sigma}{dt} + m B^{\frac{1}{m}} \sigma^{\frac{n}{m}} (\varepsilon^c)^{\frac{m-1}{m}} \quad (2.15)$$

From equation (2.11), strain can be rearranged, as follows:

$$\varepsilon^c = \varepsilon_0 - \varepsilon^e = \frac{1}{E} (\sigma_0 - \sigma) \quad (2.16)$$

Substituting equation (2.16) in equation (2.15) and rearranging, the equation becomes

$$\frac{d\sigma}{dt} = -m E B^{\frac{1}{m}} \sigma^{\frac{n}{m}} \left(\frac{\sigma_0 - \sigma}{E} \right)^{\frac{m-1}{m}} \quad (2.17)$$

It has been shown that the stress variation with time can be obtained by a simple time marching numerical algorithm where the stress gradient is evaluated over a small time step (see, for example, Becker and Hyde [1993]).

2.5 Multiaxial Creep Model

A mathematical model for creep under multiaxial stress conditions must satisfy these requirements (see, for example, Kraus [1980]):

1. The multiaxial formulation must be valid for the uniaxial case when it is appropriate.
2. The creep process is a constant volume process, i.e. $\varepsilon_1^c + \varepsilon_2^c + \varepsilon_3^c = 0$.
3. From experimental observation for creep, the equations should exclude the influence of the hydrostatic state of stress.
4. For isotropic materials, the principal directions of stress and strain should be in the same direction.

Like plasticity formulations, multiaxial creep formulations are usually based on the von Mises effective stress criterion and the Prandtl-Reuss flow rule. In any three-dimensional state of stress, there are three planes on which only the normal stress exists i.e. the shear stress is zero. These planes are called the *principal planes* and the normal stresses acting on them are called *principal stresses*, σ_1 , σ_2 and σ_3 . Conventionally, $\sigma_1 > \sigma_2 > \sigma_3$. Any stress can be divided into two different parts, a *hydrostatic part*, σ_m , and a *deviatoric part*, S_{ij} . In general, creep behaviour is caused by the deviatoric part through the shear component. In the tensor notation form, the hydrostatic and deviatoric stresses can be written as follows:

$$\sigma_m = \frac{1}{3} \sigma_{kk} \quad (2.18)$$

$$S_{ij} = \sigma_{ij} - \frac{1}{3} \delta_{ij} \sigma_{kk} \quad (2.19)$$

where i and j range from 1 to 3 and δ_{ij} is the Kronecker delta which is defined as follows:

$$\begin{aligned} \delta_{ij} &= 1 & (i=j) \\ &= 0 & (i \neq j) \end{aligned} \quad (2.20)$$

From experimental evidence, for small strains, creep is a constant volume process, and a hydrostatic stress state has no effect on creep behaviour in the primary and secondary stages. Since creep behaviour is incompressible, the principal strain rates can be written as follows:

$$\dot{\epsilon}_1^c + \dot{\epsilon}_2^c + \dot{\epsilon}_3^c = 0 \quad (2.21)$$

A von Mises effective or equivalent stress, σ_{eff} , which governs the creep behaviour in multiaxial creep formulations, is defined as follows:

$$\sigma_{eff} = \left(\frac{3}{2} S_{ij} S_{ij} \right)^{\frac{1}{2}} = \frac{1}{\sqrt{2}} \left[(\sigma_1 - \sigma_2)^2 + (\sigma_2 - \sigma_3)^2 + (\sigma_1 - \sigma_3)^2 \right]^{\frac{1}{2}} \quad (2.22)$$

or in terms of the Cartesian stresses

$$\sigma_{eff} = \frac{1}{\sqrt{2}} \left[(\sigma_{xx} - \sigma_{yy})^2 + (\sigma_{yy} - \sigma_{zz})^2 + (\sigma_{xx} - \sigma_{zz})^2 + 6(\tau_{xy}^2 + \tau_{yz}^2 + \tau_{xz}^2) \right]^{\frac{1}{2}} \quad (2.23)$$

where τ_{xy} , τ_{yz} and τ_{xz} are shear stresses.

Similarly, the effective creep strain rate, $\dot{\epsilon}_{eff}^c$, can be written as follows:

$$\dot{\varepsilon}_{eff}^c = \frac{\sqrt{2}}{3} [(\dot{\varepsilon}_1^c - \dot{\varepsilon}_2^c)^2 + (\dot{\varepsilon}_2^c - \dot{\varepsilon}_3^c)^2 + (\dot{\varepsilon}_1^c - \dot{\varepsilon}_3^c)^2]^{\frac{1}{2}} \quad (2.24)$$

or in terms of the Cartesian strains

$$\dot{\varepsilon}_{eff}^c = \frac{\sqrt{2}}{3} [(\dot{\varepsilon}_{xx}^c - \dot{\varepsilon}_{yy}^c)^2 + (\dot{\varepsilon}_{yy}^c - \dot{\varepsilon}_{zz}^c)^2 + (\dot{\varepsilon}_{xx}^c - \dot{\varepsilon}_{zz}^c)^2 + 6(\dot{\gamma}_{xy}^2 + \dot{\gamma}_{yz}^2 + \dot{\gamma}_{zx}^2)]^{\frac{1}{2}} \quad (2.25)$$

Since creep behaviour is dependent on time and load path, the constitutive equations of creep behaviour must be written in rate form. A flow rule, based on the Prandtl-Reuss plasticity flow rule, can be used as follows:

$$\dot{\varepsilon}_{ij}^c = \frac{d\varepsilon_{ij}^c}{dt} = \lambda S_{ij} \quad (2.26)$$

where λ is a factor of proportionality which can be determined experimentally from a uniaxial creep test. The proportionality factor, λ , can be obtained by substituting the flow rule of equation (2.26) into the effective creep strain rate of equation (2.25) and applying the definition of the effective stress of equation (2.23), resulting in

$$\lambda = \frac{3 \dot{\varepsilon}_{eff}^c}{2 \sigma_{eff}} \quad (2.27)$$

The use of the effective strain rate and effective stress in the multiaxial formulation is valid for the uniaxial formulation, i.e. $\sigma_{xx} > 0, \sigma_{yy} = \sigma_{zz} = 0, \sigma_{eff} = \sigma_{xx}$ and $\varepsilon_{eff}^c = \varepsilon_{xx}^c$.

Therefore, the uniaxial Norton-Bailey creep law of equation (2.7) can be written in terms of effective quantities, as follows:

$$\varepsilon_{eff}^c = B (\sigma_{eff})^n t^m \quad (2.28)$$

Differentiating this equation with time and substituting into equation (2.27), the proportionality factor, λ , can be written as follows:

$$\lambda = \frac{3}{2} m B (\sigma_{eff})^{(n-1)} t^{(m-1)} \quad (2.29)$$

For the global creep strain rates, based on time hardening rule, an expression can be obtained by substituting the proportionality factor, λ , of equation (2.29) into the flow rule of equation (2.26), as follows:

$$\dot{\epsilon}_{ij}^c = \frac{3}{2} m B (\sigma_{eff})^{(n-1)} S_{ij} t^{(m-1)} \quad (2.30)$$

Similarly, if the strain hardening rule of equation (2.10) is applied, the creep law becomes:

$$\dot{\epsilon}_{ij}^c = \frac{3}{2} m B^{\frac{1}{m}} (\sigma_{eff})^{\frac{n-m}{m}} S_{ij} (\epsilon_{eff}^c)^{\frac{m-1}{m}} \quad (2.31)$$

or can be written in the same form of the time hardening rule by changing the time t to the effective time t_{eff} as follows:

$$\dot{\epsilon}_{ij}^c = \frac{3}{2} m B (\sigma_{eff})^{(n-1)} S_{ij} t_{eff}^{(m-1)} \quad (2.32)$$

where t_{eff} is defined as follows:

$$t_{eff} = \left[\frac{\epsilon_{eff}^c}{B \sigma_{eff}^n} \right]^{\frac{1}{m}} \quad (2.33)$$

The above multiaxial formulation is based on the uniaxial creep law, therefore, it is not suitable for stress reversal situations.

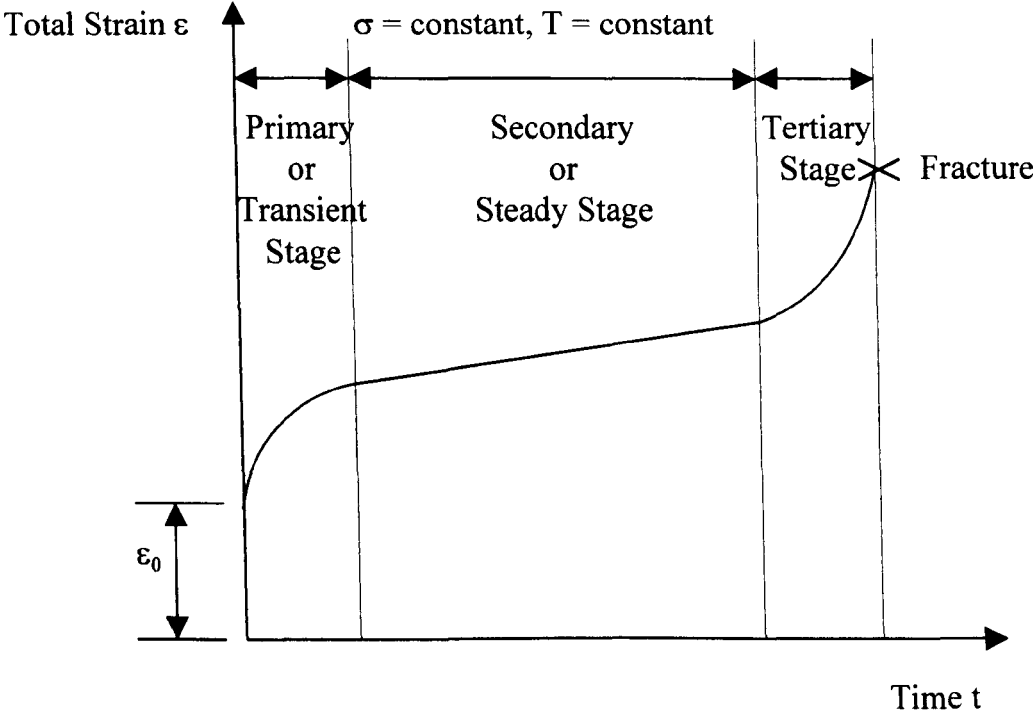


Figure 2.1 Typical Uniaxial Creep Curve.

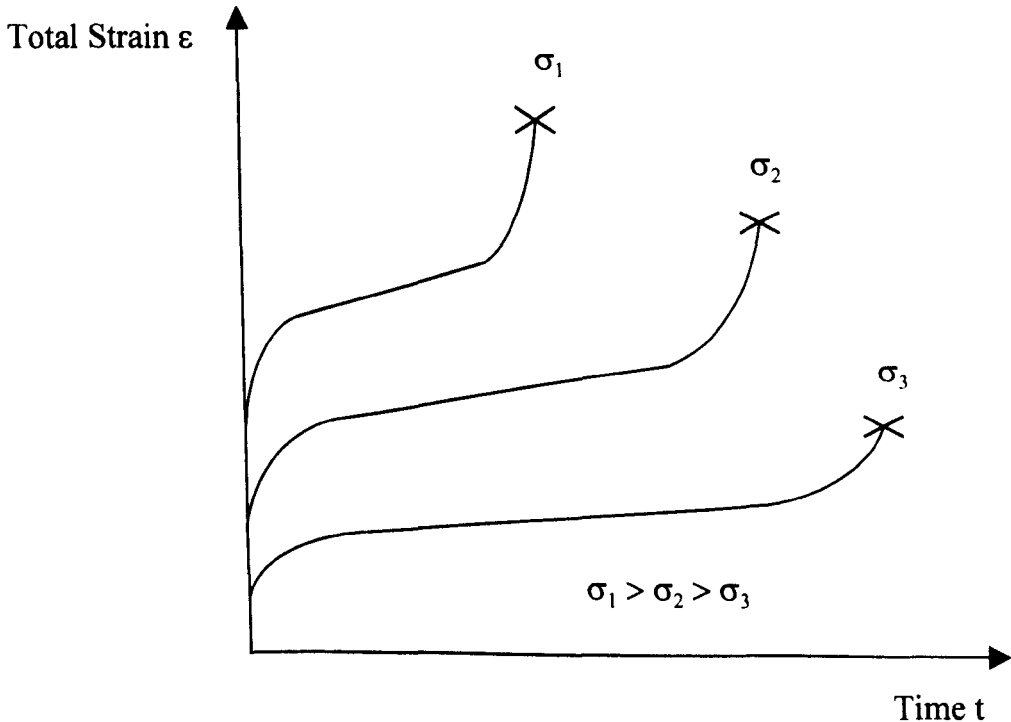


Figure 2.2 Typical Uniaxial Creep Curve for Different Loads.

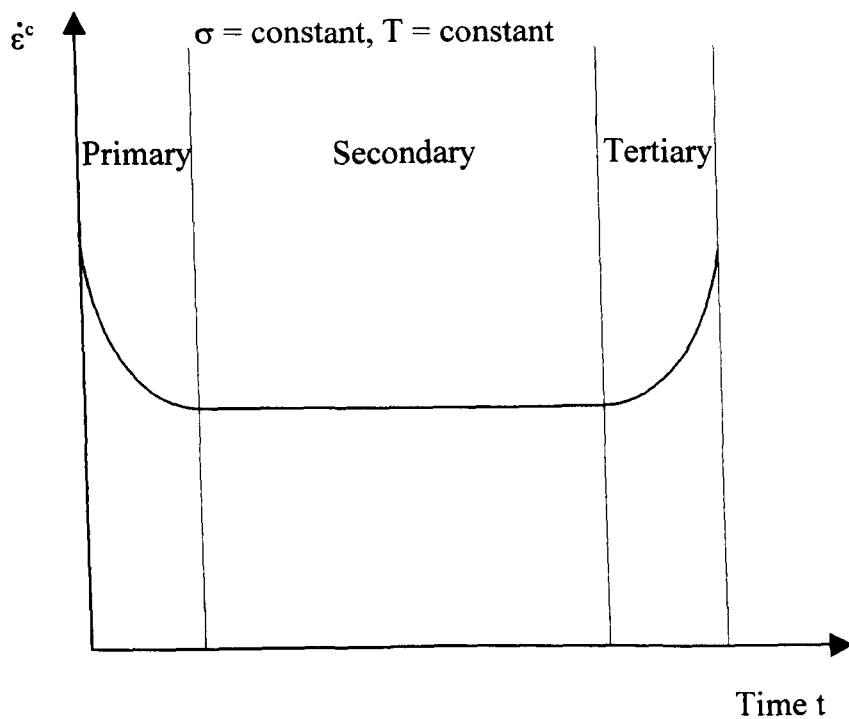


Figure 2.3 The Creep Strain Rate Response With Time.

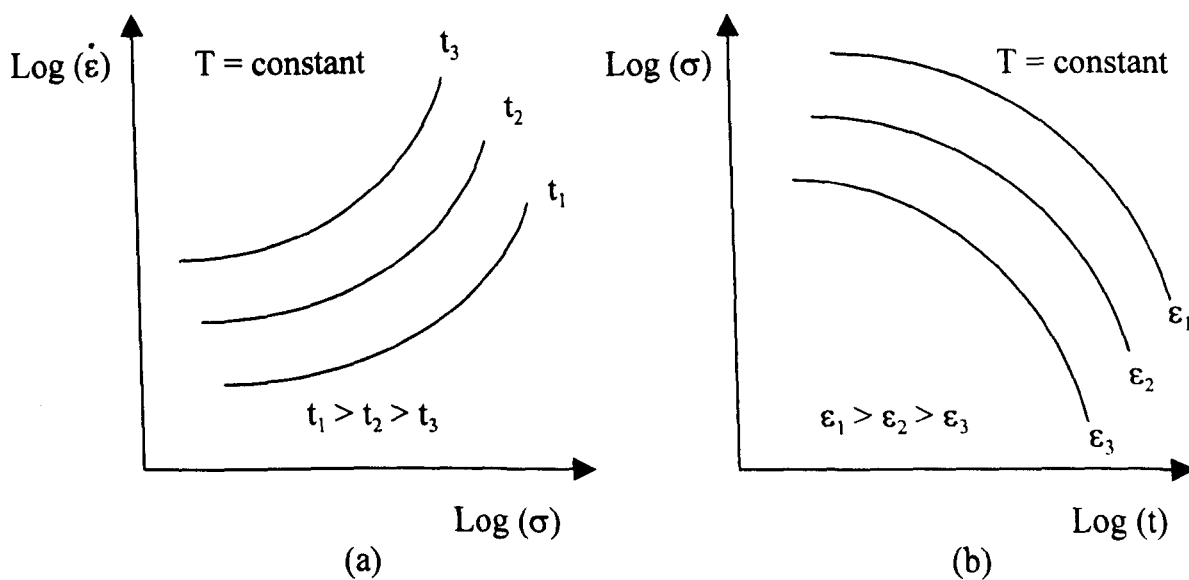


Figure 2.4 (a) Isochronous Creep Curves, (b) Isostrain Creep Curves.

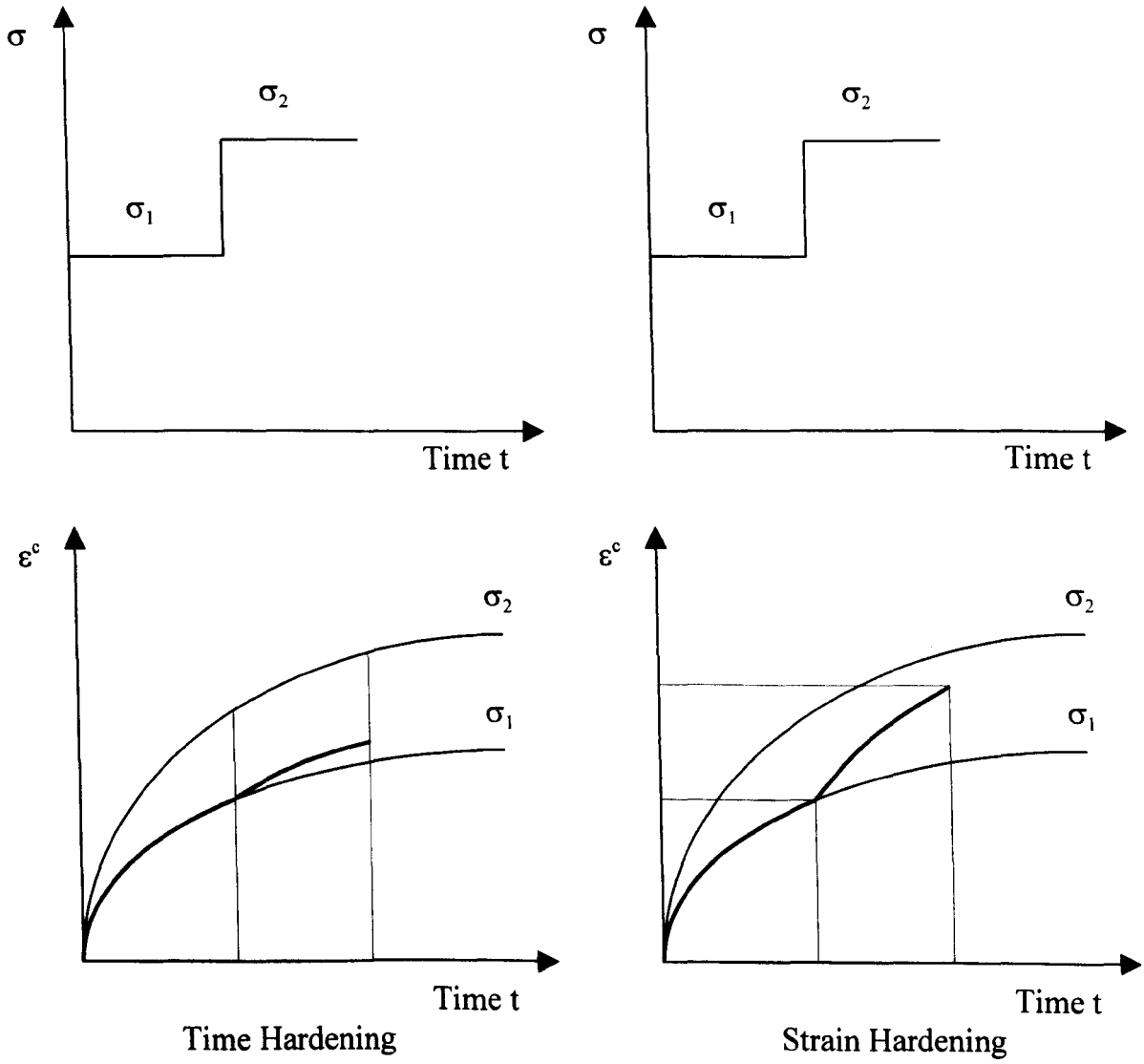


Figure 2.5 Time and Strain Hardening Assumptions.

Chapter 3

Boundary Element Method for Two-Dimensional Creep Problems

The BEM has been widely used to solve many engineering problems because of its advantages over the FEM (see, for example, Becker [1992] and El-Zafrany [1993]).

The advantages of the BEM are:

1. The dimensionality of the problem is reduced by one. This means that the two-dimensional problems are modelled on the boundary only and the surface only for the three-dimensional problems. Therefore, it takes less time for data preparation.
2. The stresses at internal points are accurate because no approximation is imposed on the solution at internal points.
3. The BEM takes less computational time for the same level of accuracy because of less number of nodes and elements.
4. The BEM can be easily applicable to incompressible materials where Poisson's ratio equals 0.5.

There are also some disadvantages of the BEM as follows:

1. The BE solution is poor for thin shell analysis where the distance between nodal points on either side of the shell thickness is very small. This causes inaccuracies in the numerical integration.
2. The BE solution matrix is fully populated and unsymmetric. Therefore, it needs a large space in the computer memory. But comparing with the FE solution for the same level of accuracy, the BE solution still needs less memory space.
3. In non-linear problems, the interior must be modelled.

In the following sections, the analytical formulation and numerical implementation of the BEM for creep problems are presented.

3.1 Analytical Formulation

The BE formulation presented in this section is based on the direct approach which uses actual physical quantities as variables. To derive the BE formulation, the displacement differential equations (Navier equations) have to be derived first and then the point load (Kelvin) solution is used to obtain the fundamental solution. Subsequently, Betti's reciprocal work theorem is used to obtain the boundary integral equation (see, for example, Telles and Brebbia [1981]).

The displacement differential equations can be derived from three relationships: equilibrium of a differential element, stress-strain equations (Hooke's law), and strain-displacement equations (strain definitions).

3.1.1 The Displacement Differential Equations (Navier Equations)

Consider a small differential element shown in Figure 3.1. The equilibrium equations can be written, as follows (see, for example, Spencer [1968]):

$$\frac{\partial \sigma_{ij}}{\partial x_i} + f_j = 0 \quad (3.1)$$

where f_j is the body force per unit volume in the j -direction.

In the absence of thermal strains, the stress-strain equations (Hooke's law) are defined as follows:

$$\begin{aligned}
 \varepsilon_{xx} &= \frac{1}{E} \left[\sigma_{xx} - \nu (\sigma_{yy} + \sigma_{zz}) \right] \\
 \varepsilon_{yy} &= \frac{1}{E} \left[\sigma_{yy} - \nu (\sigma_{xx} + \sigma_{zz}) \right] \\
 \varepsilon_{zz} &= \frac{1}{E} \left[\sigma_{zz} - \nu (\sigma_{xx} + \sigma_{yy}) \right] \\
 \varepsilon_{xy} &= \frac{1}{2\mu} \sigma_{xy} \\
 \varepsilon_{yz} &= \frac{1}{2\mu} \sigma_{yz} \\
 \varepsilon_{xz} &= \frac{1}{2\mu} \sigma_{xz}
 \end{aligned} \tag{3.2}$$

where E is Young's modulus, ν is Poisson's ratio and μ is the shear modulus. These material properties are not independent. Their relationship is defined as follows:

$$\mu = \frac{E}{2(1 + \nu)} \tag{3.3}$$

For two-dimensional plane strain conditions ($\varepsilon_{zz} = 0$), equation (3.2) becomes:

$$\begin{aligned}
 \varepsilon_{xx} &= \left(\frac{1 - \nu^2}{E} \right) \sigma_{xx} + \left[\frac{-\nu(1 + \nu)}{E} \right] \sigma_{yy} \\
 \varepsilon_{yy} &= \left[\frac{-\nu(1 + \nu)}{E} \right] \sigma_{xx} + \left(\frac{1 - \nu^2}{E} \right) \sigma_{yy} \\
 \varepsilon_{xy} &= \frac{1}{2\mu} \sigma_{xy}
 \end{aligned} \tag{3.4}$$

For two-dimensional plane stress conditions ($\sigma_{zz} = 0$), equation (3.2) becomes:

$$\begin{aligned}
\varepsilon_{xx} &= \left(\frac{1}{E}\right)\sigma_{xx} + \left(\frac{-\nu}{E}\right)\sigma_{yy} \\
\varepsilon_{yy} &= \left(\frac{-\nu}{E}\right)\sigma_{xx} + \left(\frac{1}{E}\right)\sigma_{yy} \\
\varepsilon_{xy} &= \frac{1}{2\mu}\sigma_{xy}
\end{aligned} \tag{3.5}$$

Both plane strain (equation (3.4)) and plane stress (equation (3.5)) equations can be written in one form by using new effective material properties, E^* , ν^* and μ^* . By sticking to plane strain equations, the new equations which cover both plane strain and plane stress conditions can be written, as follows:

$$\begin{aligned}
\varepsilon_{xx} &= \left(\frac{1-\nu^{*2}}{E^*}\right)\sigma_{xx} + \left(\frac{-\nu^*(1+\nu^*)}{E^*}\right)\sigma_{yy} \\
\varepsilon_{yy} &= \left(\frac{-\nu^*(1+\nu^*)}{E^*}\right)\sigma_{xx} + \left(\frac{1-\nu^{*2}}{E^*}\right)\sigma_{yy} \\
\varepsilon_{xy} &= \frac{1}{2\mu^*}\sigma_{xy}
\end{aligned} \tag{3.6}$$

where

$$\begin{aligned}
E^* &= E; \quad \nu^* = \nu; \quad \mu^* = \mu \quad \text{for plane strain} \\
E^* &= \frac{E(1+2\nu)}{(1+\nu)^2}; \quad \nu^* = \frac{\nu}{1+\nu}; \quad \mu^* = \mu \quad \text{for plane stress}
\end{aligned} \tag{3.7}$$

For convenience, the asterisk will be dropped from the material properties but are still implied unless otherwise stated. The equation (3.6) can be rearranged so that the stress is a function of the strain, as follows:

$$\sigma_{ij} = \frac{2\mu\nu}{1-2\nu}\delta_{ij}\varepsilon_{mm} + 2\mu\varepsilon_{ij} \tag{3.8}$$

where δ_{ij} is the Kronecker delta defined in equation (2.20). For small strains, the strain-displacement equations are defined, as follows:

$$\varepsilon_{ij} = \frac{1}{2} \left(\frac{\partial u_i}{\partial x_j} + \frac{\partial u_j}{\partial x_i} \right) \quad (3.9)$$

By substituting the strain-displacement relationship of equation (3.9) into the stress-strain relationship of equation (3.8), the stress-displacement equations can be obtained, as follows:

$$\sigma_{ij} = \frac{2\mu\nu}{1-2\nu} \left(\frac{\partial u_m}{\partial x_m} \right) \delta_{ij} + \mu \left(\frac{\partial u_i}{\partial x_j} + \frac{\partial u_j}{\partial x_i} \right) \quad (3.10)$$

By substituting the stress-displacement relationship of equation (3.10) into the force equilibrium of equation (3.1), the displacement differential equations can be obtained, as follows:

$$\frac{\partial^2 u_i}{\partial x_j \partial x_j} + \left(\frac{1}{1-2\nu} \right) \frac{\partial^2 u_j}{\partial x_i \partial x_j} = -\frac{f_i}{\mu} \quad (3.11)$$

The displacement differential equations are called the *Navier* equations. The Navier equations are difficult to solve analytically. It can be solved by expressing the displacement vectors in term of another vectors, as follows:

$$u_i = \frac{\partial^2 G_i}{\partial x_j \partial x_j} - \frac{1}{2(1-\nu)} \frac{\partial^2 G_j}{\partial x_i \partial x_j} \quad (3.12)$$

The vector G is called the *Galerkin* vector. By substituting equation (3.12) into Navier equation of equation (3.11), the biharmonic equations are obtained:

$$\nabla^4 G_i = \nabla^2 (\nabla^2 G_i) = -\frac{f_i}{\mu} \quad (3.13)$$

where ∇^2 is the Laplacian operator which is defined as:

$$\nabla^2 = \frac{\partial^2}{\partial x^2} + \frac{\partial^2}{\partial y^2} \quad (3.14)$$

3.1.2 Kelvin Solution

The fundamental solution of equation (3.13) can be obtained by considering the physical domain of Figure 3.2 with load point p of coordinates X_p and Y_p and a field point Q on the boundary of coordinates of x_Q and y_Q . Capital letters mean fixed coordinates and lower case letters mean variable coordinates. The Kelvin solution, which is a three-dimensional solution of a unit point force in an infinite medium, is used to obtain the fundamental solution and must satisfy two physical conditions:

- (i) All stresses must become zero as the distance between point p and Q tends to infinity.
- (ii) The stresses must be singular at ' p ' itself, i.e. the stresses become infinity as the distance between point p and Q tends to zero.

The Galerkin vectors, which are the solutions of equation (3.13) and satisfy both physical conditions, are given by:

$$G_x = G_y = \frac{1}{8\pi\mu} r^2(p, Q) \ln \left[\frac{1}{r(p, Q)} \right] \quad (3.15)$$

where $r(p, Q)$ is a distance between point p and Q and defined as follows:

$$r(p, Q) = \sqrt{(X_p - x_Q)^2 + (Y_p - y_Q)^2} \quad (3.16)$$

By substituting the Galerkin vector of equation (3.15) into the displacement vector of equation (3.12), the displacement vector can be written:

$$u_i = \frac{1}{8\pi\mu(1-\nu)} \left\{ (3-4\nu) \ln \left[\frac{1}{r(p,Q)} \right] \delta_{ij} + \frac{\partial r(p,Q)}{\partial x_i} \frac{\partial r(p,Q)}{\partial x_j} \right\} x e_j \quad (3.17)$$

The displacement vector can be written in the form of tensor functions, as follows:

$$u_i = U_{ij}(p,Q) e_j \quad (3.18)$$

where the function $U_{ij}(p,Q)$ are given by

$$U_{ij}(p,Q) = \frac{1}{8\pi\mu(1-\nu)} \left\{ (3-4\nu) \ln \left[\frac{1}{r(p,Q)} \right] \delta_{ij} + \frac{\partial r(p,Q)}{\partial x_i} \frac{\partial r(p,Q)}{\partial x_j} \right\} \quad (3.19)$$

The functions $U_{ij}(p,Q)$ are called the displacement kernels where the first subscript refers to the direction of the displacement of the boundary point Q due to a unit load at interior load point p in the direction of the second subscript.

The traction vector can be derived by differentiating the displacement vector of equation (3.17) and substituting into the stress-strain equation (3.8), as follows:

$$t_i = \frac{-1}{4\pi(1-\nu)r(p,Q)} \left(\frac{\partial r(p,Q)}{\partial n} \right) \left[(1-2\nu)\delta_{ij} + 2 \frac{\partial r(p,Q)}{\partial x_i} \frac{\partial r(p,Q)}{\partial x_j} \right] - \frac{1-2\nu}{4\pi(1-\nu)r(p,Q)} \left[\frac{\partial r(p,Q)}{\partial x_j} n_i - \frac{\partial r(p,Q)}{\partial x_i} n_j \right] x e_j \quad (3.20)$$

Similar to the displacement vector, the traction vector can be written in the form of tensor function as follows:

$$t_i = T_{ij}(p,Q) e_j \quad (3.21)$$

where the function $T_{ij}(p,Q)$ are given by

$$T_{ij}(p, Q) = \frac{-1}{4\pi(1-\nu)r(p, Q)} \left(\frac{\partial r(p, Q)}{\partial n} \right) \left[(1-2\nu)\delta_{ij} + 2 \frac{\partial r(p, Q)}{\partial x_i} \frac{\partial r(p, Q)}{\partial x_j} \right] - \frac{1-2\nu}{4\pi(1-\nu)r(p, Q)} \left[\frac{\partial r(p, Q)}{\partial x_j} n_i - \frac{\partial r(p, Q)}{\partial x_i} n_j \right] \quad (3.22)$$

The function $T_{ij}(p, Q)$ are called the traction kernels. The normal derivative $\partial r / \partial n$ is given by

$$\frac{\partial r}{\partial n} = \frac{\partial r}{\partial x} \frac{\partial x}{\partial n} + \frac{\partial r}{\partial y} \frac{\partial y}{\partial n} \quad (3.23)$$

where $\partial r / \partial x$ and $\partial r / \partial y$ are given by differentiating equation (3.16), as follows:

$$\begin{aligned} \frac{\partial r(p, Q)}{\partial x} &= \frac{x_Q - X_p}{r(p, Q)} \\ \frac{\partial r(p, Q)}{\partial y} &= \frac{y_Q - Y_p}{r(p, Q)} \end{aligned} \quad (3.24)$$

and $\partial x / \partial n$ and $\partial y / \partial n$ are the components of the unit outward normal in the x and y directions, n_x and n_y , as follows:

$$\begin{aligned} n_x &= \frac{\partial x}{\partial n} \\ n_y &= \frac{\partial y}{\partial n} \end{aligned} \quad (3.25)$$

3.1.3 Reciprocal Work Theorem (Betti's Theorem)

Consider an isotropic and elastic body in equilibrium under two different sets of stresses and strains: set (a) of applied stresses $\sigma_{ij}^{(a)}$ which cause strains $\varepsilon_{ij}^{(a)}$ and set (b) of applied stresses $\sigma_{ij}^{(b)}$ which cause strains $\varepsilon_{ij}^{(b)}$. The Betti's theorem states that the work done by the stresses of system (a) on the displacements of system (b) is equal to

the work done by the stresses of system (b) on the displacements of system (a).

Therefore, this theorem can be written, as follows:

$$\int_V \sigma_{ij}^{(a)} \varepsilon_{ij}^{(b)} dV = \int_V \sigma_{ij}^{(b)} \varepsilon_{ij}^{(a)} dV \quad (3.26)$$

The above equation can be written in terms of stresses and displacements, as follows:

$$\frac{1}{2} \int_V \sigma_{ij}^{(a)} \left[\frac{\partial u_i}{\partial x_j} + \frac{\partial u_j}{\partial x_i} \right]^{(b)} dV = \frac{1}{2} \int_V \sigma_{ij}^{(b)} \left[\frac{\partial u_i}{\partial x_j} + \frac{\partial u_j}{\partial x_i} \right]^{(a)} dV \quad (3.27)$$

Using the summation convention, the above equation can be written:

$$\int_V \sigma_{ij}^{(a)} \frac{\partial u_i}{\partial x_j}^{(b)} dV = \int_V \sigma_{ij}^{(b)} \frac{\partial u_i}{\partial x_j}^{(a)} dV \quad (3.28)$$

The left-hand side term can be expanded, as follows:

$$\int_V \sigma_{ij}^{(a)} \frac{\partial u_i}{\partial x_j}^{(b)} dV = \int_V \left[\frac{\partial(\sigma_{ij}^{(a)} u_i^{(b)})}{\partial x_j} - \frac{\partial \sigma_{ij}^{(a)}}{\partial x_j} u_i^{(b)} \right] dV \quad (3.29)$$

The last term can be substituted by equilibrium equation (3.1), as follows:

$$\int_V \sigma_{ij}^{(a)} \frac{\partial u_i}{\partial x_j}^{(b)} dV = \int_V \left[\frac{\partial(\sigma_{ij}^{(a)} u_i^{(b)})}{\partial x_j} \right] dV + \int_V f_i^{(a)} u_i^{(b)} dV \quad (3.30)$$

Applying Green's theorem (also called divergence theorem) which transforms a volume integral into a surface integral, as follows:

$$\int_V \frac{\partial f_i}{\partial x_i} dV = \int_{\Gamma} f_i \cdot n_i d\Gamma \quad (3.31)$$

into the first term of the right-hand side of equation (3.30), results in:

$$\int_V \sigma_{ij}^{(a)} \frac{\partial u_i^{(b)}}{\partial x_j} dV = \int_{\Gamma} (\sigma_{ij}^{(a)} u_i^{(b)}) n_j d\Gamma + \int_V f_i^{(a)} u_i^{(b)} dV \quad (3.32)$$

Applying the stress-traction relationship, which is, in tensor notation:

$$t_i = \sigma_{ij} n_j \quad (3.33)$$

into equation (3.32), the equation becomes:

$$\int_V \sigma_{ij}^{(a)} \frac{\partial u_i^{(b)}}{\partial x_j} dV = \int_{\Gamma} t_i^{(a)} u_i^{(b)} d\Gamma + \int_V f_i^{(a)} u_i^{(b)} dV \quad (3.34)$$

Using the same procedure as above for the right-hand side term of equation (3.28),

gives:

$$\int_V \sigma_{ij}^{(b)} \frac{\partial u_i^{(a)}}{\partial x_j} dV = \int_{\Gamma} t_i^{(b)} u_i^{(a)} d\Gamma + \int_V f_i^{(b)} u_i^{(a)} dV \quad (3.35)$$

By substituting equation (3.34) and (3.35) into equation (3.28), the equation for Betti's theorem becomes:

$$\int_{\Gamma} t_i^{(a)} u_i^{(b)} d\Gamma + \int_V f_i^{(a)} u_i^{(b)} dV = \int_{\Gamma} t_i^{(b)} u_i^{(a)} d\Gamma + \int_V f_i^{(b)} u_i^{(a)} dV \quad (3.36)$$

The above equation can be used to derive an boundary integral equation by setting set (a) to be the actual problem to be solved, where the traction and displacement vectors $t_i^{(a)}$ and $u_i^{(a)}$ are unknown and satisfy the boundary conditions of the actual problem, and set (b) to be a known set of traction and displacement vectors $t_i^{(b)}$ and $u_i^{(b)}$ which must be valid for any geometry in equilibrium. In this case, the three-dimensional

Kelvin solution for tractions and displacements at any surface point Q due to a unit load applied on an interior point p in an infinite domain is used for set (b). Therefore, the displacement and traction vectors of both systems can be written, as follows:

$$\begin{aligned} u_i^{(a)} &= u_i(Q); & t_i^{(a)} &= t_i(Q); & f_i^{(a)} &= f_i(q) \\ u_i^{(b)} &= U_{ij}(p, Q)\mathbf{e}_j; & t_i^{(b)} &= T_{ij}(p, Q)\mathbf{e}_j; & f_i^{(b)} &= 0 \end{aligned} \quad (3.37)$$

where $U_{ij}(p, Q)$ and $T_{ij}(p, Q)$ can be obtained from equation (3.19) and (3.22), respectively. Note that q is a point inside the solution domain. By substituting equation (3.37) into equation (3.36), the equation becomes:

$$\int_{\Gamma} U_{ij}(p, Q)t_i(Q)d\Gamma + \int_V U_{ij}(p, q)f_i(q)dV = \int_{\Gamma} T_{ij}(p, Q)u_i(Q)d\Gamma \quad (3.38)$$

The Kelvin solution is singular when point p coincides with point Q . To solve this problem, a sphere of an infinitesimal radius ε and surface area Γ_ε is used to surround the interior point p and examine the integrals as $\varepsilon \rightarrow 0$. Therefore, the boundary integral equation becomes:

$$u_i(p) + \int_{\Gamma} T_{ij}(p, Q)u_i(Q)d\Gamma = \int_{\Gamma} U_{ij}(p, Q)t_i(Q)d\Gamma + \int_V U_{ij}(p, q)f_i(q)dV \quad (3.39)$$

This equation is known as the Somigliana identity for the displacements. In the absence of body forces, the above equation becomes:

$$u_i(p) + \int_{\Gamma} T_{ij}(p, Q)u_i(Q)d\Gamma = \int_{\Gamma} U_{ij}(p, Q)t_i(Q)d\Gamma \quad (3.40)$$

or in terms of second-order kernels U_{ij} and T_{ij} :

$$\begin{bmatrix} u_x(p) \\ u_y(p) \end{bmatrix} + \int_{\Gamma} \begin{bmatrix} T_{xx}(p, Q) & T_{xy}(p, Q) \\ T_{yx}(p, Q) & T_{yy}(p, Q) \end{bmatrix} \begin{bmatrix} u_x(Q) \\ u_y(Q) \end{bmatrix} d\Gamma = \int_{\Gamma} \begin{bmatrix} U_{xx}(p, Q) & U_{xy}(p, Q) \\ U_{yx}(p, Q) & U_{yy}(p, Q) \end{bmatrix} \begin{bmatrix} t_x(Q) \\ t_y(Q) \end{bmatrix} d\Gamma \quad (3.41)$$

The interior stresses at point p can be obtained by differentiating the BIE of equation (3.40) at p and substituting in the Hooke's law equation (3.10), as follows (see, for example, Becker [1992]):

$$\begin{aligned} \sigma_{ij}(p) + \int_{\Gamma} \left\{ \frac{2\mu\nu}{1-2\nu} \delta_{ij} \frac{\partial T_{mk}(p, Q)}{\partial x_m} + \mu \left[\frac{\partial T_{ik}(p, Q)}{\partial x_j} + \frac{\partial T_{jk}(p, Q)}{\partial x_i} \right] \right\} u_k(Q) d\Gamma \\ = \int_{\Gamma} \left\{ \frac{2\mu\nu}{1-2\nu} \delta_{ij} \frac{\partial U_{mk}(p, Q)}{\partial x_m} + \mu \left[\frac{\partial U_{ik}(p, Q)}{\partial x_j} + \frac{\partial U_{jk}(p, Q)}{\partial x_i} \right] \right\} t_k(Q) d\Gamma \end{aligned} \quad (3.42)$$

or in terms of new third-order kernels S_{kij} and D_{kij} , as follows:

$$\sigma_{ij}(p) + \int_{\Gamma} S_{kij}(p, Q) u_k(Q) d\Gamma = \int_{\Gamma} D_{kij}(p, Q) t_k(Q) d\Gamma \quad (3.43)$$

where

$$\begin{aligned} S_{kij}(p, Q) = & \frac{\mu}{2\pi(1-\nu)} \left(\frac{1}{r^2} \right) n_i \left[2\nu \frac{\partial r}{\partial x_j} \frac{\partial r}{\partial x_k} + (1-2\nu) \delta_{jk} \right] \\ & + \frac{\mu}{2\pi(1-\nu)} \left(\frac{1}{r^2} \right) n_j \left[2\nu \frac{\partial r}{\partial x_i} \frac{\partial r}{\partial x_k} + (1-2\nu) \delta_{ik} \right] \\ & + \frac{\mu}{2\pi(1-\nu)} \left(\frac{1}{r^2} \right) n_k \left[2(1-2\nu) \frac{\partial r}{\partial x_i} \frac{\partial r}{\partial x_j} - (1-4\nu) \delta_{ij} \right] \\ & + \frac{\mu}{\pi(1-\nu)} \left(\frac{1}{r^2} \right) \left(\frac{\partial r}{\partial n} \right) \left[(1-2\nu) \delta_{ij} \frac{\partial r}{\partial x_k} + \nu \left(\delta_{jk} \frac{\partial r}{\partial x_i} + \delta_{ik} \frac{\partial r}{\partial x_j} \right) - 4 \frac{\partial r}{\partial x_i} \frac{\partial r}{\partial x_j} \frac{\partial r}{\partial x_k} \right] \end{aligned} \quad (3.44)$$

$$D_{kij}(p, Q) = \frac{1}{4\pi(1-\nu)} \left(\frac{1}{r} \right) \left[(1-2\nu) \left(\delta_{jk} \frac{\partial r}{\partial x_i} + \delta_{ik} \frac{\partial r}{\partial x_j} - \delta_{ij} \frac{\partial r}{\partial x_k} \right) + 2 \frac{\partial r}{\partial x_i} \frac{\partial r}{\partial x_j} \frac{\partial r}{\partial x_k} \right] \quad (3.45)$$

For solving the boundary-only problem, the interior load point p has to move to the boundary and referred to as P . Therefore, the boundary integral equation (3.40) can be written, as follows:

$$C_{ij}(P)u_i(P) + \int_{\Gamma} T_{ij}(P,Q)u_i(Q)d\Gamma = \int_{\Gamma} U_{ij}(P,Q)t_i(Q)d\Gamma \quad (3.46)$$

There are two approaches, direct and indirect approaches, to calculate the function $C_{ij}(P)$. In the direct approach, the boundary point P is surrounded by a small circle of radius ε and each term is taken in equation (3.46) in the limit as $\varepsilon \rightarrow 0$, as follows (see, for example, Brebbia et al. [1984]):

$$C_{ij}(P) = \delta_{ij} + \lim_{\varepsilon \rightarrow 0} \int_{\Gamma_\varepsilon} T_{ij}(P,Q)d\Gamma \quad (3.47)$$

In the indirect approach, the rigid body motion, which results in zero tractions everywhere, is used.

3.1.4 The BEM for Two-Dimensional Creep Problems

The BE formulation for creep problems can be obtained by using a similar procedure as that of the BE formulation for elastostatic problems. Mukherjee [1982b] has shown that the BE formulation for time-dependent (creep) viscoplasticity has the same form as that for time-independent (plastic) viscoplasticity, except for two differences. The first is that the plastic strain rates are replaced by the creep strain rates. The second is that a rate form is used with real time. Generally, there are two types of the BE formulations for creep. One is based on an initial strain approach, and the other is based on an initial stress approach. In this chapter, the initial strain approach is used because this approach is suitable for traction-controlled problems and for strain hardening materials.

The above boundary integral equations are for elasticity which assume that the total strain consists of the elastic strain only. To derive the boundary integral equations for creep problems, the total strain is assumed to comprise the elastic strain (ε^e) and the creep strain (ε^c) as follows:

$$\varepsilon = \varepsilon^e + \varepsilon^c \quad (3.48)$$

Since creep behaviour is time and path dependent, the BE formulation must be written in rate form. Therefore, the total strain in rate form can be written as follows:

$$\dot{\varepsilon} = \dot{\varepsilon}^e + \dot{\varepsilon}^c \quad (3.49)$$

The elastic strain rate can be written in terms of the total strain rate and the creep strain rate as follows:

$$\dot{\varepsilon}^e = \dot{\varepsilon} - \dot{\varepsilon}^c \quad (3.50)$$

The force equilibrium equation (3.1) can be written in rate form as follows:

$$\frac{\partial \dot{\sigma}_{ij}}{\partial x_i} + \dot{f}_j = 0 \quad (3.51)$$

The stress-strain equation (3.8) can be written in the rate form as follows:

$$\dot{\sigma}_{ij} = \frac{2\mu\nu}{1-2\nu} \delta_{ij} \dot{\varepsilon}_{mm} + 2\mu \dot{\varepsilon}_{ij} \quad (3.52)$$

And the strain-displacement equation (3.9) can be written in the rate form as follows:

$$\dot{\epsilon}_{ij} = \frac{1}{2} \left(\frac{\partial \dot{u}_i}{\partial x_j} + \frac{\partial \dot{u}_j}{\partial x_i} \right) \quad (3.53)$$

Substituting equation (3.50) into equation (3.52), the equation becomes:

$$\dot{\sigma}_{ij} = \frac{2\mu\nu}{1-2\nu} \delta_{ij} \dot{\epsilon}_{mm} + 2\mu \dot{\epsilon}_{ij} - \left(\frac{2\mu\nu}{1-2\nu} \delta_{ij} \dot{\epsilon}_{mm}^c + 2\mu \dot{\epsilon}_{ij}^c \right) \quad (3.54)$$

Substituting equation (3.53) into equation (3.54) and then applying the result into equation (3.51), the displacement differential equation can be obtained as follows:

$$\frac{\partial \dot{u}_i}{\partial x_j} + \frac{1}{1-2\nu} \frac{\partial \dot{u}_j}{\partial x_i} - \left[k \left(\frac{\partial \dot{\epsilon}_{mm}^c}{\partial x_i} \right) + 2 \left(\frac{\partial \dot{\epsilon}_{ij}^c}{\partial x_j} \right) \right] = -\frac{\dot{f}_i}{\mu} \quad (3.55)$$

where the effective material properties of equation (3.7) are still held and the parameter k is defined as:

$$\begin{aligned} k &= 0 && \text{for plane strain } (\epsilon_{zz} = 0) \\ k &= \frac{2\nu}{1-2\nu} && \text{for plane stress } (\sigma_{zz} = 0) \end{aligned} \quad (3.56)$$

The direct BE formulation for creep based on an initial strain approach can be obtained by using Betti's theorem and including the effects of creep. Therefore, the boundary integral equation, excluding body force effects, can be written as before for the elastostatic problems with an additional term containing an initial strain rate as follows (see, for example, Lee and Fenner [1986]):

$$\dot{u}_i(p) + \int_{\Gamma} T_{ij}(p, Q) \dot{u}_j(Q) d\Gamma(Q) = \int_{\Gamma} U_{ij}(p, Q) \dot{v}_j(Q) d\Gamma(Q) + \int_A W_{kij}(p, q) \dot{\epsilon}_{ij}^c(q) dA(q) \quad (3.57)$$

where the kernels T_{ij} and U_{ij} are the same kernels as those of elastostatic problems and W_{kij} is the third-order kernel for the stress at the field point due to a unit orthogonal load at the load point in the k^{th} direction and can be expressed as follows:

$$W_{kij}(p,q) = \frac{-1}{4\pi(1-\nu)} \left(\frac{1}{r} \right) \left[(1-2\nu) \left(\delta_{jk} \frac{\partial r}{\partial x_i} + \delta_{ik} \frac{\partial r}{\partial x_j} - k_1 \delta_{ij} \frac{\partial r}{\partial x_k} \right) + 2 \frac{\partial r}{\partial x_i} \frac{\partial r}{\partial x_j} \frac{\partial r}{\partial x_k} \right] \quad (3.58)$$

where the parameter k_1 is given as follows:

$$\begin{aligned} k_1 &= \frac{1}{1-2\nu} && \text{for plane strain} \\ k_1 &= 1 && \text{for plane stress} \end{aligned} \quad (3.59)$$

To solve the boundary-only problem, the interior load point p has to move to the boundary and referred to it as P . Therefore, the equation (3.57) can be written as follows:

$$C_{ij}(P)\dot{u}_i(P) + \int_{\Gamma} T_{ij}(P,Q)\dot{u}_j(Q)d\Gamma(Q) = \int_{\Gamma} U_{ij}(P,Q)\dot{v}_j(Q)d\Gamma(Q) + \int_A W_{kij}(P,q)\dot{\epsilon}_{ij}^c(q)dA(q) \quad (3.60)$$

3.2 Numerical Implementation

To solve the BIE solution of any shape of the boundary, numerical integration is the only method to obtain the solution. To perform the numerical integration of the boundary integral equation (3.60), the boundary and domain must be divided into a number of boundary elements and domain elements or cells. Each element and cell are defined by some nodal points. Over each element and cell, the variation of the

geometry and variables, which can be constant, linear, quadratic, cubic or higher order, must be derived.

In this section, isoparametric quadratic elements for boundary elements and eight-node quadrilateral elements for domain cells (see Figure 3.3), which use the quadratic order of variation for both the geometry and unknown variables, are used since they give the best compromise between accuracy and efficiency.

3.2.1 Division of the Boundary into Elements and the Domain into Cells

(a) Division of the Boundary into Elements

The boundary of the solution domain is divided into a number of connected elements. As mentioned previously, isoparametric quadratic elements are used. It is convenient to use a new coordinate system that is local to the element using an intrinsic variable ξ with its origin at the midpoint node and values -1 and +1 at the end nodes, as shown in Figure 3.3(a). Therefore, the geometry of an element can be described by the coordinates of its three nodes and the shape function, as follows:

$$x_i(\xi) = \sum_{c=1}^3 N_c(\xi)(x_i)_c = N_1(\xi)(x_i)_1 + N_2(\xi)(x_i)_2 + N_3(\xi)(x_i)_3 \quad (3.61)$$

where the shape functions $N_c(\xi)$ are quadratic functions that satisfy two conditions:

1. $N_c(\xi) = 1$ at the node c and,
2. $N_c(\xi) = 0$ at the other two nodes.

and are given as follows:

$$\begin{aligned}
N_1(\xi) &= \frac{-\xi}{2}(1-\xi) \\
N_2(\xi) &= (1+\xi)(1-\xi) \\
N_3(\xi) &= \frac{\xi}{2}(1+\xi)
\end{aligned} \tag{3.62}$$

Since the elements are isoparametric, the same shape functions can be used for the solution variables, as follows:

$$\begin{aligned}
\dot{u}_i(\xi) &= \sum_{c=1}^3 N_c(\xi)(\dot{u}_i)_c = N_1(\xi)(\dot{u}_i)_1 + N_2(\xi)(\dot{u}_i)_2 + N_3(\xi)(\dot{u}_i)_3 \\
i_i(\xi) &= \sum_{c=1}^3 N_c(\xi)(i_i)_c = N_1(\xi)(i_i)_1 + N_2(\xi)(i_i)_2 + N_3(\xi)(i_i)_3
\end{aligned} \tag{3.63}$$

(b) Division of the Domain into Cells

For the domain discretisation, the geometry of a quadrilateral element and the solution variables can be described by a quadratic shape function $N_c(\xi)$ of two local intrinsic coordinates, ξ_1 and ξ_2 , which vary from -1 to +1 (see Figure 3.3(b)) as follows:

$$\begin{aligned}
x_i(\xi_1, \xi_2) &= \sum_{c=1}^8 N_c(\xi_1, \xi_2)(x_i)_c \\
\dot{u}_i(\xi_1, \xi_2) &= \sum_{c=1}^8 N_c(\xi_1, \xi_2)(\dot{u}_i)_c \\
i_i(\xi_1, \xi_2) &= \sum_{c=1}^8 N_c(\xi_1, \xi_2)(i_i)_c \\
\dot{\varepsilon}_{ij}^c(\xi_1, \xi_2) &= \sum_{c=1}^8 N_c(\xi_1, \xi_2)(\dot{\varepsilon}_{ij}^c)_c
\end{aligned} \tag{3.64}$$

where the shape function $N_c(\xi_1, \xi_2)$ is given as follows:

$$\begin{aligned}
N_1(\xi_1, \xi_2) &= \frac{-1}{4}(1-\xi_1)(1-\xi_2)(1+\xi_1+\xi_2) \\
N_2(\xi_1, \xi_2) &= \frac{1}{2}(1-\xi_1^2)(1-\xi_2) \\
N_3(\xi_1, \xi_2) &= \frac{-1}{4}(1+\xi_1)(1-\xi_2)(1-\xi_1+\xi_2) \\
N_4(\xi_1, \xi_2) &= \frac{1}{2}(1+\xi_1)(1-\xi_2^2) \\
N_5(\xi_1, \xi_2) &= \frac{-1}{4}(1+\xi_1)(1+\xi_2)(1-\xi_1-\xi_2) \\
N_6(\xi_1, \xi_2) &= \frac{1}{2}(1-\xi_1^2)(1+\xi_2) \\
N_7(\xi_1, \xi_2) &= \frac{-1}{4}(1-\xi_1)(1+\xi_2)(1+\xi_1-\xi_2) \\
N_8(\xi_1, \xi_2) &= \frac{1}{2}(1-\xi_1)(1-\xi_2^2)
\end{aligned} \tag{3.65}$$

3.2.2 Numerical Integration of the Kernels

Since the variable from the boundary curve Γ has to transform to the local intrinsic coordinate ξ , the Jacobian of transformation, $J(\xi)$, must be calculated, as follows:

$$J(\xi) = \frac{d\Gamma}{d\xi} = \sqrt{\left(\frac{dx(\xi)}{d\xi}\right)^2 + \left(\frac{dy(\xi)}{d\xi}\right)^2} \tag{3.66}$$

To determine the components of the unit outward normal, the unit tangential vector, \mathbf{m} , is defined, as follows:

$$\mathbf{m} = \frac{m_x \mathbf{e}_x}{|\mathbf{m}|} + \frac{m_y \mathbf{e}_y}{|\mathbf{m}|} \tag{3.67}$$

where the magnitude of the vector \mathbf{m} is given by

$$|\mathbf{m}| = \sqrt{(m_x)^2 + (m_y)^2} = \sqrt{\left(\frac{dx(\xi)}{d\xi}\right)^2 + \left(\frac{dy(\xi)}{d\xi}\right)^2} \tag{3.68}$$

which is equal to the Jacobian $J(\xi)$. Therefore, the components of the unit tangential vector can be written, as follows:

$$\begin{aligned} m_x &= \frac{1}{J(\xi)} \left[\frac{dx(\xi)}{d\xi} \right] \\ m_y &= \frac{1}{J(\xi)} \left[\frac{dy(\xi)}{d\xi} \right] \end{aligned} \quad (3.69)$$

The normal vector is equal to the cross product of the vector \mathbf{m} and \mathbf{e}_z , which is the unit vector in the z-direction normal to the two-dimensional plane, as follows:

$$\begin{aligned} \mathbf{n} &= \mathbf{m} \times \mathbf{e}_z \\ &= \begin{vmatrix} \mathbf{e}_x & \mathbf{e}_y & \mathbf{e}_z \\ \frac{1}{J(\xi)} \left[\frac{dx(\xi)}{d\xi} \right] & \frac{1}{J(\xi)} \left[\frac{dy(\xi)}{d\xi} \right] & 0 \\ 0 & 0 & 1 \end{vmatrix} \\ &= \frac{1}{J(\xi)} \left[\frac{dy(\xi)}{d\xi} \right] \mathbf{e}_x - \frac{1}{J(\xi)} \left[\frac{dx(\xi)}{d\xi} \right] \mathbf{e}_y \end{aligned} \quad (3.70)$$

Therefore, the components of the unit outward normal can be written, as follows:

$$\begin{aligned} n_x &= \frac{1}{J(\xi)} \left[\frac{dy(\xi)}{d\xi} \right] \\ n_y &= -\frac{1}{J(\xi)} \left[\frac{dx(\xi)}{d\xi} \right] \end{aligned} \quad (3.71)$$

The differentials of the coordinates $x(\xi)$ and $y(\xi)$ with respect to ξ are given by

$$\begin{aligned} \frac{dx(\xi)}{d\xi} &= \frac{dN_1(\xi)}{d\xi} x_1 + \frac{dN_2(\xi)}{d\xi} x_2 + \frac{dN_3(\xi)}{d\xi} x_3 \\ \frac{dy(\xi)}{d\xi} &= \frac{dN_1(\xi)}{d\xi} y_1 + \frac{dN_2(\xi)}{d\xi} y_2 + \frac{dN_3(\xi)}{d\xi} y_3 \end{aligned} \quad (3.72)$$

where the differentials of the shape functions are given by

$$\begin{aligned}\frac{dN_1(\xi)}{d\xi} &= \xi - \frac{1}{2} \\ \frac{dN_2(\xi)}{d\xi} &= -2\xi \\ \frac{dN_3(\xi)}{d\xi} &= \xi + \frac{1}{2}\end{aligned}\tag{3.73}$$

For quadrilateral elements, the Jacobian of transformation, $J(\xi_1, \xi_2)$, can be written as follows:

$$\begin{aligned}J(\xi_1, \xi_2) &= \frac{\partial(x, y)}{\partial(\xi_1, \xi_2)} \\ &= \begin{vmatrix} \frac{\partial x}{\partial \xi_1} & \frac{\partial x}{\partial \xi_2} \\ \frac{\partial y}{\partial \xi_1} & \frac{\partial y}{\partial \xi_2} \end{vmatrix} \\ &= \frac{\partial x}{\partial \xi_1} \frac{\partial y}{\partial \xi_2} - \frac{\partial x}{\partial \xi_2} \frac{\partial y}{\partial \xi_1}\end{aligned}\tag{3.74}$$

The boundary integral equations (3.60) can now be written in terms of the local coordinate ξ, ξ_1, ξ_2 as follows:

$$\begin{aligned}C_{ij}(P)\dot{u}_i(P) + \sum_{m=1}^M \sum_{c=1}^3 \dot{u}_j(Q) \int_{-1}^{+1} T_{ij}(P, Q) N_c(\xi) J(\xi) d\xi &= \sum_{m=1}^M \sum_{c=1}^3 i_j(Q) \int_{-1}^{+1} U_{ij}(P, Q) N_c(\xi) J(\xi) d\xi \\ + \sum_{d=1}^D \sum_{c=1}^8 \dot{\epsilon}_{ij}^c(q) \int_{-1}^{+1} \int_{-1}^{+1} W_{kij}(P, q) N_c(\xi_1, \xi_2) J(\xi_1, \xi_2) d\xi_1 d\xi_2\end{aligned}\tag{3.75}$$

where M is the total number of the boundary elements and D is the total number of the domain cells. By taking each node in turn as the load point p and performing the integration, a set of linear equations can be written as follows:

$$[A][\dot{u}] = [B][\dot{i}] + [W][\dot{\epsilon}^c]\tag{3.76}$$

where the matrices $[A]$, $[B]$ and $[W]$ contain the integrals of the kernels T_{ij} , U_{ij} , and W_{kij} , respectively. Note that the parameter $C_{ij}(P)$ contributes only to the diagonal coefficients of the $[A]$ matrix (when P is equal to Q).

3.2.3 Singularity Treatment

For the boundary integrations, the U_{ij} and T_{ij} kernels contain terms of the order $\ln(1/r)$ and $(1/r)$, respectively. Therefore, the kernels are singular as $r \rightarrow 0$. Since the kernels are dependent on the distance between P and Q , there are three possibilities of the positions of P and Q .

1. P and Q are in different elements. In this case, the U_{ij} and T_{ij} kernels are not singular. Therefore, the integrals can be determined by using the standard Gaussian quadrature, as follows:

$$\int_{-1}^{+1} f(\xi) d\xi = \sum_{g=1}^G f(\xi_g) w_g \quad (3.77)$$

where G is the total number of Gaussian integration points and ξ_g is the Gaussian coordinate with an associated weighting function w_g .

2. P and Q are in the same element but $P \neq Q$. In this case, the U_{ij} and T_{ij} kernels are singular but the shape function $N_c(\xi)$ in the vicinity of P is of the order $r(P,Q)$. Therefore, the product of the kernels and the shape function is not singular and the integrals can be evaluated by using the standard Gaussian quadrature.

3. P and Q are in the same element and $P = Q$. In this case, the U_{ij} and T_{ij} kernels are singular and the standard Gaussian quadrature cannot be used. The U_{ij} kernel is singular of the order $\ln(1/r)$ as $r \rightarrow 0$. This form of integral can be accurately calculated by using the special logarithmic Gaussian quadrature and changing the limits of integration to become 0 to 1, as follows:

$$\int_0^1 f(\eta) \ln\left(\frac{1}{\eta}\right) d\eta = \sum_{gl=1}^{Gl} f(\eta_{gl}) w_{gl} \quad (3.78)$$

where Gl is the total number of logarithmic Gaussian integration points and η_{gl} is the Gaussian coordinate with an associated weighting function w_{gl} . A simple linear transformation can be used to accommodate the 0 and 1 integration limits, as follows:

1. If P is the first node of the element, $\eta = 0.5 (1 + \xi)$.
2. If P is the second node of the element, the element is divided into two sub-elements: $\eta = -\xi$ (for $-1 < \xi < 0$) and $\eta = \xi$ (for $0 < \xi < 1$).
3. If P is the third node of the element, $\eta = 0.5 (1 - \xi)$.

The T_{ij} kernel is singular of the order $1/r$ as $r \rightarrow 0$. This means the diagonal coefficients of the $[A]$ matrix are singular. To evaluate these coefficients, this singular kernel needs a special treatment. Since the BIE matrices must apply to any physical problem with a unique solution, any physical problem can be chosen as long as the solution does not depend on the geometry. In elastostatic problems, the rigid body motion (constant displacement of all the nodes in any direction) is chosen. This motion results in zero tractions everywhere which makes the right-hand side of equation (3.76) zero:

$$[A][u_c] = [B][0] = 0 \quad (3.79)$$

where u_c is a constant arbitrary displacement in any direction. Therefore, the sum of all the coefficients in any row of $[A]$ must be zero. The diagonal terms of $[A]$ can then be calculated as the sum of all the other non-diagonal coefficients, as follows:

$$[A]_{ii} = - \sum_{\substack{j=1 \\ j \neq i}}^N [A]_{ij} \quad (3.80)$$

where i and j are the row and column counters, respectively, while N is the total number of nodes.

On the domain integrations, the domain integral containing the W_{kij} kernel which is singular of order $1/r$ requires special treatment. There are two possibilities for the position of load point p .

1. When p is not a node of domain elements. In this case, there is no singularity of the W_{kij} kernel. Therefore, the standard Gaussian quadrature (for area integrals) can be used as follows:

$$\int_{-1}^{+1} \int_{-1}^{+1} f(\xi_1, \xi_2) d\xi_1 d\xi_2 = \sum_{m=1}^{G_m} \sum_{n=1}^{G_n} f(\xi_m, \xi_n) w_m w_n \quad (3.81)$$

where G_m and G_n are the total number of Gaussian integration points and ξ_m and ξ_n are the Gaussian coordinates with associated weighting functions w_m and w_n , respectively.

2. When p is a node of a domain element. In this case, the W_{kij} kernel is singular of order $1/r$. To deal with this singularity, the domain element must be divided into two or three triangular sub-elements depending on whether p is a corner or midpoint node, as shown in Figure 3.4. The new set of local intrinsic coordinates, η_1 and η_2 , with their

origin at the centre of the element and vary from -1 to +1, must be used and a new set of linear shape functions is defined as follows:

$$\begin{aligned}\xi_1(\eta_1, \eta_2) &= L_1(\eta_1, \eta_2)(\xi_1)_1 + L_2(\eta_1, \eta_2)(\xi_1)_2 + L_3(\eta_1, \eta_2)(\xi_1)_3 + L_4(\eta_1, \eta_2)(\xi_1)_4 \\ \xi_2(\eta_1, \eta_2) &= L_1(\eta_1, \eta_2)(\xi_2)_1 + L_2(\eta_1, \eta_2)(\xi_2)_2 + L_3(\eta_1, \eta_2)(\xi_2)_3 + L_4(\eta_1, \eta_2)(\xi_2)_4\end{aligned}\quad (3.82)$$

where the linear rectangular shape functions L_1, L_2, L_3 and L_4 are defined as follows:

$$\begin{aligned}L_1(\eta_1, \eta_2) &= \frac{1}{4}(1-\eta_1)(1-\eta_2) \\ L_2(\eta_1, \eta_2) &= \frac{1}{4}(1+\eta_1)(1-\eta_2) \\ L_3(\eta_1, \eta_2) &= \frac{1}{4}(1+\eta_1)(1+\eta_2) \\ L_4(\eta_1, \eta_2) &= \frac{1}{4}(1-\eta_1)(1+\eta_2)\end{aligned}\quad (3.83)$$

When p is located at the vertex, the points 1 and 2 of rectangular are jointed together as follows:

$$\begin{aligned}(\xi_1)_1 &= (\xi_1)_2 \\ (\xi_2)_1 &= (\xi_2)_2\end{aligned}\quad (3.84)$$

The Jacobian of transformation, $J(\eta_1, \eta_2)$, is defined as :

$$\begin{aligned}J(\eta_1, \eta_2) &= \frac{\partial(\xi_1, \xi_2)}{\partial(\eta_1, \eta_2)} \\ &= \begin{vmatrix} \frac{\partial \xi_1(\eta_1, \eta_2)}{\partial \eta_1} & \frac{\partial \xi_1(\eta_1, \eta_2)}{\partial \eta_2} \\ \frac{\partial \xi_2(\eta_1, \eta_2)}{\partial \eta_1} & \frac{\partial \xi_2(\eta_1, \eta_2)}{\partial \eta_2} \end{vmatrix} \\ &= \frac{\partial \xi_1(\eta_1, \eta_2)}{\partial \eta_1} \frac{\partial \xi_2(\eta_1, \eta_2)}{\partial \eta_2} - \frac{\partial \xi_2(\eta_1, \eta_2)}{\partial \eta_1} \frac{\partial \xi_1(\eta_1, \eta_2)}{\partial \eta_2}\end{aligned}\quad (3.85)$$

where the differentials of the coordinates, ξ_1 and ξ_2 , with respect to η_1 and η_2 can be written as follows:

$$\begin{aligned}
\frac{\partial \xi_1(\eta_1, \eta_2)}{\partial \eta_1} &= \frac{\partial L_1(\eta_1, \eta_2)(\xi_1)_1}{\partial \eta_1} + \frac{\partial L_2(\eta_1, \eta_2)(\xi_1)_2}{\partial \eta_1} + \frac{\partial L_3(\eta_1, \eta_2)(\xi_1)_3}{\partial \eta_1} + \frac{\partial L_4(\eta_1, \eta_2)(\xi_1)_4}{\partial \eta_1} \\
\frac{\partial \xi_2(\eta_1, \eta_2)}{\partial \eta_1} &= \frac{\partial L_1(\eta_1, \eta_2)(\xi_2)_1}{\partial \eta_1} + \frac{\partial L_2(\eta_1, \eta_2)(\xi_2)_2}{\partial \eta_1} + \frac{\partial L_3(\eta_1, \eta_2)(\xi_2)_3}{\partial \eta_1} + \frac{\partial L_4(\eta_1, \eta_2)(\xi_2)_4}{\partial \eta_1} \\
\frac{\partial \xi_1(\eta_1, \eta_2)}{\partial \eta_2} &= \frac{\partial L_1(\eta_1, \eta_2)(\xi_1)_1}{\partial \eta_2} + \frac{\partial L_2(\eta_1, \eta_2)(\xi_1)_2}{\partial \eta_2} + \frac{\partial L_3(\eta_1, \eta_2)(\xi_1)_3}{\partial \eta_2} + \frac{\partial L_4(\eta_1, \eta_2)(\xi_1)_4}{\partial \eta_2} \\
\frac{\partial \xi_2(\eta_1, \eta_2)}{\partial \eta_2} &= \frac{\partial L_1(\eta_1, \eta_2)(\xi_2)_1}{\partial \eta_2} + \frac{\partial L_2(\eta_1, \eta_2)(\xi_2)_2}{\partial \eta_2} + \frac{\partial L_3(\eta_1, \eta_2)(\xi_2)_3}{\partial \eta_2} + \frac{\partial L_4(\eta_1, \eta_2)(\xi_2)_4}{\partial \eta_2}
\end{aligned}
\tag{3.86}$$

where the differentials of the linear shape functions are given in Appendix A. Since the Jacobian $J(\eta_1, \eta_2)$ is of order r , the singularity of the W_{kij} kernel is removed. Therefore, the integrals for these triangular sub-elements can be calculated by using standard Gaussian quadrature of equation (3.81).

3.2.4 Application of the Boundary Conditions

At this step, all of the coefficients of the $[A]$, $[B]$ and $[W]$ matrices have been calculated. The boundary conditions must be applied to obtain a unique solution. There are typically three types of boundary conditions: prescribed displacement rates, prescribed traction (or stress) rates and linear relationship between traction and displacement rates (e.g. spring attached to the boundary). Assuming that there are N nodal points on the boundary, each node has four variables, u_x , u_y , t_x and t_y . Therefore, there are $4N$ variables on the boundary. Equation (3.60) shows that there are two equations for each nodal point on the boundary or $2N$ equations for all the nodal points on the boundary. For the unique solution, half the variables must be prescribed on

every nodal point. Therefore, a particular nodal point must have both displacements or both tractions or a displacement component and a traction component prescribed. If a nodal point has no prescribed value of any kind, it is automatically assumed that both tractions are set to zero (i.e. stress free).

There are $2N$ unknowns after giving $2N$ prescribed value of variables. The $2N$ equations are needed to solve the problem. To create these equations, a force is placed at node 1 and the displacements and tractions at every node from 1 to N are calculated using the fundamental solution. This gives the first set of two linear equations. To obtain the second set of two linear equations, the force is placed at node 2 and the displacements and tractions at every node from 1 to N are calculated using the fundamental solution. This procedure is repeated until the force is placed at the last node N . Therefore, there are $2N$ equations with $2N$ unknowns which produce a unique solution. Note that the matrices $[A]$ and $[B]$ are square matrices of size $2N \times 2N$ and the matrix $[W]$ is of size $2N \times 3J$ where J is the total number of domain nodes.

To be able to use a standard solver, after applying the boundary conditions, the equation (3.76) must be rearranged such that all the unknown variables are on the left-hand side and all the known variables on the right-hand side. Therefore, the system of linear algebraic equations can be written, as follows:

$$\begin{aligned} [A^*][\dot{x}] &= [B^*][\dot{y}] + [W][\dot{\epsilon}^c] \\ &= [C] + [W][\dot{\epsilon}^c] \end{aligned} \quad (3.87)$$

where $[\dot{x}]$ contains the unknown displacement and traction rates at the boundary and $[\dot{y}]$ contains all the prescribed values of displacement and traction rates. Therefore, the

vector $[C]$ is known. In creep problems, the creep strain rates are known from the creep law. Therefore, equation (3.87) can be written as follows:

$$[A^*][\dot{x}] = [C^*] \quad (3.88)$$

where $[C^*]$ is a known vector which contains the effect of creep strain rates in the domain. The $[A^*]$ matrix is not symmetric and fully populated with non-zero coefficients. Because of this, the Gaussian elimination is suitably the choice of solution solver, although any other direct technique can be used.

In practical elastostatic problems, the displacement magnitudes are usually several orders of magnitude less than the traction magnitudes (because of the very high value of Young's modulus). This means that the values of the $[A]$ coefficients are several orders of magnitude larger than the $[B]$ coefficients. Since the $[A]$ and $[B]$ coefficients are placed together in the $[A^*]$ matrix before solving the equations, they should be roughly of the same order of magnitude to avoid suffering from numerical inaccuracies. This can be achieved by multiplying the matrix $[B]$ by a suitable scaling factor, as follows:

$$[A][u] = s[B] \times \frac{1}{s}[t] \quad (3.89)$$

where the scaling factor, s , is defined, as follows:

$$s = \frac{E}{L_{\max}} \quad (3.90)$$

where E is Young's modulus and L_{\max} is the maximum distance between any two nodes.

3.2.5 Calculation of the Boundary Stress and Strain Rates

To calculate the boundary stresses, Figure 3.5 is used to show the directions of tractions at any node on the boundary. The unit tangential vector \mathbf{m} , which has two components m_x and m_y in the x and y directions, respectively, is defined in equation (3.67). The local directions 1 and 2 are defined as tangential and normal directions, respectively. Therefore, the load tangential component of the displacement vector u_1 can be written in terms of the Cartesian displacements, as follows:

$$\dot{u}_1(\xi) = \dot{u}_x(\xi)m_x + \dot{u}_y(\xi)m_y \quad (3.91)$$

Using the shape functions from equation (3.63), the above equation becomes

$$\dot{u}_1(\xi) = \left[\sum_{c=1}^3 N_c(\xi)(\dot{u}_x)_c \right] m_x + \left[\sum_{c=1}^3 N_c(\xi)(\dot{u}_y)_c \right] m_y \quad (3.92)$$

Differentiating the above equation with respect to the tangential direction, the tangential strain ε_{11} is obtained, as follows:

$$\dot{\varepsilon}_{11}(\xi) = \frac{1}{J(\xi)} \left\{ \left[\sum_{c=1}^3 \frac{\partial N_c(\xi)}{\partial \xi} (\dot{u}_x)_c \right] m_x + \left[\sum_{c=1}^3 \frac{\partial N_c(\xi)}{\partial \xi} (\dot{u}_y)_c \right] m_y \right\} \quad (3.93)$$

Note that the Jacobian, $J(\xi)$, is used in the above equation because of the relationship between the intrinsic coordinate ξ and the boundary path Γ .

The local components of the traction vector, t_1 and t_2 , can be defined as the tangential and normal tractions to the surface, respectively, as shown in Figure 3.5. The local traction rates can be written in terms of the Cartesian global tractions, as follows:

$$\begin{aligned} \dot{t}_1 &= -\dot{t}_x \sin \alpha + \dot{t}_y \cos \alpha \\ \dot{t}_2 &= \dot{t}_x \cos \alpha + \dot{t}_y \sin \alpha \end{aligned} \quad (3.94)$$

where α is the angle between the normal traction and the global x-direction. Note that the positive tangential traction should point to the left of the outward normal. To obtain the stresses in the local directions 1 and 2, the stress-strain relationships (Hooke's law) of equation (3.2) are used, as follows:

$$\begin{aligned} \dot{\epsilon}_{11}^e &= \frac{1}{E} [\dot{\sigma}_{11} - \nu(\dot{\sigma}_{22} + \dot{\sigma}_{33})] \\ \dot{\epsilon}_{22}^e &= \frac{1}{E} [\dot{\sigma}_{22} - \nu(\dot{\sigma}_{11} + \dot{\sigma}_{33})] \\ \dot{\epsilon}_{33}^e &= \frac{1}{E} [\dot{\sigma}_{33} - \nu(\dot{\sigma}_{11} + \dot{\sigma}_{22})] \end{aligned} \quad (3.95)$$

and

$$\begin{aligned} \dot{\sigma}_{12} &= \dot{t}_1 \\ \dot{\sigma}_{22} &= \dot{t}_2 \end{aligned} \quad (3.96)$$

Creep deformation is an incompressible process. Therefore, the following expression can be written:

$$\dot{\epsilon}_{11}^c + \dot{\epsilon}_{22}^c + \dot{\epsilon}_{33}^c = 0 \quad (3.97)$$

For plane stress case ($\dot{\sigma}_{33} = 0$), the local tangential stress rate can be derived by substituting $\dot{\sigma}_{33} = 0$ and equation (3.96) into the first equation (3.95) as follows:

$$\dot{\sigma}_{11} = \nu \dot{t}_2 + E(\dot{\epsilon}_{11} - \dot{\epsilon}_{11}^c) \quad (3.98)$$

For plane strain case ($\dot{\epsilon}_{33} = 0$), the local tangential stress rate and the local stress rate in the third direction can be obtained by substituting $\dot{\epsilon}_{33} = 0$ into the third equation (3.95) and then substituting the results into the first equation (3.95) and applying equation (3.97), as follows:

$$\begin{aligned}\dot{\sigma}_{11} &= \frac{\nu}{1-\nu} \dot{i}_2 + \frac{E\nu}{1-\nu^2} (\dot{\epsilon}_{11}^c + \dot{\epsilon}_{22}^c) + \frac{E}{1-\nu^2} (\dot{\epsilon}_{11} - \dot{\epsilon}_{11}^c) \\ \dot{\sigma}_{33} &= \nu(\dot{\sigma}_{11} + \dot{i}_2) + E(\dot{\epsilon}_{11}^c + \dot{\epsilon}_{22}^c)\end{aligned}\quad (3.99)$$

Note that the material properties of equation (3.98) and (3.99) are actual (not effective) material properties. The local stress rates can be transformed to the global Cartesian stress rates by using a transformation matrix as follows:

$$\begin{bmatrix} \dot{\sigma}_{xx} \\ \dot{\sigma}_{yy} \\ \dot{\sigma}_{xy} \end{bmatrix} = \begin{bmatrix} \sin^2 \alpha & \cos^2 \alpha & -2 \sin \alpha \cos \alpha \\ \cos^2 \alpha & \sin^2 \alpha & 2 \sin \alpha \cos \alpha \\ -\sin \alpha \cos \alpha & \sin \alpha \cos \alpha & (\cos^2 \alpha - \sin^2 \alpha) \end{bmatrix} \begin{bmatrix} \dot{\sigma}_{11} \\ \dot{\sigma}_{22} \\ \dot{\sigma}_{12} \end{bmatrix}\quad (3.100)$$

where α is the angle between the normal traction and the global x-direction. Inversely, the local stress rates can be obtained from the global Cartesian stress rates by using the inversion of the transformation matrix.

3.2.6 Calculation of the Interior Variables

After solving the boundary integral equation, all values of displacement and traction rates at the boundary are known. Using the boundary integral equation (3.57) with known displacement and traction rates at the boundary, the interior displacement rates can be obtained. The strain and stress rates can be obtained by analytically differentiating the boundary integral equation (3.57) to obtain strain rates and then

using the stress-strain relationships to obtain stress rates (see, for example, Lee and Fenner [1986]). There is another approach to calculate the strain and stress rates at internal points by differentiating via the shape functions (see, for example, Gun [1997]). The numerical differentiation is used in this work, since it is easier to implement in a numerical scheme.

The differentials of the displacement vector components with respect to the local intrinsic coordinates, ξ_1 and ξ_2 , can be written as follows:

$$\begin{aligned}
 \frac{\partial \dot{u}_1}{\partial \xi_1} &= \frac{\partial \dot{u}_1}{\partial x_1} \frac{\partial x_1}{\partial \xi_1} + \frac{\partial \dot{u}_1}{\partial x_2} \frac{\partial x_2}{\partial \xi_1} \\
 \frac{\partial \dot{u}_1}{\partial \xi_2} &= \frac{\partial \dot{u}_1}{\partial x_1} \frac{\partial x_1}{\partial \xi_2} + \frac{\partial \dot{u}_1}{\partial x_2} \frac{\partial x_2}{\partial \xi_2} \\
 \frac{\partial \dot{u}_2}{\partial \xi_1} &= \frac{\partial \dot{u}_2}{\partial x_1} \frac{\partial x_1}{\partial \xi_1} + \frac{\partial \dot{u}_2}{\partial x_2} \frac{\partial x_2}{\partial \xi_1} \\
 \frac{\partial \dot{u}_2}{\partial \xi_2} &= \frac{\partial \dot{u}_2}{\partial x_1} \frac{\partial x_1}{\partial \xi_2} + \frac{\partial \dot{u}_2}{\partial x_2} \frac{\partial x_2}{\partial \xi_2}
 \end{aligned} \tag{3.101}$$

or in the matrix form,

$$\begin{aligned}
 \begin{bmatrix} \frac{\partial \dot{u}_1}{\partial \xi_1} \\ \frac{\partial \dot{u}_1}{\partial \xi_2} \end{bmatrix} &= \begin{bmatrix} \frac{\partial x_1}{\partial \xi_1} & \frac{\partial x_2}{\partial \xi_1} \\ \frac{\partial x_1}{\partial \xi_2} & \frac{\partial x_2}{\partial \xi_2} \end{bmatrix} \begin{bmatrix} \frac{\partial \dot{u}_1}{\partial x_1} \\ \frac{\partial \dot{u}_1}{\partial x_2} \end{bmatrix} = [J] \begin{bmatrix} \frac{\partial \dot{u}_1}{\partial x_1} \\ \frac{\partial \dot{u}_1}{\partial x_2} \end{bmatrix} \\
 \begin{bmatrix} \frac{\partial \dot{u}_2}{\partial \xi_1} \\ \frac{\partial \dot{u}_2}{\partial \xi_2} \end{bmatrix} &= \begin{bmatrix} \frac{\partial x_1}{\partial \xi_1} & \frac{\partial x_2}{\partial \xi_1} \\ \frac{\partial x_1}{\partial \xi_2} & \frac{\partial x_2}{\partial \xi_2} \end{bmatrix} \begin{bmatrix} \frac{\partial \dot{u}_2}{\partial x_1} \\ \frac{\partial \dot{u}_2}{\partial x_2} \end{bmatrix} = [J] \begin{bmatrix} \frac{\partial \dot{u}_2}{\partial x_1} \\ \frac{\partial \dot{u}_2}{\partial x_2} \end{bmatrix}
 \end{aligned} \tag{3.102}$$

where $[J]$ is the Jacobian matrix. Therefore, the differentials of the displacement rates with respect to x_1 and x_2 directions can be written as follows:

$$\begin{bmatrix} \frac{\partial \dot{u}_1}{\partial x_1} \\ \frac{\partial \dot{u}_1}{\partial x_2} \end{bmatrix} = [J]^{-1} \begin{bmatrix} \frac{\partial \dot{u}_1}{\partial \xi_1} \\ \frac{\partial \dot{u}_1}{\partial \xi_2} \end{bmatrix} \quad (3.103)$$

$$\begin{bmatrix} \frac{\partial \dot{u}_2}{\partial x_1} \\ \frac{\partial \dot{u}_2}{\partial x_2} \end{bmatrix} = [J]^{-1} \begin{bmatrix} \frac{\partial \dot{u}_2}{\partial \xi_1} \\ \frac{\partial \dot{u}_2}{\partial \xi_2} \end{bmatrix}$$

where $[J]^{-1}$ is the inverse of the Jacobian and defined as follows:

$$[J]^{-1} = \frac{1}{\begin{pmatrix} \frac{\partial x_1}{\partial \xi_1} & \frac{\partial x_2}{\partial \xi_1} \\ \frac{\partial x_1}{\partial \xi_2} & \frac{\partial x_2}{\partial \xi_2} \end{pmatrix}} \begin{vmatrix} \frac{\partial x_2}{\partial \xi_2} & -\frac{\partial x_2}{\partial \xi_1} \\ -\frac{\partial x_1}{\partial \xi_2} & \frac{\partial x_1}{\partial \xi_1} \end{vmatrix} \quad (3.104)$$

The differentials of x_1 and x_2 with respect to the coordinates ξ_1 and ξ_2 can be written as follows:

$$\begin{aligned} \frac{\partial x_1}{\partial \xi_1} &= \sum_{c=1}^8 \frac{\partial N_c(\xi_1, \xi_2)}{\partial \xi_1} (x_1)_c \\ \frac{\partial x_1}{\partial \xi_2} &= \sum_{c=1}^8 \frac{\partial N_c(\xi_1, \xi_2)}{\partial \xi_2} (x_1)_c \\ \frac{\partial x_2}{\partial \xi_1} &= \sum_{c=1}^8 \frac{\partial N_c(\xi_1, \xi_2)}{\partial \xi_1} (x_2)_c \\ \frac{\partial x_2}{\partial \xi_2} &= \sum_{c=1}^8 \frac{\partial N_c(\xi_1, \xi_2)}{\partial \xi_2} (x_2)_c \end{aligned} \quad (3.105)$$

where the differentials of the shape function with respect to the local coordinates ξ_1 and ξ_2 are given in Appendix B.

From equation (3.9), the total strain rates can be written as follows:

$$\begin{aligned}
\dot{\epsilon}_{xx} &= \frac{\partial \dot{u}_1}{\partial x_1} \\
\dot{\epsilon}_{yy} &= \frac{\partial \dot{u}_2}{\partial x_2} \\
\dot{\epsilon}_{xy} &= \frac{1}{2} \left(\frac{\partial \dot{u}_1}{\partial x_2} + \frac{\partial \dot{u}_2}{\partial x_1} \right)
\end{aligned} \tag{3.106}$$

For plane stress case ($\dot{\sigma}_{zz} = 0$), the total strain rates in the third direction ($\dot{\epsilon}_{zz}$) can be obtained by using equation (3.54) as follows:

$$\dot{\epsilon}_{zz} = \frac{-\nu}{1-\nu} (\dot{\epsilon}_{xx} + \dot{\epsilon}_{yy}) - \frac{1-2\nu}{1-\nu} (\dot{\epsilon}_{xx}^c + \dot{\epsilon}_{yy}^c) \tag{3.107}$$

Note that in the above equation, the Poisson's ratio is the actual (not effective) Poisson's ratio.

For the plane stress case ($\dot{\sigma}_{zz} = 0$), the stress rates can be obtained from equation (3.54) and equation (3.107) as follows:

$$\begin{aligned}
\dot{\sigma}_{xx} &= \frac{2\mu\nu}{1-2\nu} (\dot{\epsilon}_{xx} + \dot{\epsilon}_{yy} - \dot{\epsilon}_{xx}^c - \dot{\epsilon}_{yy}^c) + 2\mu (\dot{\epsilon}_{xx} - \dot{\epsilon}_{xx}^c) \\
\dot{\sigma}_{yy} &= \frac{2\mu\nu}{1-2\nu} (\dot{\epsilon}_{xx} + \dot{\epsilon}_{yy} - \dot{\epsilon}_{xx}^c - \dot{\epsilon}_{yy}^c) + 2\mu (\dot{\epsilon}_{yy} - \dot{\epsilon}_{yy}^c) \\
\dot{\sigma}_{xy} &= 2\mu (\dot{\epsilon}_{xy} - \dot{\epsilon}_{xy}^c)
\end{aligned} \tag{3.108}$$

For the plane strain case ($\dot{\epsilon}_{zz} = 0$), the stress rates can be obtained from equation (3.54) as follows:

$$\begin{aligned}
\dot{\sigma}_{xx} &= \frac{2\mu\nu}{1-2\nu}(\dot{\epsilon}_{xx} + \dot{\epsilon}_{yy}) + 2\mu(\dot{\epsilon}_{xx} - \dot{\epsilon}_{xx}^c) \\
\dot{\sigma}_{yy} &= \frac{2\mu\nu}{1-2\nu}(\dot{\epsilon}_{xx} + \dot{\epsilon}_{yy}) + 2\mu(\dot{\epsilon}_{yy} - \dot{\epsilon}_{yy}^c) \\
\dot{\sigma}_{zz} &= \frac{2\mu\nu}{1-2\nu}(\dot{\epsilon}_{xx} + \dot{\epsilon}_{yy}) + 2\mu(\dot{\epsilon}_{xx}^c + \dot{\epsilon}_{yy}^c) \\
\dot{\sigma}_{xy} &= 2\mu(\dot{\epsilon}_{xy} - \dot{\epsilon}_{xy}^c)
\end{aligned} \tag{3.109}$$

Note that the material properties in equation (3.108) and (3.109) are the effective material properties.

3.3 BE-Creep Algorithm

The algorithm for BE-creep can be summarised in the following steps:

Step 1 – Solve for elastic solution

- At $t = 0$, $\epsilon_{ij}^c = 0$, obtain the elastic solution using equation (3.46) with prescribed displacements and tractions.
- The displacements (u_i) and tractions (t_i) at boundary nodes are now known.
- The stresses at boundary nodes are calculated using equation (3.96) and (3.98) or (3.99) in non-rate form and the transformation matrix (equation (3.100)) in non-rate form is used to transform stresses from local to global coordinates.
- The strains at boundary nodes are calculated using Hooke's Law equation (3.2).

Step 2 – Calculate elastic stresses and strains

- Use equation (3.40) with known displacements and tractions at boundary to solve for displacements at internal nodes. Now displacements at all nodes (domain and boundary) are known.
- The strains (ε_{ij}) at internal nodes are calculated using differentiation via the shape functions.
- The stresses (σ_{ij}) at internal nodes are then calculated from the strains using equation (3.8).
- At this point, displacements, strains and stresses at all boundary and interior nodes are known.
- Store the solution matrix $[A^*]$.
- Choose the initial time increment or time step Δt (for the first calculation).

Step 3 – Solve for creep solution

- Calculate the creep strain rates ($\dot{\varepsilon}_{ij}^c$) from equation (2.30) for time hardening or equation (2.32) for strain hardening. Note that these equations use total time and, for the first calculation, time t is zero.
- Substitute the creep strain rates ($\dot{\varepsilon}_{ij}^c$) in the right hand side (RHS) of equation (3.87) with prescribed displacement and traction rates which are zero where constant prescribed values are used (i.e. $[B^*][\dot{y}] = 0$ and note that $[A^*]$, and $[W]$ are not changed) and solve for $[\dot{x}]$, the unknown displacement and traction rates at boundary nodes. Then all displacement rates (\dot{u}_i) and traction rates (\dot{t}_i) at boundary nodes are known.

- Use equation (3.57) to solve for displacement rates at all internal nodes. Now all displacement rates (\dot{u}_i) at all nodes are known.
- Store the solution matrix $[W]$.

Step 4 – Calculate creep stresses and strains

- (a) **Boundary nodes**: use displacement rates (\dot{u}_i) and traction rates (\dot{t}_i) to calculate stress rates ($\dot{\sigma}_{ij}$) using equation (3.96) and equation (3.98) or equation (3.99) and the transformation matrix (3.100), then use Hooke's law equation (3.95) to obtain strain rates ($\dot{\epsilon}_{ij}$).
- (b) **Internal nodes**: strain rates ($\dot{\epsilon}_{ij}$) are obtained by differentiation via the shape function, then stress rates ($\dot{\sigma}_{ij}$) are calculated by equation (3.54).

Step 5 – Check the convergence

- Check the convergence using the following equation.

$$e_{\min} \leq \frac{|\Delta t_I (\dot{\epsilon}_I - \dot{\epsilon}_{I-1})|}{|\epsilon_I|} \leq e_{\max} \quad \text{or} \quad e_{\min} \leq \frac{|\Delta t_I (\dot{\sigma}_I - \dot{\sigma}_{I-1})|}{|\sigma_I|} \leq e_{\max} \quad (3.110)$$

- (a) **No Convergence**: If the difference is not smaller than or equal to maximum prescribed tolerance (e_{\max}) multiply Δt by a factor ($f_1 < 1$), say 0.5, and check the convergence again. This process will be repeated until convergence is achieved. If the number of iterations exceeds a set number (say 50), then stop the program.
- (b) **Convergence**: If the difference is smaller than or equal to maximum prescribed tolerance, then update all variables using Euler's method as follows:

$$y_{I+1} = y_I + \Delta t_I \dot{y}_I \quad (3.111)$$

and update the time, $t_{I+1} = t_I + \Delta t_I$.

Step 6 – Select the next time increment

- If the difference is between minimum and maximum prescribed tolerances, the current time increment (Δt) is used for next calculation.
- If the difference is less than minimum prescribed tolerance (e_{\min}), the current time increment (Δt) is multiplied by a factor ($f_2 > 1$), say 2.0, and is used for the next calculation.

Step 7

- Repeat steps 3-6 until t_{I+1} equals the final time.

For primary creep problems where $m < 1$, the creep strain rates ($\dot{\epsilon}_{ij}^c$) of both time hardening and strain hardening at $t = 0$ cannot be found because the creep strain rates are infinite at $t = 0$. This problem can be solved by using an incremental form coupled with the initial time increment Δt as follows:

$$\Delta \epsilon_{ij}^c = \frac{3}{2} B(\sigma_{eff})^{(n-1)} S_{ij} (t_{I+1}^m - t_I^m) \quad (3.112)$$

where I is a counter and t_I is zero and t_{I+1} is equal to Δt . Therefore, the creep strain rate ($\dot{\epsilon}_{ij}^c$) at time $t = 0$ can be defined as follows:

$$(\dot{\epsilon}_{ij}^c)_{t=0} = \frac{\Delta \epsilon_{ij}^c}{\Delta t} \quad (3.113)$$

The flow chart for BE creep program is shown in Figure 3.6.

3.4 Convergence Criteria

The Euler method which is used to update the variables at each time step has a form as follows:

$$y_{i+1} = y_i + \Delta t_i \dot{y}_i \quad (3.114)$$

Although it is relatively simple to apply, Euler method is a very slow process if a constant time step is employed. To enhance the Euler method, the automatic time step control which will automatically select the next time step for the next calculation is implemented. The main idea is to compare the error, e , at each time step, with the two predefined errors or prescribed tolerances, the maximum error, e_{max} and the minimum error, e_{min} . Therefore, there will be three possibilities:

- (i) If $e > e_{max}$, the current time step is reduced by a factor of less than 1.0 and the analysis is repeated.
- (ii) If $e_{max} > e > e_{min}$, the current time step is used for the next calculation.
- (iii) If $e_{min} > e$, the current time step is increased by a factor of greater than 1.0 for the next calculation.

The creep strain error which occurs in each time step can be defined as follows (see, Mukherjee [1982b]):

$$e = \frac{|\Delta t_i (\dot{\epsilon}_i^c - \dot{\epsilon}_{i-1}^c)|}{|\epsilon_i^c|} \quad (3.115)$$

where $\dot{\varepsilon}_i^c$ is the creep strain rate at i th step and ε_i^c is the total creep strain. Note that the stress rate can alternatively be used in equation (3.115) instead of the creep strain rate.

Since there are a number of nodes in one problem and each node has six components of the stress or the strain, only one maximum value of the stress error or strain error is needed to compare with the prescribed errors. To evaluate this value, there are four possible methods as follows:

1. Method one is called 'Criterion 1' which uses the maximum magnitudes of the components of the stresses or strains. This method will calculate the error e using the equation (3.115) for all components and all nodes and then choose the maximum one as the maximum error of this time step.
2. Method two is called 'Criterion 2' which uses the maximum magnitudes of the effective stress or strain. The effective stress or strain will be calculated at each node and then used in equation (3.115) to calculate the error e for each node. The node that has the maximum value of the error will be used to compare with the prescribed tolerances.
3. Method three is called 'Criterion 3' which uses the norm of the stress or strain components. The norm is defined as follows:

$$e = \sqrt{\sum_{i=1}^n (e_i)^2} \quad (3.116)$$

where n is the total number of nodes. This method will calculate the error e in each stress or strain component for all nodes using equation (3.115) and then use equation (3.116) to calculate the norm of the error of each

component. The norm of the error of the component that has a maximum value will be used as a maximum error to compare with the prescribed tolerances. Note that if the average value is used, the term inside the square root must be divided by n and the error will be less.

4. Method four is called 'Criterion 4' which uses the norm of the error of the effective stress or strain. This method will calculate the effective stress or strain at each node and use equation (3.115) to calculate the error e_i at each node and then use equation (3.116) to calculate the error e which is used to compare with the prescribed tolerances.

In this work, the factor used to reduce the current time step is 0.5 and the factor used to increase the current time step is 2.0.

3.5 The Creep Computer Program

The structure of a typical BEM program for elasticity can be found, for example, in Becker [1992] and El-Zafrany [1993]. The BEACON program for BE elasticity is developed to solve creep problems. Thousands of lines of the creep computer program are written using Fortran code. The computer program is debugged and checked for errors. Additional subroutines are written to analyse creep problems and listed as below:

Subroutine Name	Purpose
ARRBCU2	To arrange the prescribed displacement after solving the equations.
ASSEMB	To assemble the equations in matrix form.
CELLDOM	To specify the cell number in each domain (used for multidomain problems).
CONTROL	To input the analysis parameters.
CPDAMAGE	To analysis creep damage.
CPDATA	To read creep parameters.
CPDATA	To input creep parameters and convergence criterion.
CPOUT	To output creep strains and stresses.
CPRHS	To calculate the right hand side matrix of equation (3.88).
CREEP	To analyse creep.
DBLTIME	To check current time step if it needs to increase for next calculation.
DMDATA	To input damage parameters.
EFFBOTH	To check convergence of both stresses and creep strains using criterion 2.
EFSTRAIN	To check convergence of creep strains using criterion 2.
EFSTRESS	To check convergence of stresses using criterion 2.
INPUT	To read the data modules.
L2EFBOTH	To check convergence of both stresses and creep strains using criterion 4.

Subroutine Name	Purpose
L2EFSTRN	To check convergence of creep strains using criterion 4.
L2EFSTRS	To check convergence of stresses using criterion 4.
L2MXBOTH	To check convergence of both stresses and creep strains using criterion 3.
L2MXSTRN	To check convergence of creep strains using criterion 3.
L2MXSTRS	To check convergence of stresses using criterion 3.
MAXBOTH	To check convergence of both stresses and creep strains using criterion 1.
MXSTRAIN	To check convergence of creep strains using criterion 1.
MXSTRESS	To check convergence of stresses using criterion 1.
NODEDOM	To specify the internal node number in each domain (used for multidomain problems).
OUT2D	To output the elastic variables.
PLASTIC	To analyse combined plasticity and creep (full load approach).
PLCREEP	To analyse combined plasticity and creep (part-load approach).
PLDIFF	To calculate the internal creep variables using differentiation of displacements via the shape functions.
PLINT	To calculate the internal displacement.
STRAIN	To calculate the strains from stresses at the boundary.
STRES2D	To calculate the stresses at the boundary.
UPDATE	To update the variables using Euler method.
ZEROINC	To initialise all incremental variables.

Subroutine Name

Purpose

ZEROTOT

To initialise all total variables.

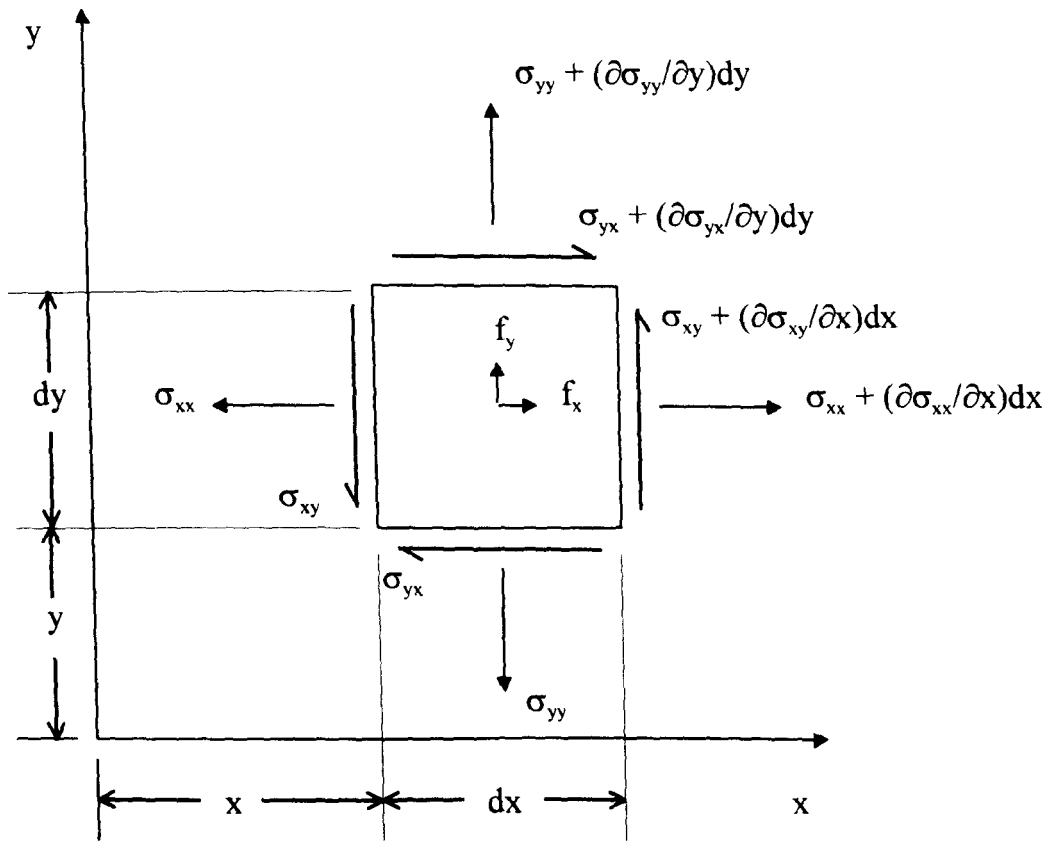


Figure 3.1 A small differential element.

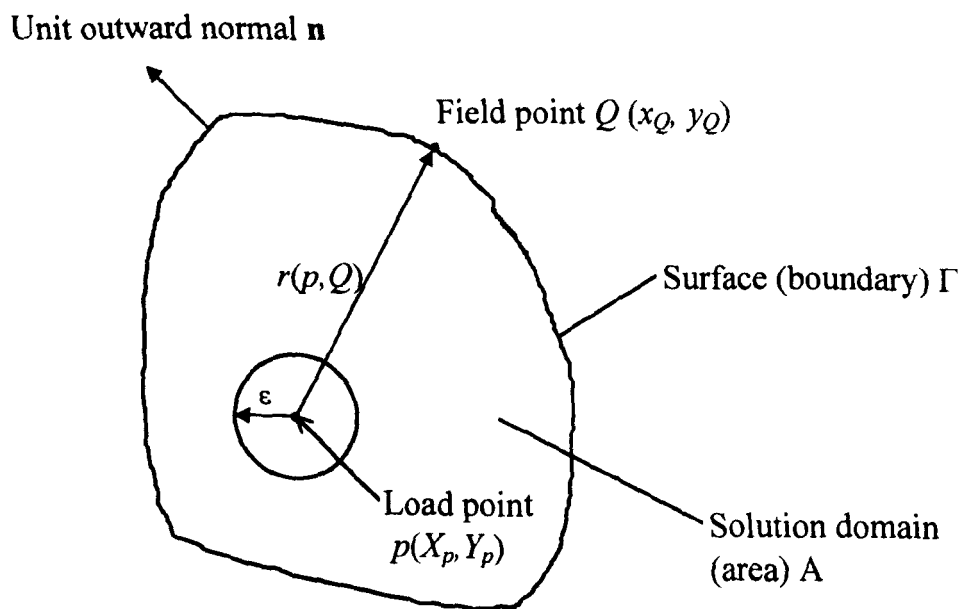


Figure 3.2 A two-dimensional physical domain.

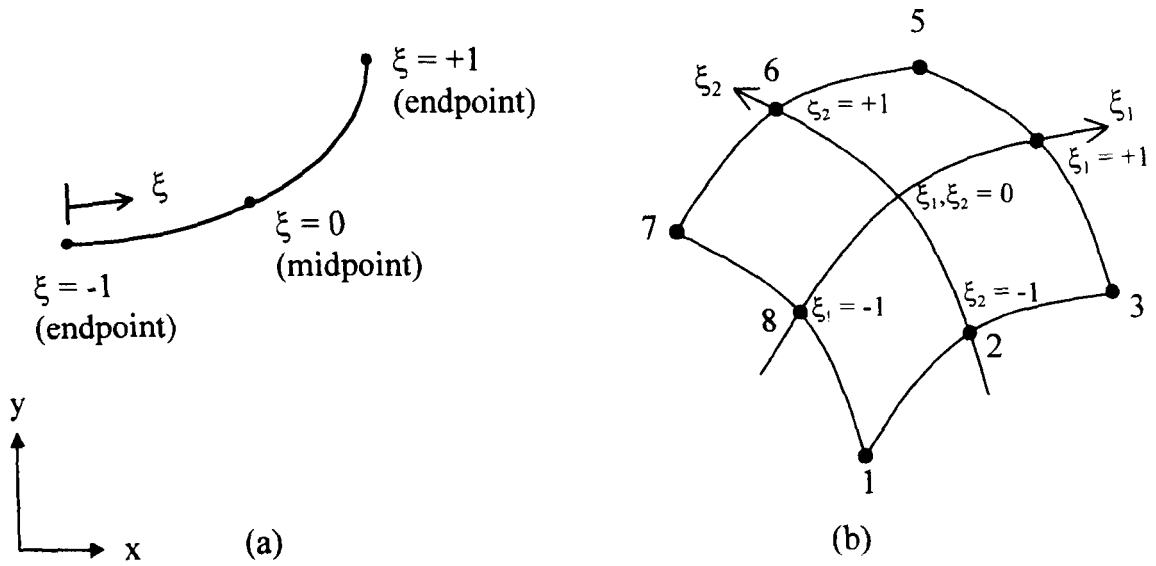


Figure 3.3 (a) An isoparametric quadratic element, (b) Eight-noded quadrilateral element.

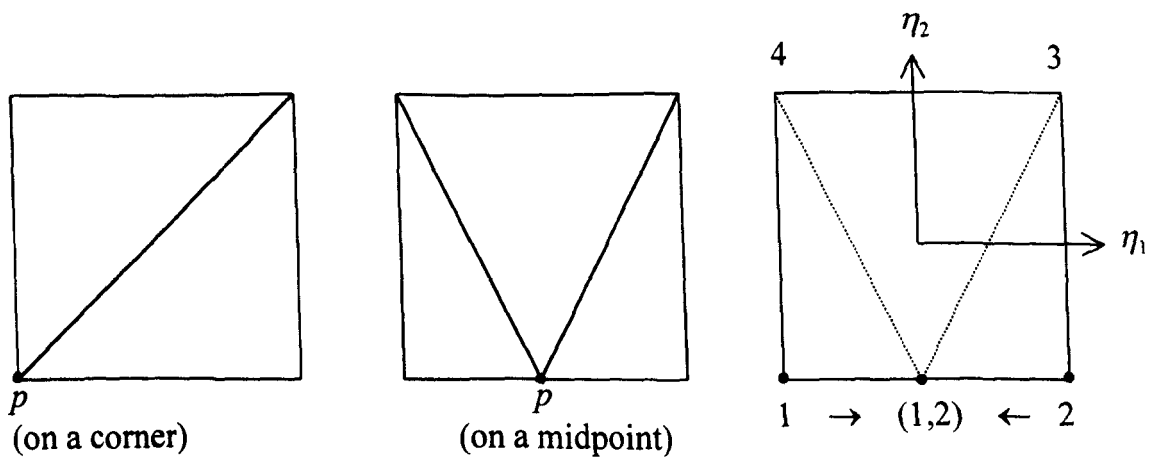


Figure 3.4 Subdivision of the quadrilateral element into triangular sub-elements.

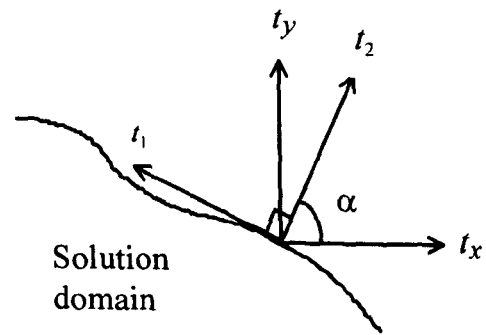


Figure 3.5 Local and Cartesian components of the traction vector.

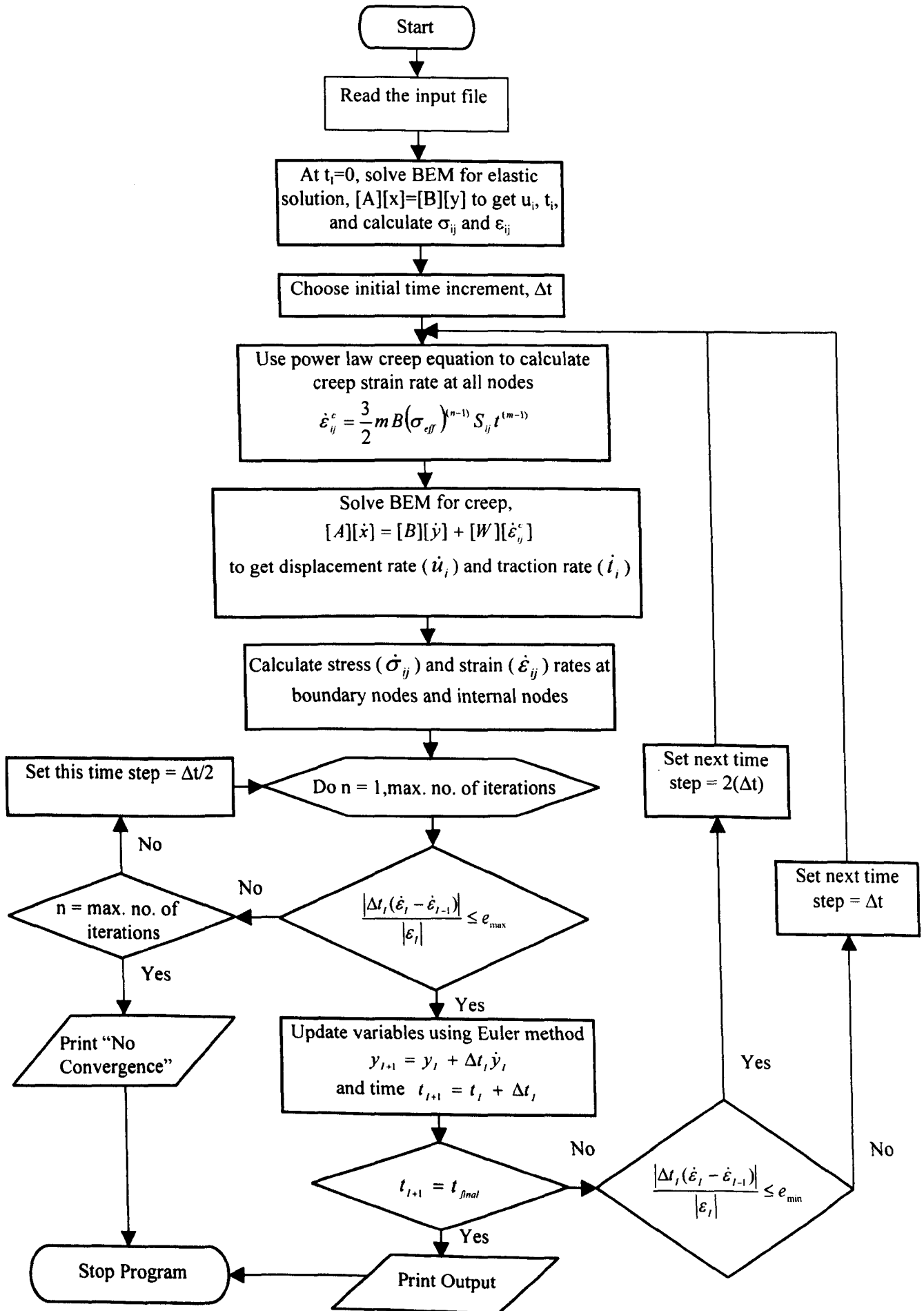


Figure 3.6 Flow chart of BEM for creep

Chapter 4

Creep Examples Using the Boundary Element Method

The boundary element formulation for creep problems is implemented in a computer program and is used to analyse the creep problems of a square plate subjected to biaxial constant stress and constant displacement loads, a plate with a circular hole and a plate with a semicircular notch subjected to a constant tensile stress load. The results are compared with the analytical solutions (Becker and Hyde [1993]) and the finite element solutions using ABAQUS [1997].

4.1 Square Plate Tests

Four cases of square plates subjected to constant stress loads, constant displacement loads and variable stress loads are tested. These tests include both primary creep and secondary creep. The dimensions of the square plate are 100 mm x 100 mm. The boundary and domain are divided into 4 boundary elements and 1 cells, respectively. The BE mesh is shown in Figure 4.1. The creep parameters and mechanical material properties are as follows:

Creep Parameters:

$$B = 3.125 \times 10^{-14} \quad (\text{stress in MPa, time in hour})$$

$$m = 1.0 \quad \text{for secondary creep}$$

$$m = 0.5 \quad \text{for primary creep}$$

$$n = 5$$

Material Properties:

$$\text{Young's Modulus (E)} = 200 \times 10^3 \text{ N/mm}^2$$

$$\text{Poisson's Ratio (v)} = 0.3$$

The boundary conditions are as follows:

$$u_y = 0 \text{ along line ab}$$

$$u_x = 0 \text{ along line ad}$$

The details of the 4 tests are listed below:

1. TEST 1. The square plate is subjected to biaxial constant tensile stresses of 200 N/mm². This test is the plane stress and secondary creep problem. The test is performed for 100 hours using the automatic time step control (criterion 4) with the maximum and minimum stress tolerances of 10⁻³ and 10⁻⁴, respectively. The initial time step of 10⁻³ hour and 6 integration points are used. The time hardening law is applied. The creep strains at BE node 1 with coordinates (0,0) are plotted against time and shown in Figure 4.2. The results are compared with analytical solutions and shows very good agreement with the error being less than 0.005%.
2. TEST 2. The square plate is subjected to biaxial constant tensile stresses of 200 N/mm². This test is the plane stress and primary creep problem. The test is performed for 100 hours using the automatic time step control (criterion 4) with the maximum and minimum creep strain tolerances of 10⁻³ and 10⁻⁴, respectively. The initial time step of 10⁻³ hour and 6 integration points are used. The time hardening law is implemented. The creep strains at BE node 1 are plotted against time and shown in Figure 4.3. It can be seen that the results are in good agreement with analytical solutions with the error being less than 0.4%.

3. TEST 3. The square plate is subjected to biaxial constant tensile displacements of 0.1 mm. This test is the plane stress and primary creep problem. The test is performed for 100 hours using the automatic time step control (criterion 2) with the maximum and minimum stress tolerances of 10^{-3} and 10^{-4} , respectively. The initial time step of 10^{-4} hour and 6 integration points are used. Both time hardening and strain hardening law are employed. The stresses at BE node 1 in the x-direction are plotted against time and shown in Figure 4.4. It can be seen that the stresses drop sharply in a short time period at the beginning. This period requires very small time steps. The results for both creep laws agree very well with analytical solutions with the error being less than 1%.
4. TEST 4. The square plate is subjected to biaxial variable constant tensile stresses of 200 N/mm^2 and 250 N/mm^2 . This test is the plane stress and primary creep problem. The test is performed for 100 hours for the first applied stresses of 200 N/mm^2 and for another 100 hours for the second applied stresses of 250 N/mm^2 . The automatic time step control (criterion 4) with the maximum and minimum creep strain tolerances of 10^{-4} and 10^{-5} , respectively, is used. The initial time step of 10^{-3} hour and 6 integration points are employed. Both time hardening and strain hardening laws are applied. The creep strains at BE node 1 in the x-direction are plotted against time and shown in Figure 4.5. The results are in good agreement with analytical solutions for both creep laws with the error being less than 0.1%. It can be seen that the strain hardening assumption predicts higher creep strain.

4.2 Plate with a Circular Hole Test

A plate with a circular hole at the centre is tested. Because of symmetry, only a quarter of the plate is used. The quarter of the plate with a circular hole has the dimensions of 10 mm x 18 mm with a hole of a radius of 5 mm. The boundary and domain are discretised into 24 boundary elements and 32 cells, respectively. The BE mesh is shown in Figure 4.6. The boundary conditions are as follows:

$$u_y = 0 \quad \text{along line ab.}$$

$$u_x = 0 \quad \text{along line de.}$$

The creep parameters and mechanical material properties are the same as those used in the square plate test. The plate with a circular hole is subjected to a constant tensile stress of 50 N/mm² in the x-direction. This test is the plane stress and secondary creep problem. The test is conducted for 10 hours. The initial time step of 10⁻³ hour and 4 integration points are used. The automatic time step control (criterion 4) with the maximum and minimum stress tolerances of 0.1 and 0.01 is employed. The time hardening law is used.

The results are compared with finite element solutions, with the same mesh, using ABAQUS [1997]. The stresses in the x-direction is plotted along the root of the plate and shown in Figure 4.7 where y/r is the ratio of the distance along the y-axis to the hole radius. The results agree well with the finite element solutions with the error being less than 1% except for the nodes at $y/r = 1.25$, 1.75 and 2.0 which have percentages of error of 3.32%, 10.11% and 6.74%, respectively.

4.3 Plate with a Semicircular Notch Test

A plate with a semicircular notch is tested. Similar to the plate with a circular hole, only a quarter of the plate is used. The dimensions of the plate are 10 mm x 18 mm with a semicircle of the radius of 5 mm. The boundary and domain are divided into 24 boundary elements and 32 cells, respectively. The BE mesh is shown in Figure 4.8. The boundary conditions are as follows:

$$u_y = 0 \quad \text{along line cd.}$$

$$u_x = 0 \quad \text{along line de.}$$

The creep parameters and mechanical material properties are the same as those of the square plate test. The plate with a semicircular notch is subjected to a constant tensile stress of 50 N/mm² in the x-direction. This test is the plane stress and secondary creep problem. The test is conducted for 10 hours. The initial time step of 10⁻³ hour and 4 integration points are used. The automatic time step control (criterion 4) with the maximum and minimum stress tolerances of 0.1 and 0.01 is employed. The time hardening law is used.

The results are compared with the finite element solutions, with the same mesh, using ABAQUS [1997]. The stresses in the x-direction is plotted along the root of the plate and shown in Figure 4.9 where y/r is the ratio of the distance along the y-axis to the notch radius. The results agree well with the finite element solutions with the error being less than 4%. It can be seen that the common nodes have higher difference. This might be because the average value is used at the common nodes.

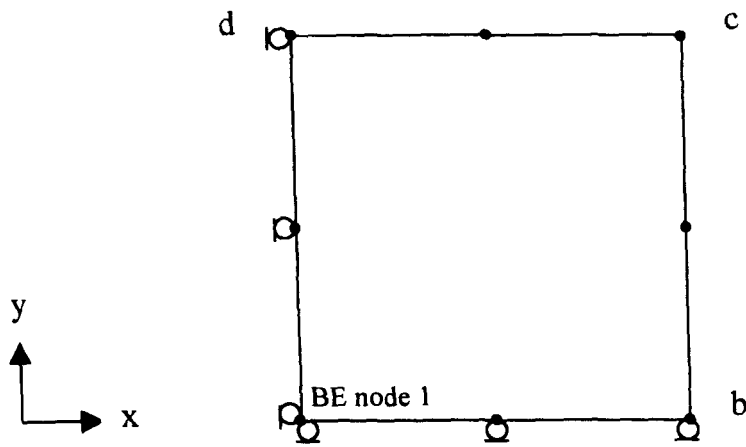


Figure 4.1 BE mesh of the square plate, 4 boundary elements and 1 cell.

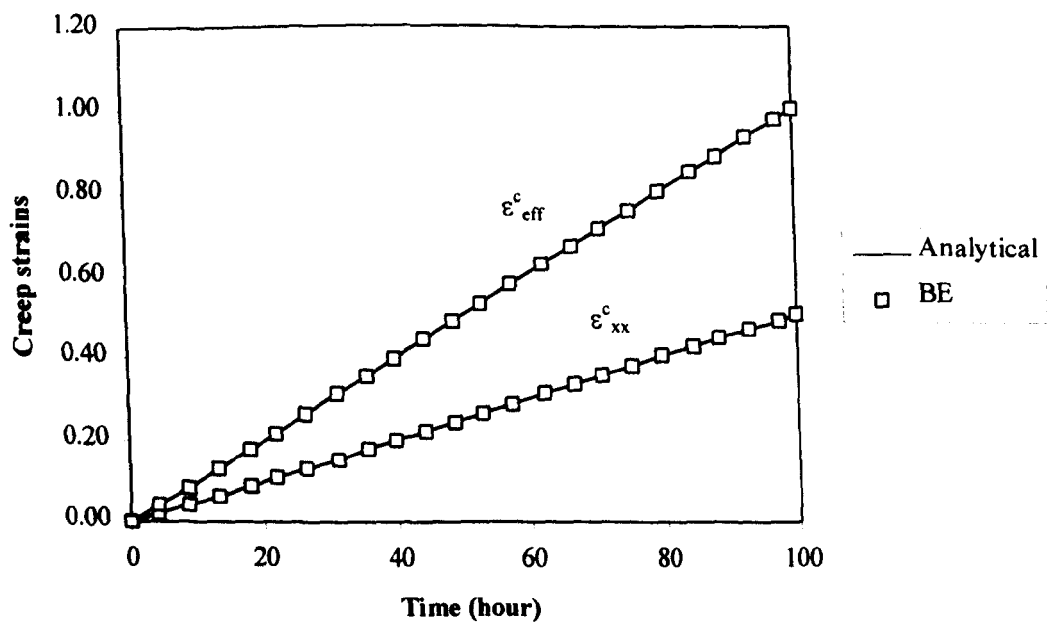


Figure 4.2 The solutions of the square plate, TEST 1, plane stress, secondary creep.

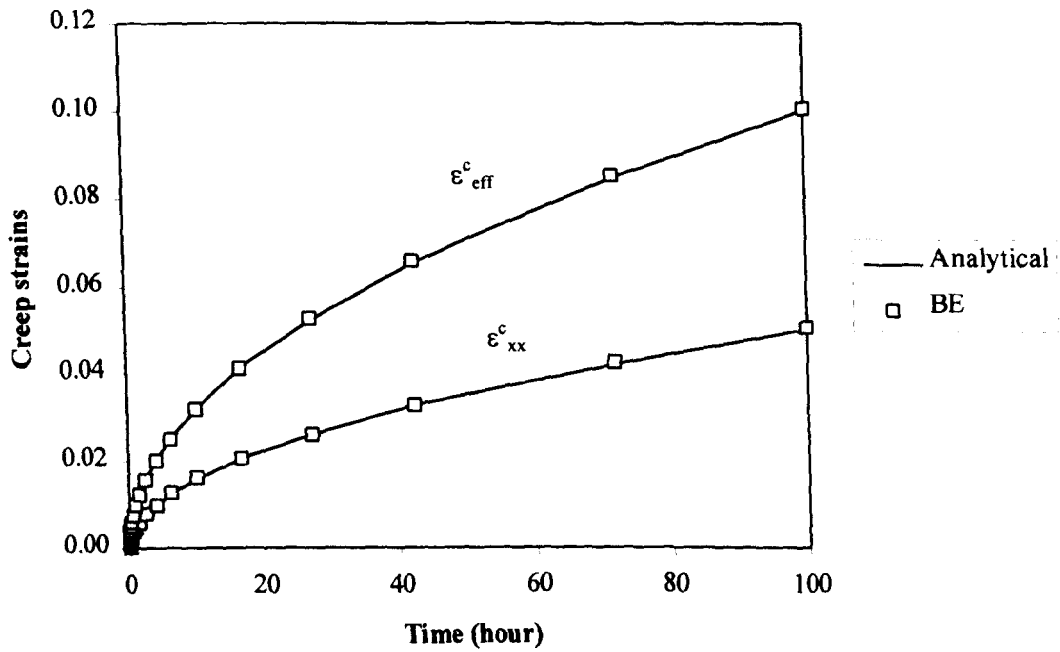


Figure 4.3 The solutions of the square plate, TEST 2, plane stress, primary creep.

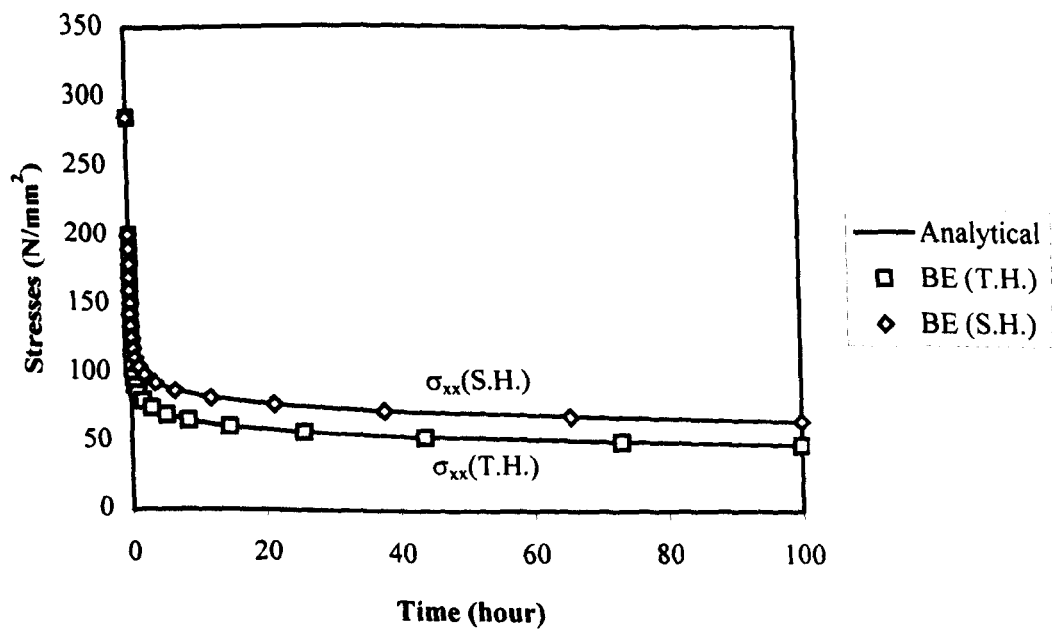


Figure 4.4 The solutions of the square plate, TEST 3, plane stress, primary creep.

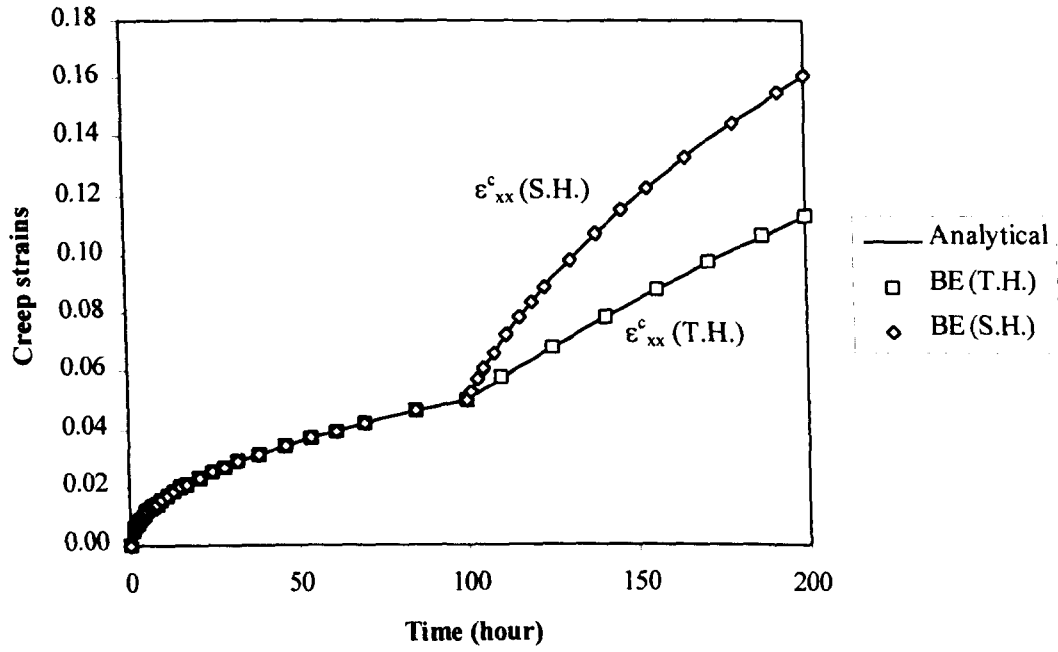


Figure 4.5 The solutions of the square plate, TEST 4, plane stress, primary creep.

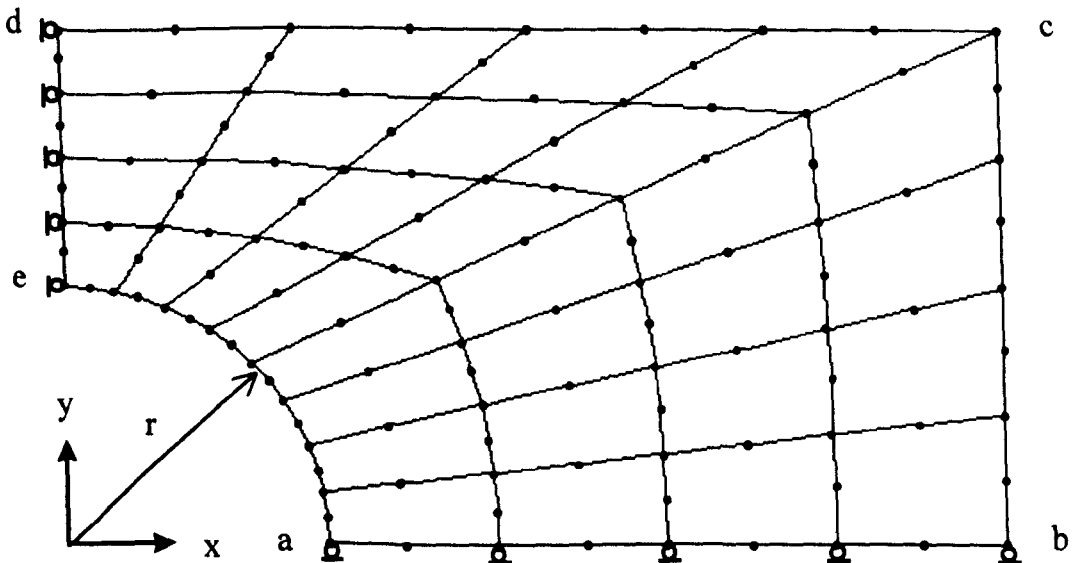


Figure 4.6 BE and FE meshes of the plate with a circular hole,
24 boundary elements and 32 cells.

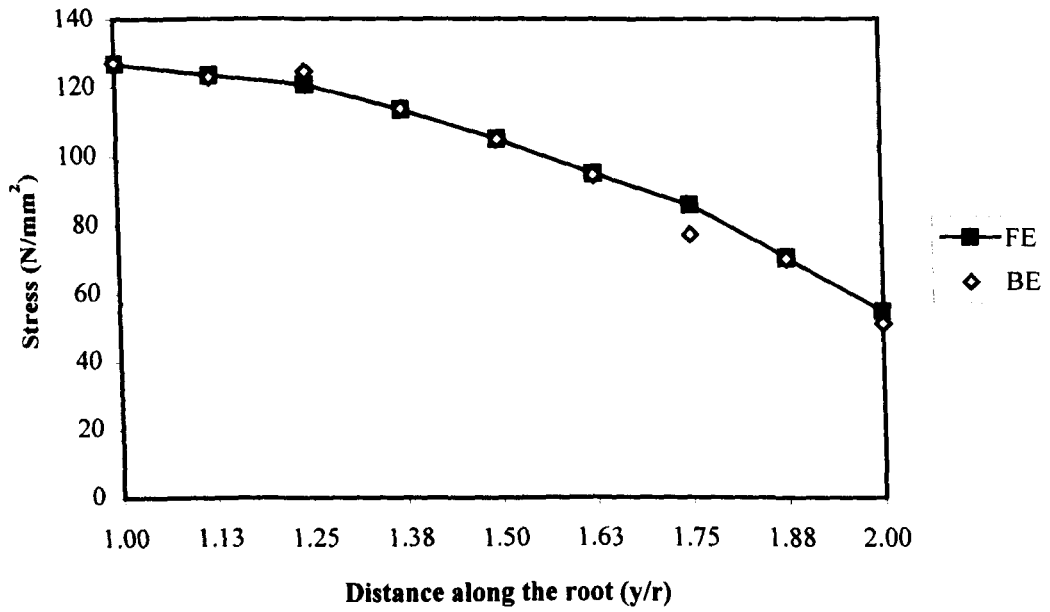


Figure 4.7 The solutions along the root of the plate with a circular hole.

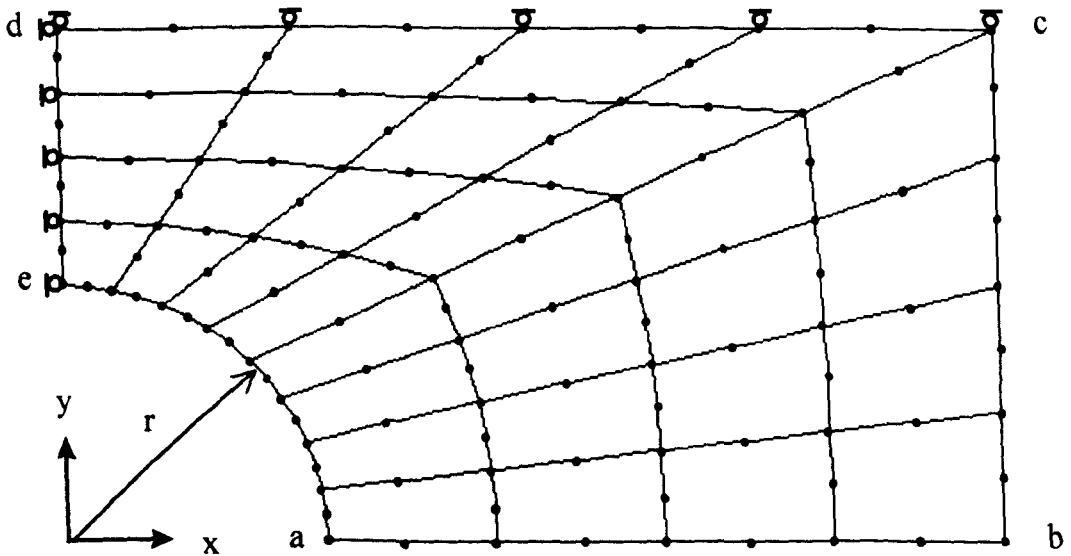


Figure 4.8 BE and FE meshes of the plate with a semicircular notch,
24 boundary elements and 32 cells.

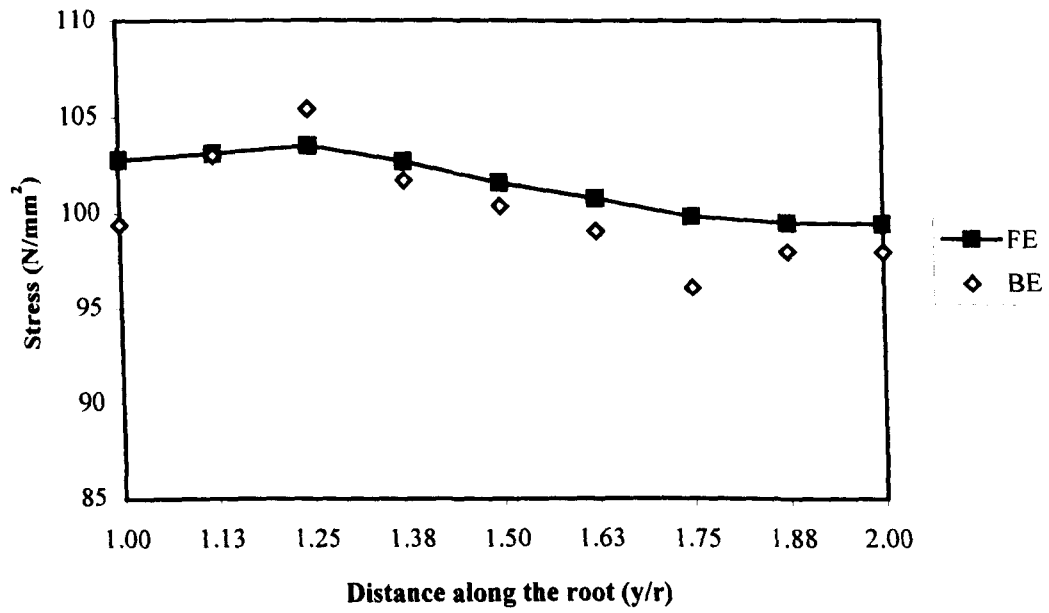


Figure 4.9 The solutions along the root of the plate with a semicircular notch.

Chapter 5

The Effects of Gaussian Integration Points, Initial Time Steps and Tolerances

Since the accuracy of the results of running the BE creep program is dependent on the number of Gaussian integration points, initial time steps and tolerances used, the following work is to investigate the effects of these factors. Before investigating the effects of these factors, the four convergence criteria must be compared in order to choose the best criterion to investigate these effects. Single precision is used for all tests.

5.1 Comparison of Convergence Criteria

In order to compare the four convergence criteria, a number of test cases are analysed as follows: (a) a square plate subjected to biaxial tensile stresses of 200 N/mm^2 , (b) square plate subjected to biaxial tensile displacements of 0.1 mm . All tests are plane stress and include primary and secondary creep for 10 hours. The square plate is divided into 8 boundary elements and 4 cells. The BE meshes are shown in Figure 5.1. The automatic time step control is used with the maximum and minimum prescribed tolerances of 10^{-3} and 10^{-4} , respectively. The initial time step of 10^{-3} hour and 6 Gaussian integration points are employed. The convergence criteria are based on creep strains. The creep parameters and material properties are as follows: $B = 3.125 \times 10^{-14}$ (stress in MPa, time in hour), $m = 1$ for secondary creep and $m = 0.5$ for primary creep, $n = 5$, $E = 200 \times 10^3 \text{ N/mm}^2$, and $\nu = 0.3$. The results of the square plate are compared

with the analytical benchmark of Becker and Hyde [1993] with the tolerance of 10^{-3} for the constant displacement load cases. The BE solutions of the square plate cases are shown in Table 5.1. The results show that criterion 4 is more effective than the others by comparing the accuracy.

5.2 The Effect of the Integration Points

The number of Gaussian integration points which can be used in this program are 4, 6, 8 and 10 points. The same problems as above are tested with varying the Gaussian integration points. The initial time step is 10^{-3} hour. The automatic time step control with the maximum and minimum tolerances of 10^{-3} and 10^{-4} , respectively, is used. The convergence criterion 4 based on creep strain is implemented. The tests are performed for 10 hours. The results are compared with the analytical benchmark of Becker and Hyde [1993] and shown in Table 5.2. It can be seen that the solutions are not stable for 4 Gaussian integration points. It seems that, for the straight side, 6 Gaussian integration points is suitable to use in the program because it gives the same level of accuracy compared to 8 and 10 Gaussian integration points but uses less computational time. Note that in some problems the number of time steps is the same for all Gaussian integration points.

5.3 The Effect of the Initial Time Steps

The size of the initial time step is very crucial for the case of primary creep problem, in which the creep strain rates decrease with time, and the case of constant displacement

load problem, in which stress relaxation occurs. The Euler method used to update the variables assumes that the rates of variables are constant over the time step. Figure 5.2 shows the stress relaxation with time in which two initial time steps Δt_1 and Δt_2 may be used. It can be seen that the larger initial time step (Δt_2) gives the greater error of stress ($\Delta\sigma_2$). This initial error will spread to the next time step. Consequently, the accumulated error at the final time will be very large. The same problems as those in section 5.1 are tested for 10 hours. The automatic time step control with the maximum and minimum tolerances of 10^{-3} and 10^{-4} , respectively, is used. Six Gaussian integration points are used. The convergence criterion 4 based on creep strain is employed. The initial time steps are varied from 10^{-1} hour through 10^{-6} hour. The results are compared with the analytical benchmark of Becker and Hyde [1993] and shown in Table 5.3. It can be seen that the initial time step of 10^{-2} hour is acceptable for use in the program except the problem of primary creep and constant displacement load which needs the initial time step of 10^{-4} . In this case considerable error occurs if the initial time step is larger than 10^{-4} . Therefore, the results may be incorrect if the initial time step is not small enough. From the results, after the solutions converge at a certain initial time step, the solutions are almost not changed and the number of time steps increase as the initial time step gets smaller.

5.4 The Effect of the Tolerances

Tolerances are used in convergence criteria to determine the next time step for the next calculation. If automatic time step control is used, the maximum and minimum tolerances must be prescribed. In this program, the minimum tolerance is determined

by dividing the maximum tolerance by 10. Therefore, the minimum tolerance is one order less than the maximum tolerance. To investigate the effect of the tolerances, the same problems as those in section 5.1 are tested for 10 hours with varying the maximum tolerances from 10^{-1} to 10^{-6} . The convergence criterion 4 based on creep strain is employed. The initial time step is 10^{-3} hour. Six Gaussian integration points are used. The results are compared with the analytical benchmark of Becker and Hyde [1993] and shown in Table 5.4. It can be seen that the maximum tolerance of 10^{-3} is acceptable for use by comparing the accuracy. Note that, in most cases, the number of time steps increases by about three times while the maximum tolerance decreases by one order. Unlike the initial time steps, the solutions improve as the maximum tolerance gets smaller.

Constant stress load	Benchmark solution	Constant time step	Criterion 1	Criterion 2	Criterion 3	Criterion 4
Stress xx (N/mm ²)	200	200	200 - 200.2	197.1 – 203.2	200 – 200.2	199.9 – 200.2
Strain xx (x10 ⁻²)	5	4.999	4.999 – 5.009	4.999 – 5.01	4.999 – 5.009	4.999 – 5.01
No. of time steps	-	10,000	1,458	75	1,600	88

Constant displacement load	Benchmark solution	Constant time step	Criterion 1	Criterion 2	Criterion 3	Criterion 4
Stress xx (N/mm ²)	48.62	48.63	48.38	48.28	48.46	48.46
Strain xx (x10 ⁻⁴)	8.298	8.298	8.307	8.310	8.304	8.304
No. of time steps	-	10,000	392	329	690	682

(a)

Constant stress load	Benchmark solution	Constant time step	Criterion 1	Criterion 2	Criterion 3	Criterion 4
Stress xx (N/mm ²)	200	200	200	200	200	200
Strain xx (x10 ⁻²)	1.581	1.585	1.585	1.592	1.584	1.587
No. of time steps	-	10,000	948	351	1,091	728

Constant displacement load*	Benchmark solution	Constant time step	Criterion 1	Criterion 2	Criterion 3	Criterion 4
Stress xx (N/mm ²)	64.80	64.72	64.32	64.23	64.50	64.50
Strain xx (x10 ⁻⁴)	7.732	7.734	7.749	7.752	7.743	7.743
No. of time steps	-	99,937	316	251	524	517

* Use initial time step of 10⁻⁴ hour.

(b)

Table 5.1 Square plate tests with varying convergence criteria,

(a) secondary creep, (b) primary creep.

Constant stress load	Benchmark solution	Integration points = 4	Integration points = 6	Integration points = 8	Integration points = 10
Stress xx (N/mm ²)	200	181.8 – 201.8	199.9 – 200.2	199.9 – 200.2	199.9 – 200.2
Strain xx (x10 ⁻²)	5	4.343 – 5.083	4.999 – 5.01	5.0 – 5.001	4.999 – 5.001
No. of time steps	-	145	88	96	86

Constant displacement load	Benchmark solution	Integration points = 4	Integration points = 6	Integration points = 8	Integration points = 10
Stress xx (N/mm ²)	48.62	48.46 – 48.47	48.46	48.46	48.46
Strain xx (x10 ⁻⁴)	8.298	8.297 – 8.307	8.304	8.304	8.304
No. of time steps	-	682	682	682	682

(a)

Constant stress load	Benchmark solution	Integration points = 4	Integration points = 6	Integration points = 8	Integration points = 10
Stress xx (N/mm ²)	200	196.4 – 200.6	200	200	200
Strain xx (x10 ⁻²)	1.581	1.535 – 1.597	1.587	1.586	1.586
No. of time steps	-	730	728	728	728

Constant displacement load*	Benchmark solution	Integration points = 4	Integration points = 6	Integration points = 8	Integration points = 10
Stress xx (N/mm ²)	64.80	64.49 – 64.52	64.50	64.50	64.50
Strain xx (x10 ⁻⁴)	7.732	7.742 – 7.746	7.743	7.743	7.743
No. of time steps	-	517	517	517	517

* Use initial time step of 10⁻⁴ hour.

(b)

Table 5.2 Square plate tests with varying Gaussian integration points,

(a) secondary creep, (b) primary creep.

Constant Stress load	Benchmark solution	Initial time steps (hour)					
		10^{-1}	10^{-2}	10^{-3}	10^{-4}	10^{-5}	10^{-6}
Stress xx (N/mm ²)	200	199.1 – 202.8	199.9 – 200.3	199.9 – 200.2	199.9 – 202.4	200.0 – 200.2	199.5 – 201.0
Strain xx ($\times 10^{-2}$)	5	4.999 – 5.009	4.999 – 5.009	4.999 – 5.010	4.999 – 5.009	4.999 – 5.009	4.999 – 5.009
No. of time steps	-	94	79	88	107	96	92

Constant displacement load	Benchmark solution	Initial time steps (hour)					
		10^{-1}	10^{-2}	10^{-3}	10^{-4}	10^{-5}	10^{-6}
Stress xx (N/mm ²)	48.62	-48.56	48.45	48.46	48.47	48.47	48.46
Strain xx ($\times 10^{-4}$)	8.298	11.70	8.304	8.304	8.304	8.304	8.304
No. of time steps	-	525	407	682	776	805	815

(a)

Constant Stress load	Benchmark solution	Initial time steps (hour)					
		10^{-1}	10^{-2}	10^{-3}	10^{-4}	10^{-5}	10^{-6}
Stress xx (N/mm ²)	200	200	200	200	200	200	200
Strain xx ($\times 10^{-2}$)	1.581	1.586	1.586	1.587	1.586	1.587	1.587
No. of time steps	-	370	550	728	911	1,091	1,270

Constant displacement load	Benchmark solution	Initial time steps (hour)					
		10^{-1}	10^{-2}	10^{-3}	10^{-4}	10^{-5}	10^{-6}
Stress xx (N/mm ²)	64.80	-66.28	-65.06	16.90	64.50	64.57	64.58
Strain xx ($\times 10^{-4}$)	7.732	12.32	12.28	9.408	7.743	7.740	7.740
No. of time steps	-	964	542	15	517	796	1,004

(b)

Table 5.3 Square plate tests with varying initial time steps,

(a) secondary creep, (b) primary creep.

Constant Stress load	Benchmark solution	Maximum tolerances (e_{max})					
		10^{-1}	10^{-2}	10^{-3}	10^{-4}	10^{-5}	10^{-6}
Stress xx (N/mm ²)	200	180.7 - 225.7	198.7 - 201.3	199.9 - 200.2	200.0 - 200.3	200.0 - 200.2	200.0 - 200.2
Strain xx ($\times 10^{-2}$)	5	5.065 - 6.442	4.998 - 5.025	4.999 - 5.01	4.999 - 5.01	4.999 - 5.009	4.999 - 5.01
No. of time steps	-	107	78	88	127	168	407

Constant displacement load	Benchmark solution	Maximum tolerances (e_{max})					
		10^{-1}	10^{-2}	10^{-3}	10^{-4}	10^{-5}	10^{-6}
Stress xx (N/mm ²)	48.62	47.28	48.15	48.46	48.58	48.62	48.63
Strain xx ($\times 10^{-4}$)	8.298	8.345	8.315	8.304	8.300	8.298	8.298
No. of time steps	-	84	223	682	2,143	6,552	20,992

(a)

Constant Stress load	Benchmark solution	Maximum tolerances (e_{max})					
		10^{-1}	10^{-2}	10^{-3}	10^{-4}	10^{-5}	10^{-6}
Stress xx (N/mm ²)	200	187.0 - 213.8	200	200	200	200	200
Strain xx ($\times 10^{-2}$)	1.581	1.623 - 1.643	1.597	1.587	1.583	1.582	1.581
No. of time steps	-	85	243	728	2,234	7,092	22,475

Constant displacement load*	Benchmark solution	Maximum tolerances (e_{max})					
		10^{-1}	10^{-2}	10^{-3}	10^{-4}	10^{-5}	10^{-6}
Stress xx (N/mm ²)	64.80	62.75	64.01	64.50	64.66	64.72	64.74
Strain xx ($\times 10^{-4}$)	7.732	7.804	7.760	7.743	7.737	7.735	7.734
No. of time steps	-	65	175	517	1,571	4,977	15,765

* Use initial time step of 10^{-4} hour.

(b)

Table 5.4 Square plate tests with varying tolerances,

(a) secondary creep, (b) primary creep.

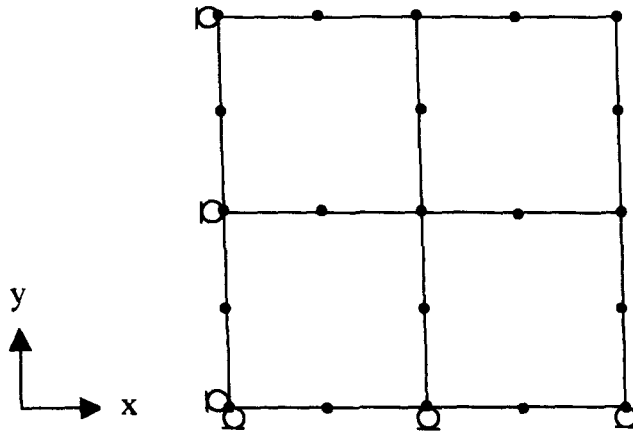


Figure 5.1 BE mesh of the square plate, 8 boundary elements and 4 cells.

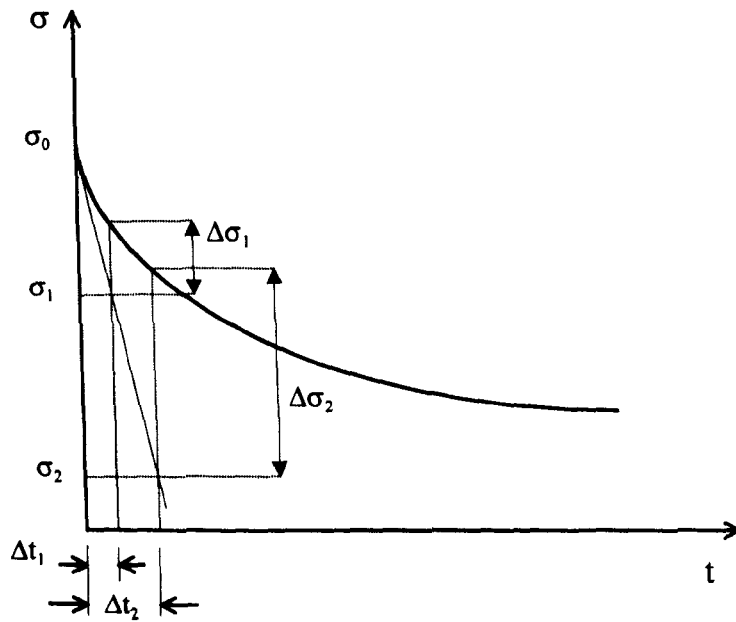


Figure 5.2 The stress relaxation with time.

Chapter 6

Boundary Element Method for Creep Damage Problems

The only numerical method that has been used so far to solve the creep continuum damage problems is the finite element method. Most of the FE work (see, for example, Hyde et al. [1990] and Dyson and Hayhurst [1993]) has been done using constitutive equations based on a phenomenological approach which uses one or many internal variables called damage parameters, ω , to characterise the deterioration of material. This approach is considered as macroscale. Another approach called a physical approach, which uses microscopic mechanisms such as the rate of formation of voids and the rate of growth of void size, can be used. This approach is considered as microscale.

For the boundary element method, the constitutive damage equations used in the finite element method can be adopted. In this work a single damage parameter is used.

6.1 Creep Damage Constitutive Equations

There are two types of creep rupture; *ductile and brittle* ruptures. In ductile rupture, as the tensile specimen elongates due to creep, the cross-sectional area decreases. Since the creep deformation is a constant volume process and the load is held constant, the stress increases during decreasing of the cross-sectional area. Finally, it causes the specimen to neck and fail. At rupture, the cross-sectional area of the specimen reduces to zero. The ductile failure time, t_f^D , can be determined (see, for example, Boyle and Spence [1983]).

In brittle rupture, as the tensile specimen elongates due to creep, voids appear and grow and grain boundaries begin to crack due to the increase in stress in these regions. This reduces the effective load-bearing area of the specimen. A damage parameter, ω , is introduced to describe this phenomenon and defined as the ratio of the area of voids at any cross-section to the overall cross-sectional area (A_0). The effective area is given by $(1 - \omega) A_0$ and the actual stress is

$$\sigma = \frac{P}{A} = \frac{P}{(1 - \omega) A_0} = \frac{\sigma_0}{1 - \omega} \quad (6.1)$$

where ω ranges from zero at the initial state to unity at rupture. In practice, ω never reaches unity. Therefore, the creep rate of equation (2.30) based on time hardening can include the damage parameter as follows (see, for example, Chen and Hsu [1987]):

$$\dot{\epsilon}_{ij}^c = \frac{3}{2} m B \left(\frac{\sigma_{eff}^{(n-1)}}{(1 - \omega)^n} \right) S_{ij} t^{(m-1)} \quad (6.2)$$

It is assumed that the damage evolution depends on the current stress and damage parameter and can be defined as follows (see, for example, Smith et al. [1989] and Duan et al. [1991]):

$$\dot{\omega} = \frac{M[\alpha \hat{\sigma} + (1 - \alpha) \sigma_{eff}]^\chi t^{(m-1)}}{(1 + \phi)(1 - \omega)^\phi} \quad (6.3)$$

where m , M , α , χ , and ϕ are material constants and $\hat{\sigma}$ is the maximum tensile principal stress.

6.2 BE Creep Damage Algorithm

The BE algorithm of creep damage problems is similar to that of creep problems by replacing the creep strain rate of equation (2.30) with equation (6.2) and adding equation (6.3) in the program. The BE algorithm for creep damage problems can be summarised as follows:

1. At $t = 0$, $\varepsilon_{ij}^c = 0$ and $\omega = 0$. Solve the elastic solution and calculate stresses and strains at boundary and internal nodes as before.
2. Calculate the strain rates from equation (6.2) and substitute the strain rates into RHS of equation (3.87) and then solve for the creep damage. Note that, for the first calculation, time t and damage parameter ω are zero.
3. Calculate the maximum tensile principal stress and effective stress at each node and then substitute in equation (6.3) to obtain the damage parameter rate at each node.
4. Calculate the stresses and strains at boundary and internal nodes as before.
5. Check the convergence as before. After converging, update the variables, time and damage parameter using Euler method as follows:

$$\omega_{i+1} = \omega_i + \Delta t \dot{\omega}_i \quad (6.4)$$

6. Select the next time step for next calculation as before.
7. Repeat 2 – 6, until the final time is reached or the rupture occurs.

In this BE program, the value of damage parameter at rupture can be specified at the beginning and the program will stop when this value at one node is reached. Usually, the value of damage parameter is equal to one at the rupture. It is impractical at $\omega = 1$

since the creep strain rates approach infinity. Therefore, ω at rupture is set at 0.9. It should be noted that while ω approach one, the time steps needed will be very small.

6.3 BE Creep Damage Examples

The boundary element formulation for creep damage problems is implemented in a computer program and is used to analyse the creep damage problems of a rectangular plate and a square plate with a circular hole subjected to a uniaxial constant tensile stress load. The results are compared with the finite element solutions using ABAQUS UMAT.

Since the creep strain rate equation has been changed to incorporate damage evolution, ABAQUS allows users to put their own creep law by using ABAQUS UMAT Code. In this work, the ABAQUS UMAT Damage Code of SAQ KONTROLL AB, Sweden, modified for 2-D problems by Sun et al. [1999] is used. The constitutive equations used in ABAQUS UMAT Damage Code are as follows:

$$\dot{\epsilon}_{ij}^c = \frac{3}{2} B \sigma_{eff}^{(n-1)} S_{ij} \left[(1-\rho) + \frac{1}{(1-\omega)^n} \right] \quad (6.4)$$

$$\dot{\omega} = gA \frac{[\alpha \hat{\sigma} + (1-\alpha) \sigma_{eff}]^\nu}{(1+\phi)(1-\omega)^\phi} \quad (6.5)$$

where B , n , ρ , g , A , α , ν and ϕ are material constants. When $m = 1$ (secondary creep) in equation (6.2) and (6.3) and $\rho = g = 1$ in equation (6.4) and (6.5), equation (6.2) and (6.3) are identical to equation (6.4) and (6.5), respectively, by using equivalent material constants as shown in the table below:

Equation (6.2) and (6.3)	B	n	$m (=1)$	M	χ	---	ϕ	---	α
Equation (6.4) and (6.5)	B	n	---	A	ν	$g (=1)$	ϕ	$\rho (=1)$	α

6.3.1 A Rectangular Plate

A rectangular plate of CrMoV steel subjected to a uniaxial constant stress load of 54 MPa in the y-direction is tested. This test is plane stress and secondary creep problem with damage. The dimensions of the rectangular plate are 25 mm x 100 mm. The boundary and domain are divided into 10 boundary elements and 4 cells, respectively. The meshes of BE and FE are the same and shown in Figure 6.1. The creep damage parameters and mechanical material properties of CrMoV Steel at 640° C (see Sun et al. [1999]) based on BE creep damage constitutive equations are as follows:

Creep Damage Parameters (based on stress in MPa and time in hour):

$$B = 6.599 \times 10^{-16}$$

$$m = 1.0$$

$$n = 6.108$$

$$M = 5.998 \times 10^{-14}$$

$$\phi = 4.5$$

$$\chi = 5.767$$

$$\alpha = 0.3$$

Material Properties:

$$\text{Young's Modulus (E)} = 200 \times 10^3 \text{ N/mm}^2$$

$$\text{Poisson's Ratio (}\nu\text{)} = 0.3$$

The boundary conditions are as follows:

$$u_y = 0 \text{ along line ab}$$

$$u_x = 0 \text{ along line ad}$$

The test is performed for 1,700 hours and the value of damage parameter at rupture in the BE program is set at 0.9. The program will stop when either the total time or the set maximum value of damage parameter at rupture is reached. The automatic time step control (criterion 4) with the maximum and minimum creep strain tolerances of 10^{-7} and 10^{-8} , respectively, is employed. The initial time step of 10^{-3} hour and 8 Gaussian integration points are used.

The total numbers of time steps used in BE and FE are 77,366 and 4,848, respectively. The BE program uses much more time steps than FE because a simple time integration (Euler) is used in the BE algorithms. The creep strain at BE node 1 with coordinate (0,0) in the y-direction and creep damage parameter are plotted against time and shown in Figure 6.2. The BE and FE curves are plotted every 900 and 50 time steps, respectively. The results are compared with the finite element solutions using ABAQUS UMAT Damage Code and show very good agreement. It can be seen that after sharp curve the time steps are very small.

6.3.2 A Square Plate With a Circular Hole

A square plate with a circular hole of Titanium Alloy subjected to a uniaxial constant stress load of 140 MPa in the y-direction is tested. This test is plane stress and secondary creep problem with damage. Because of symmetry, only a quarter of plate is used and has dimensions of 50 mm x 50 mm with a hole radius of 10 mm. The boundary and domain are divided into 32 boundary elements and 64 cells, respectively. The BE and FE meshes are the same and shown in Figure 6.3. The creep damage parameters and mechanical material properties of Titanium Alloy at 650° C (see Sun et al. [1999]) based on BE creep damage constitutive equations are as follows:

Creep Damage Parameters (based on stress in MPa and time in hour):

$$B = 5.623 \times 10^{-16}$$

$$m = 1.0$$

$$n = 5.911$$

$$M = 1.114 \times 10^{-15}$$

$$\phi = 4.8$$

$$\chi = 5.416$$

$$\alpha = 0.0$$

Material Properties:

$$\text{Young's Modulus (E)} = 200 \times 10^3 \text{ N/mm}^2$$

$$\text{Poisson's Ratio (}\nu\text{)} = 0.3$$

The boundary conditions are as follows:

$$u_y = 0 \text{ along line ab}$$

$$u_x = 0 \text{ along line de}$$

The test is performed for 300 hours and the value of damage parameter at rupture is set at 0.9. The program will stop when either the total time or the set maximum value of damage parameter at rupture is reached. The automatic time step control (criterion 4) with the maximum and minimum creep strain tolerances of 10^{-4} and 10^{-5} , respectively, is employed. The initial time step of 10^{-3} hour and 8 Gaussian integration points are used.

The total numbers of time steps used in BE and FE are 8,050 and 1,036, respectively. The stress and creep strain in the y-direction and damage parameter at BE node 1 are plotted against time and shown in Figure 6.4. The BE and FE curves are plotted every 300 and 30 time steps, respectively. The results are compared with the finite element solutions using ABAQUS UMAT Damage Code and show good agreement with the error being less than 17.0%.

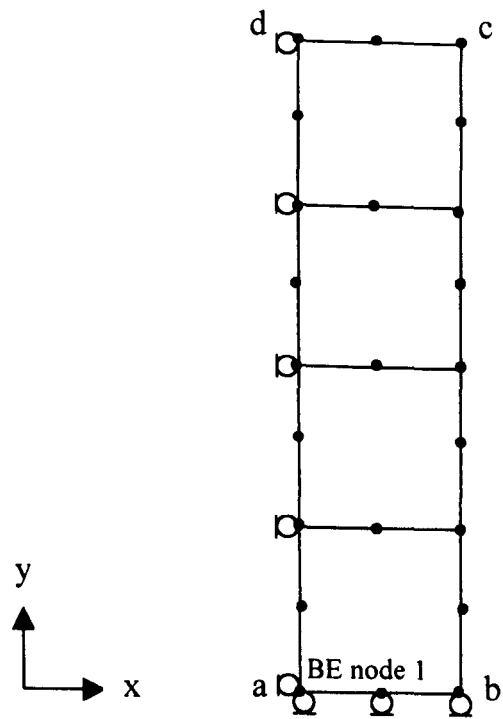
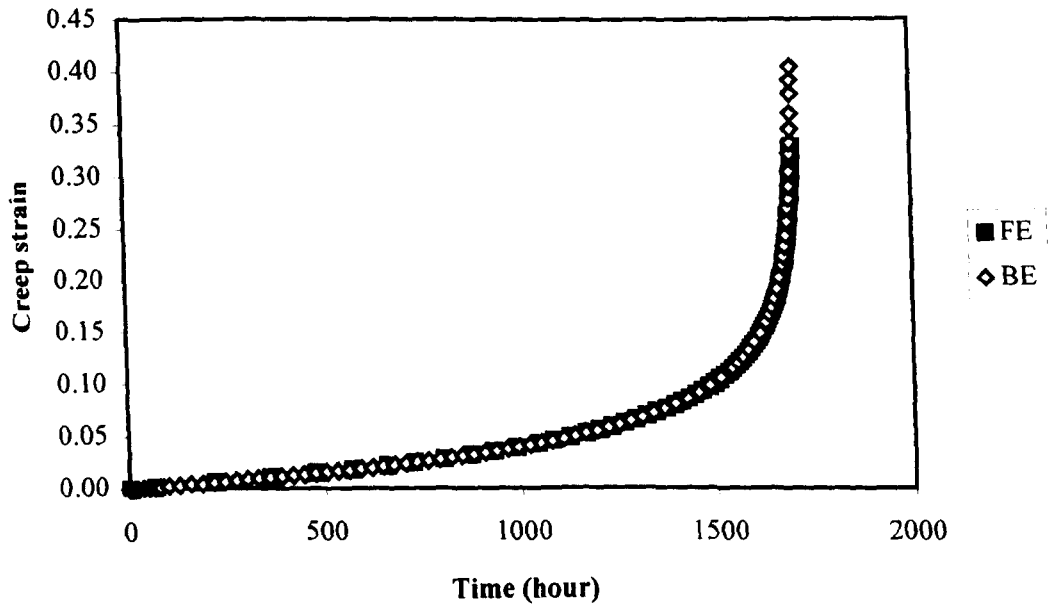
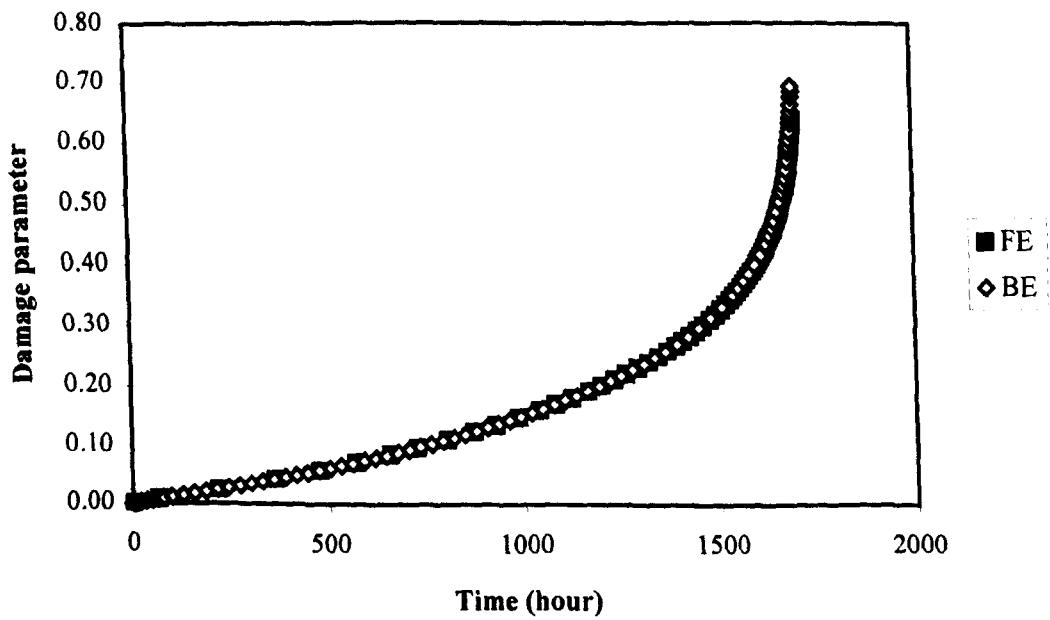


Figure 6.1 BE and FE meshes of the rectangular plate, 10 elements and 4 cells.



(a)



(b)

Figure 6.2 (a) creep strain against time, (b) creep damage parameter against time.

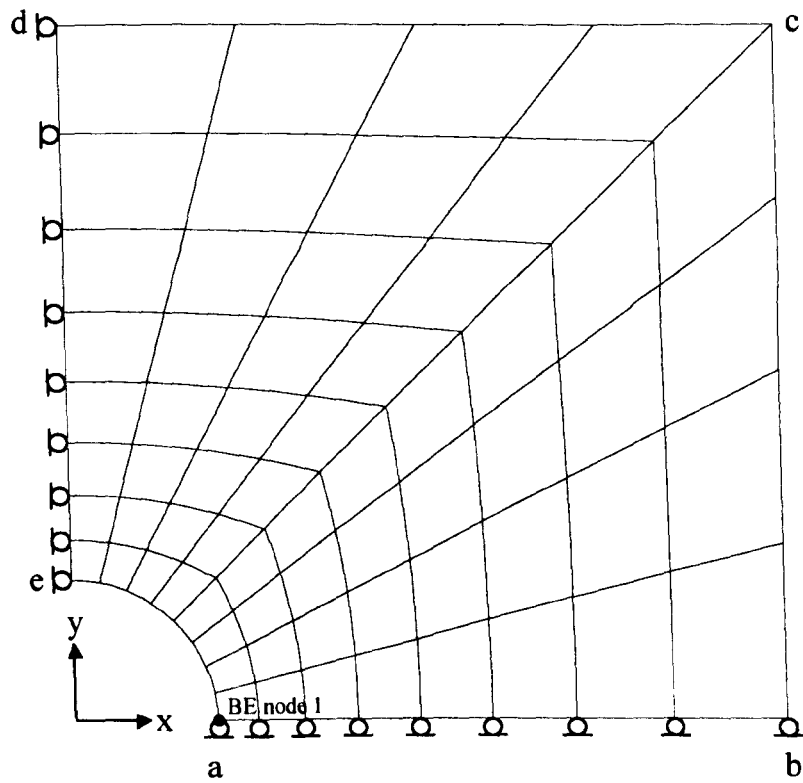


Figure 6.3 BE and FE meshes of the square plate with a circular hole,
32 boundary elements and 64 cells.

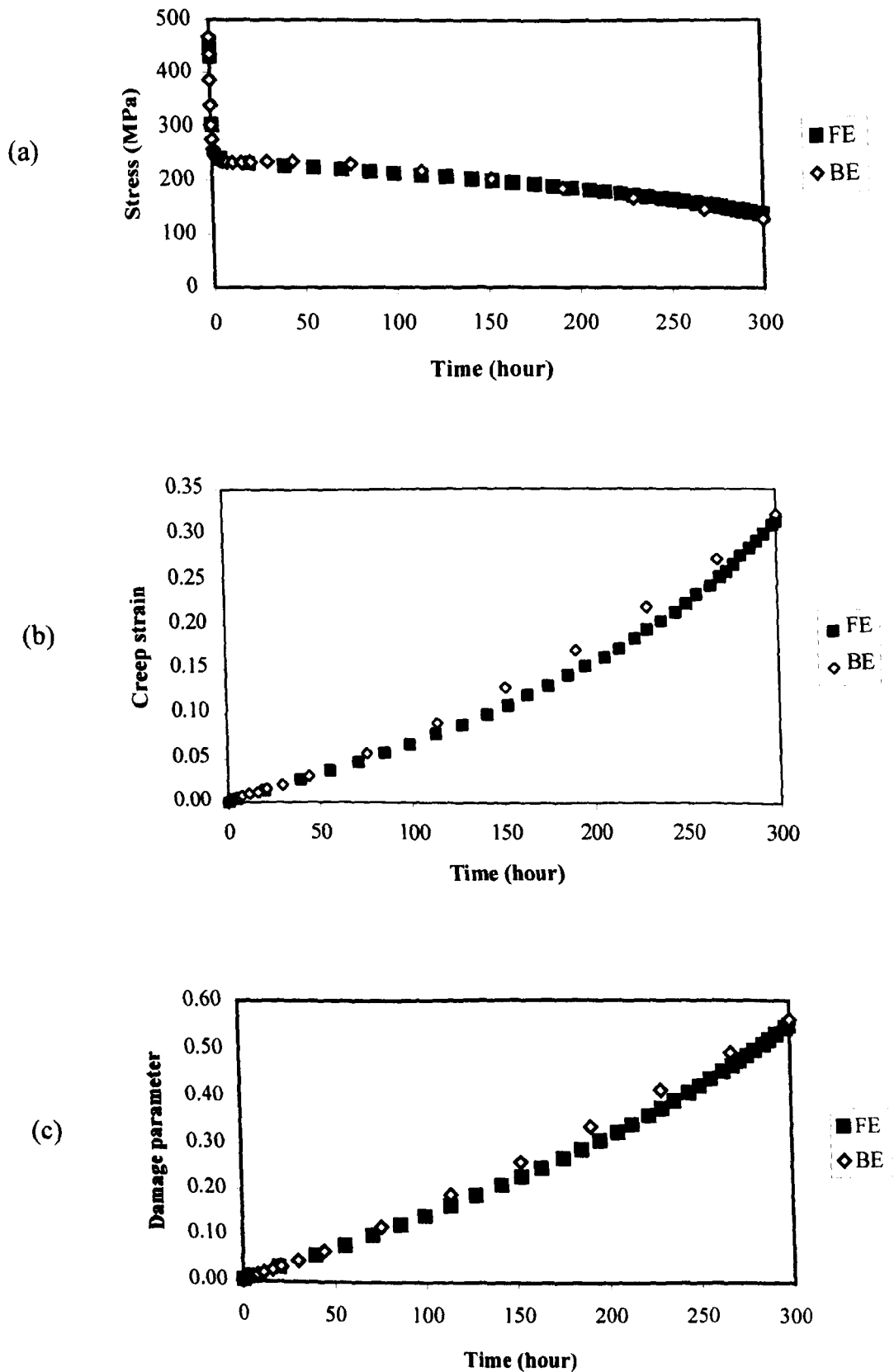


Figure 6.4 At BE node 1; (a) stress, (b) creep strain and (c) creep damage parameter.

Chapter 7

The Boundary Element Method for Combined Plasticity and Creep

Problems

In this chapter, plasticity and creep is modelled by including the plastic strain in the total strain. For isothermal condition, the total strain rate consists of the elastic, plastic and creep strain rates as follows:

$$\dot{\epsilon} = \dot{\epsilon}^e + \dot{\epsilon}^p + \dot{\epsilon}^c \quad (7.1)$$

where $\dot{\epsilon}$ is the total strain rate and $\dot{\epsilon}^e$, $\dot{\epsilon}^p$ and $\dot{\epsilon}^c$ are the elastic, plastic and creep strain rates, respectively.

7.1 The Constitutive Equations

The constitutive equation for time hardening creep can be written as follows:

$$\dot{\epsilon}_{ij}^c = \frac{3}{2} m B (\sigma_{eff})^{(n-1)} S_{ij} t^{(m-1)} \quad (7.2)$$

where B , m and n are the material constant dependent on the temperature.

The constitutive equation for plasticity based on von-Mises yield criterion and Prandtl-Reuss flow rule can be written as follows (see, for example Lee [1983] and Gun [1997]).

$$\dot{\epsilon}_{ij}^p = \frac{3}{2} \left(\frac{\dot{S}_k \dot{\epsilon}_k}{1 + \frac{H}{3\mu}} \right) \frac{\dot{S}_{ij}}{(\dot{\sigma}_{eff})^2} \quad (7.3)$$

where H is the plastic hardening modulus and μ is the shear modulus. The details of the BE formulation for elastoplasticity can be found, for example, in Lee [1983] and Gun [1997]. Since the BE for elastoplasticity is a time-independent process and the BE for creep is a time-dependent process, it is assumed that the plasticity and creep processes are separable. Therefore, superposition is used to combine the plastic and creep parts.

7.2 BE Combined Plasticity and Creep Algorithm

The numerical BE algorithm for elastoplasticity can be briefly summarised as follows (see, for example, Gun [1997] for more details):

1. Solve the elastic solutions with the full applied load to find the highest stress node.
2. Scale down the full applied load such that the highest stress node begins yielding.
3. Divide the applied load from the first yielding to the full applied load into a small number of incremental applied loads.
4. Solve the BE for elastoplasticity with an incremental applied load.
5. After convergence, update the variables.
6. Repeat step 4 - 5 until the full applied load is reached.

In this work, two approaches are used. The first approach called ‘full load approach’ is that the BE for elastoplasticity is applied first until the full applied load is reached and then the BE for creep is performed until the final time is reached. Another approach called ‘part-load approach’ is that the BE for elastoplasticity is applied for an

incremental applied load and then the BE creep analysis is performed for a small finite time. The procedure is repeated until the full applied load and the final time are reached.

The BE combined plasticity and creep algorithm for full load approach can be summarised as follows:

1. Follow steps 1 to 6 as in the plasticity algorithm above.
2. After the plastic solutions are solved, apply the BE for creep using algorithm as mentioned in section 3.3 until the total time is reached.

The BE combined plasticity and creep algorithm for part-load approach can be summarised as follows:

1. Follow step 1 to 5 as in the plasticity algorithm above.
2. Apply the BE for creep for a small finite time using the creep algorithm as mentioned in section 3.3.
3. Repeat the plasticity for another load increment followed by a finite creep time, until the full applied load and total time are reached.

7.3 BE Combined Plasticity and Creep Examples

The BE formulation for plasticity and creep has been tested for the problems of a square plate, a plate with a circular hole, and a plate with a semicircular notch subjected to a uniaxial tensile load. All results are compared with the finite element solutions using ABAQUS [1997]. The finite element solutions are obtained using the same

procedure as the BE solutions. For the part-load approach, the finite element data file needs first yield load information from the BE solutions in order to obtain the corresponding applied load.

7.3.1 Square Plate

A square plate subjected to a uniaxial tensile stress of 300 N/mm^2 in the x-direction is examined. The square plate has the dimension of $100 \text{ mm} \times 100 \text{ mm}$. The material properties and creep parameters are as follows:

Material properties:

$$E = 207 \times 10^3 \text{ N/mm}^2$$

$$\nu = 0.3$$

$$\sigma_y = 250 \text{ N/mm}^2$$

$$H = 4223.8267 \text{ N/mm}^2$$

Creep parameters:

$$B = 3.125 \times 10^{-14} \text{ (stress in MPa, time in hour)}$$

$$m = 1.0 \text{ for secondary creep}$$

$$n = 5$$

The BE mesh and boundary conditions are the same as Figure 4.1. The initial time step of 10^{-3} hour and Gaussian integration points of 6 are used. The automatic time step control (criterion 4) with the maximum and minimum creep strain tolerances of 10^{-4}

and 10^{-5} is employed. This test is secondary creep and plane stress problem. The test is performed for the total time of 1 hour for both full load and part-load approaches. The first yield occurs at the applied stress of 250 N/mm^2 . The rest of the applied load after first yield is divided into 10 incremental applied loads of 5 N/mm^2 . For the part-load approach, after solving the BE plastic solutions for each incremental applied load, the BE for creep is performed for 0.1 hour. The results at the final time are compared with the analytical solutions and the corresponding finite element solutions of the same mesh using ABAQUS [1997] and shown in Tables 7.1 and 7.2. The results are in good agreement with the analytical solutions and the finite element solutions. The analytical plastic strain solutions can be found in Appendix C. The percentage of BE error is less than 2%. It can be seen that the finite element solutions are very close to the analytical solutions. The total plastic strains for both approaches are the same while the total creep strains of part-load approach are less than that of full load approach. This is because the creep strains depend on current stresses.

7.3.2 Plate with a Circular Hole

A plate with a circular hole is subjected to a uniaxial tensile stress of 12 N/mm^2 in the x-direction. Because of symmetry, only a quarter of the plate with a circular hole is used and has the dimensions of 10 mm x 18 mm with a hole radius of 5 mm. The material properties and creep parameters are as follows:

Material properties:

$$E = 7000 \text{ N/mm}^2$$

$$\nu = 0.2$$

$$\sigma_y = 24.3 \text{ N/mm}^2$$

$$H = 224 \text{ N/mm}^2$$

Creep parameters:

$$B = 3.125 \times 10^{-10} \text{ (stress in MPa, time in hour)}$$

$$m = 1.0 \text{ for secondary creep}$$

$$n = 5$$

The BE mesh and the boundary conditions are the same as Figure 4.6. The test is secondary creep and plane stress problem and conducted for the total time of 1 hour. The initial time step of 10^{-3} hour and Gaussian integration points of 6 are used. The automatic time step control (criterion 4) with the maximum and minimum creep strain tolerances of 10^{-3} and 10^{-4} is employed. The first yield occurs at the applied stress of 5.598 N/mm^2 . The applied load is divided into 10 increments of 0.6402 N/mm^2 . For the part-load approach, the BE for creep is performed for 0.1 hour after solving the BE plastic solutions for each incremental load. The stress results in the x-direction at the final time are compared with the finite element solutions of the same mesh using ABAQUS [1997] and shown in Figure 7.1 and 7.2 where y/r is the ratio of the distance along the root in the y-direction to the hole radius. The results agree well with the finite element solutions with the error being less than 10.0% except at $y/r = 1.88$ and 2.0 which have the percentages of error of 12.91% and 30.92%, respectively, for the full load approach and 16.16% and 17.67% for the part-load approach.

7.3.3 Plate with a Semicircular Notch

A plate with a semicircular notch is subjected to a uniaxial tensile stress of 12 N/mm^2 in the x-direction. Because of symmetry, a quarter of the plate with a semicircular notch is used and has the dimensions of $10 \text{ mm} \times 18 \text{ mm}$ with a semicircular notch radius of 5 mm . The material properties and creep parameters are the same as those used in the plate with a circular hole problem.

The BE mesh and the boundary conditions are the same as Figure 4.8. The test is secondary creep and plane stress problem and conducted for the total time of 1 hour. The initial time step of 10^{-3} hour and Gaussian integration points of 6 are used. The automatic time step control (criterion 4) with the maximum and minimum creep strain tolerances of 10^{-3} and 10^{-4} is employed. The first yield occurs at the applied stress of 7.5408 N/mm^2 . The applied load is divided into 10 increments of 0.44592 N/mm^2 . For the part-load approach, the BE for creep is calculated for 0.1 hour after solving the BE plastic solutions for each incremental load. The stress results in the x-direction at the final time are compared with the finite element solutions of the same mesh using ABAQUS [1997] and shown in Figures 7.3 and 7.4 where y/r is the ratio of the distance along the root in the y-direction to the notch radius. The results agree well with the finite element solutions with the error being less than 4%.

	Stress (N/mm ²)	Plastic strains		Creep strains	
		σ_{xx}	ϵ_{xx}^p	ϵ_{yy}^p	ϵ_{xx}^c
FE	300	1.1838E-02	-5.9188E-03	7.5934E-02	-3.7968E-02
BE	299.2	1.173E-02	-5.859E-03	7.481E-02	-3.737E-02
Analytical	300	1.1838E-02	-5.9188E-03	7.5934E-02	-3.7969E-02
%FE error	0	0	0	0	-0.003
%BE error	-0.27	-0.91	-1.01	-1.48	-1.58

Table 7.1 The solutions of the square plate, full load approach.

	Stress (N/mm ²)	Plastic strains		Creep strains	
		σ_{xx}	ϵ_{xx}^p	ϵ_{yy}^p	ϵ_{xx}^c
FE	300	1.1838E-02	-5.9188E-03	5.2804E-02	-2.6402E-02
BE	299.2	1.173E-02	-5.859E-03	5.197E-02	-2.596E-02
Analytical	300	1.1838E-02	-5.9188E-03	5.2804E-02	-2.6402E-02
%FE error	0	0	0	0	0
%error	-0.27	-0.91	-1.01	-1.58	-1.67

Table 7.2 The solutions of the square plate, part-load approach.

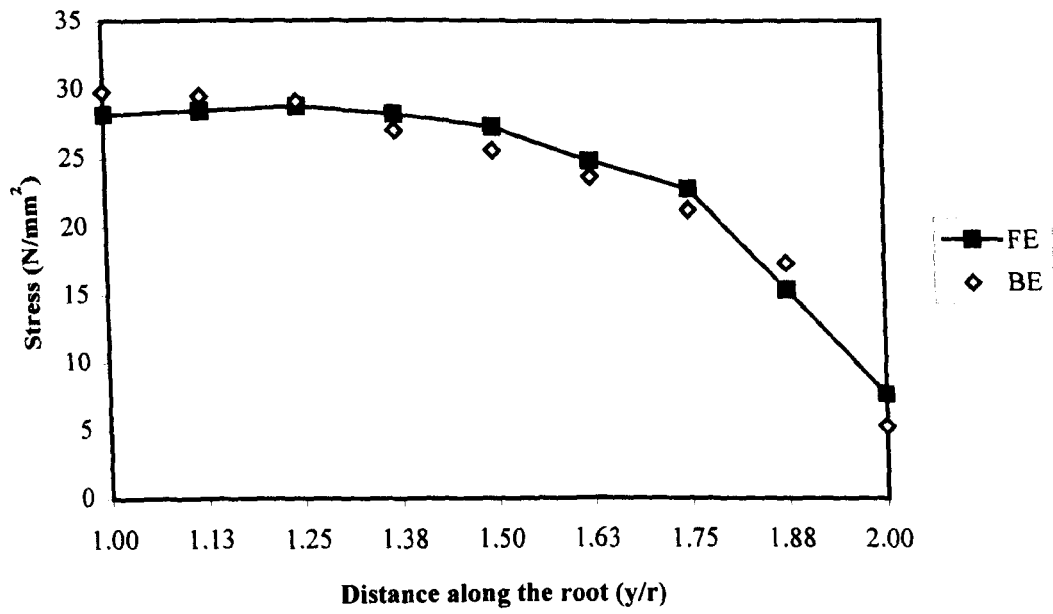


Figure 7.1 The solutions of the plate with a circular hole, full load approach.

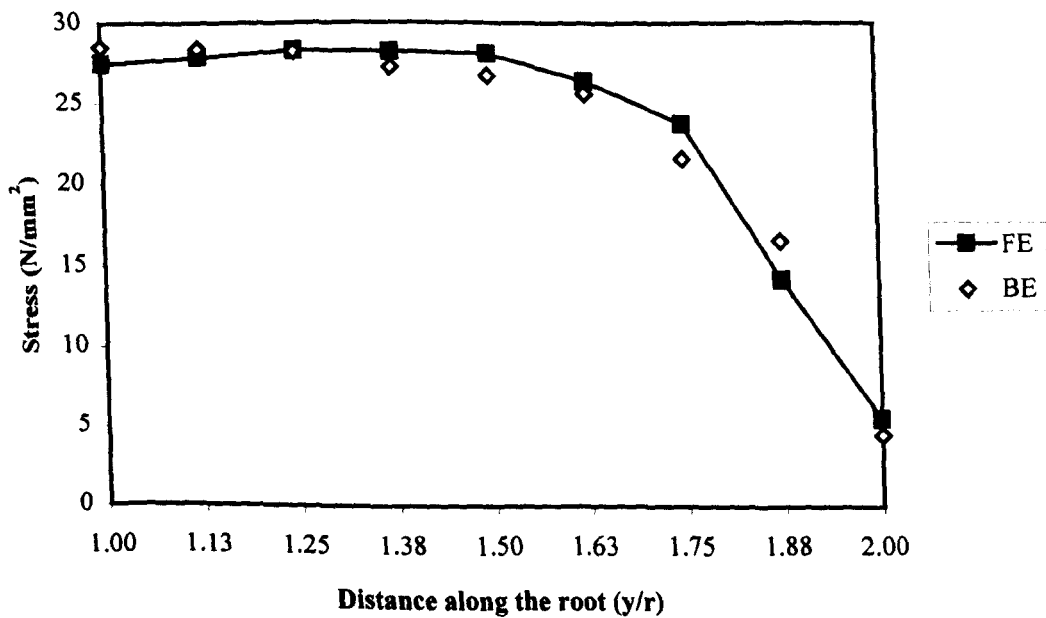


Figure 7.2 The solutions of the plate with a circular hole, part-load approach.

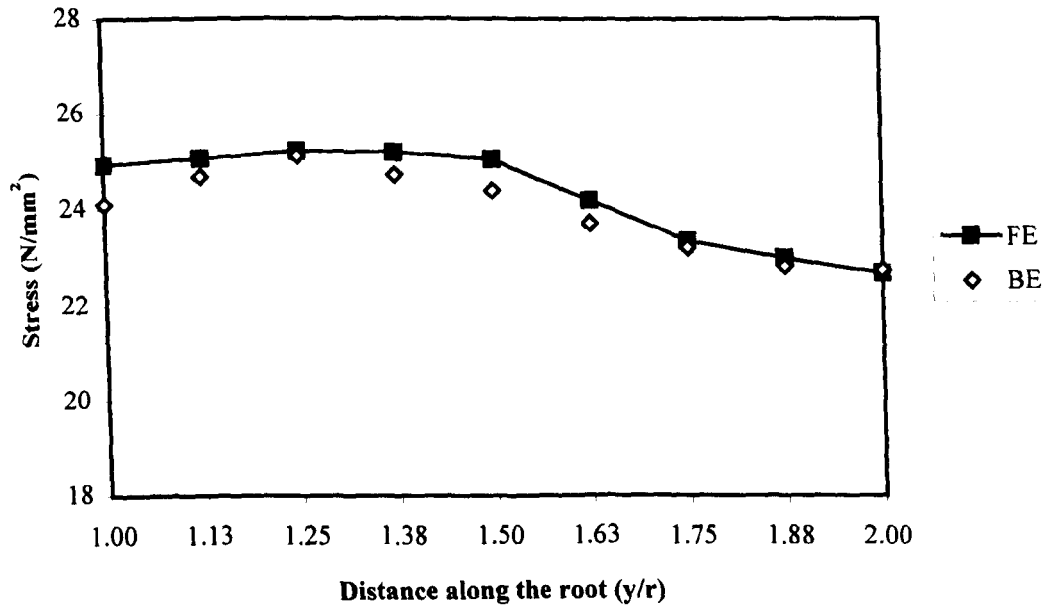


Figure 7.3 The solutions of the plate with a semicircular notch, full load approach.

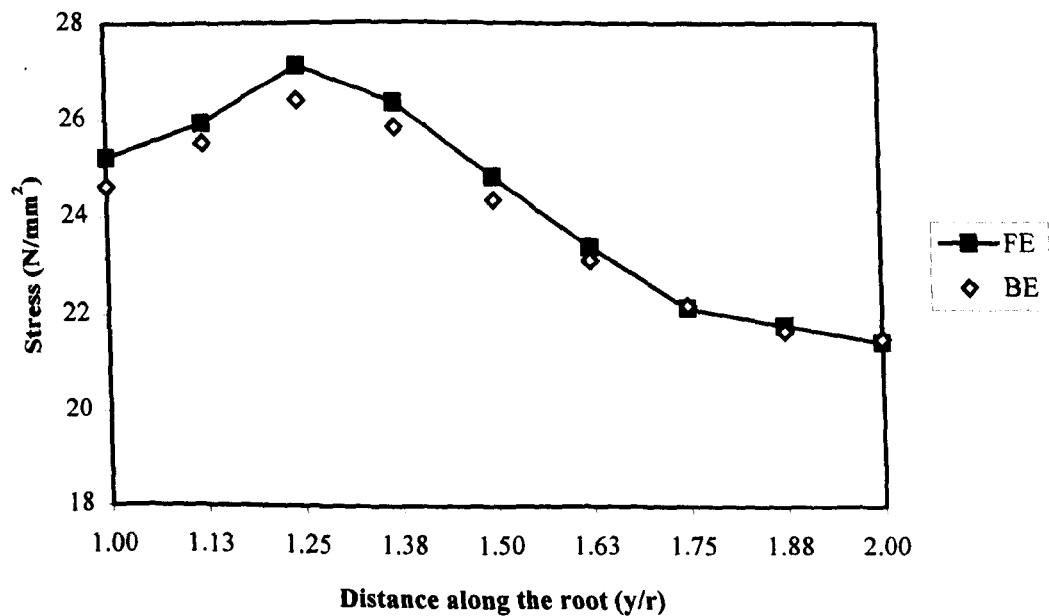


Figure 7.4 The solutions of the plate with a semicircular notch, part-load approach.

Chapter 8

Boundary Element Method for Creep Contact Problems

The boundary element method has been successfully applied to contact problems (see, for example, Olukoko et al. [1993]). Contact problems are non-linear problems in nature since the contact area for non-conforming contact problems is usually unknown in advance and does not change linearly with the applied load. Therefore, the prescribed displacements and tractions of the nodes on the contact surface are unknown as well. But there are two relationships that the nodes on the contact surface must satisfy (see, for example, Becker [1992]):

1. Continuity of displacements in the normal contact direction.
2. Equilibrium conditions (i.e. equal and opposite tractions).

There are usually two types of contacts: frictionless contact and frictional contact. For frictionless contact, only normal compressive stresses are present at the contact area. For frictional contact, both normal and shear stresses are present in the contact area. The applications of creep and contact problems can be found in Hyde et al. [1996a, 1996b]. In this chapter, the frictionless contact with creep is investigated using the boundary element method. The results are compared with the finite element solutions using ABAQUS [1997].

8.1 Contact Conditions

The contact conditions for frictionless contact problems must satisfy the continuity and equilibrium relationships. This results in four relationships as follows:

$$\begin{aligned}
u_n^A &= u_n^B \\
u_t^A &= u_t^B + \delta_t \\
t_n^B &= -t_n^A \\
t_t^A &= t_t^B = 0
\end{aligned}
\tag{8.1}$$

where the superscripts A and B refer to body A and body B , respectively, and the subscripts n and t refer to normal and tangential directions, respectively. δ_t is the amount of the slip displacement in the tangential direction. The normal and tangential directions of the contact surface can be shown as Figure 8.1.

8.2 BE Creep Contact Algorithm

Since the contact problems are non-linear and the actual contact area is usually unknown in advance, the iterative procedure is needed. The boundary element method for contact problems based on an iterative procedure is used in this work. To solve the contact problems, the contact area is usually assumed first. Then the boundary element method for elasticity for multi-domain can be applied with the help of contact conditions of equation (8.1). When two bodies come into contact, the boundary on each domain can be divided into two parts, the boundary outside the contact area (Γ_o) and the boundary inside the contact area (Γ_c). The boundary conditions of Γ_o can be used as mentioned in section 3.2.4. In the contact area, each node pair has eight variables, $u_n^A, u_t^A, t_n^A, t_t^A, u_n^B, u_t^B, t_n^B$ and t_t^B , but only four equations can be established from boundary integral equations (two equations per node for each domain). To get a unique solution, equation (8.1) must be applied for each node pair.

After the first iteration (first assumed contact area), the pairs of elements in the assumed contact area must be checked for edge overlap and tensile stress. If edge overlap occurs just outside the assumed contact area, this means the assumed contact area is too small. Therefore, the next iteration must include the overlapped element pairs. If the tensile stress occurs in the contacting elements in the assumed contact area, this means the assumed contact area is too large. Therefore, the next iteration must release these elements. The iterations are terminated when there are no edge overlap and no tensile stress elements. The numerical algorithm of elastic contact problems can be found, for example, in Becker [1992].

Like plasticity, contact problems are time-independent. To combine contact with creep, it is assumed that the contact and creep processes are separable. The BE creep contact algorithm can be summarised as follows:

1. At $t = 0$, solve elastic contact solutions and calculate stresses and strains at all nodes. At this point, the actual contact area is known.
2. Solve the multi-domain creep solutions using the creep algorithm as mentioned in section (3.3) coupled with the contact conditions of equation (8.1).

8.3 BE Creep Contact Examples

The boundary element program for creep contact problems has been established. Two kinds of contact problems, a punch on a foundation and a cylinder on a foundation, are investigated. The results are compared with the corresponding finite element solutions using ABAQUS [1997].

8.3.1 A Punch on a Foundation

A punch compressed on a foundation is investigated. Because of symmetry, only a half of the geometry is used. The dimensions of the punch and the foundation are 2 mm x 2 mm and 8 mm x 4 mm, respectively. The boundary and domain of the punch are discretised into 24 boundary elements and 40 cells, respectively. The boundary and domain of the foundation is divided into 28 boundary elements and 72 cells, respectively. The BE and FE meshes are the same and shown in Figure 8.2. The creep parameters and mechanical material properties are as follows:

Creep Parameters:

$$B = 3.125 \times 10^{-14} \quad (\text{stress in MPa, time in hour})$$

$$m = 1.0 \quad \text{for secondary creep}$$

$$n = 5$$

Material Properties:

$$\text{Young's Modulus (E)} = 200 \times 10^3 \text{ N/mm}^2$$

$$\text{Poisson's Ratio (}\nu\text{)} = 0.3$$

The boundary conditions are as follows:

$$u_y = 0 \quad \text{along line ab.}$$

$$u_x = 0 \quad \text{along line af.}$$

The punch is subjected to a constant compressive stress of 200 N/mm² in the y-direction. This test is the plane strain and secondary creep problem based on time

hardening law. The test is conducted for creep for 1 hour after solving the BE frictionless contact solutions. The initial time step of 10^{-3} hour and Gaussian integration points of 6 are used. The automatic time step control (criterion 4) with the maximum and minimum stress tolerances of 0.1 and 0.01 is employed. In this test, the actual contact area is known in advance and six pairs of elements are in contact. The normal stresses of the punch at the final time are plotted along the contact interface and compared with the corresponding finite element solutions using ABAQUS [1997] and shown in Figure 8.3. The results show a good agreement with the finite element solutions. From Figure 8.3 (a), it can be seen that the elastic solutions of BE are different from those of FE at the element near the end of contact area. This might be because: (i) the effects of the high stresses at the corner of the punch and (ii) the BE program use the average value of stress at common nodes. From Figure 8.3 (b), the normal stresses along contact interface seem to converge to one value except at the end element of the contact area.

8.3.2 A Cylindrical Punch on a Flat Foundation

A cylindrical punch compressed on a flat foundation is investigated. Because of symmetry, only a half of the geometry is used. The diameter of the cylindrical punch is 2 mm and the dimensions of the foundation are 4 mm x 2 mm. The boundary and domain of the cylindrical punch are discretised into 44 boundary elements and 120 cells, respectively. The boundary and domain of the foundation are divided into 32 boundary elements and 80 cells, respectively. The BE and FE meshes are the same and shown in Figure 8.4. The creep parameters and mechanical material properties are as follows:

Creep Parameters:

$$B = 3.125 \times 10^{-20} \quad (\text{stress in MPa, time in hour})$$

$$m = 1.0 \quad \text{for secondary creep}$$

$$n = 5$$

Material Properties:

$$\text{Young's Modulus (E)} = 200 \times 10^3 \text{ N/mm}^2$$

$$\text{Poisson's Ratio (}\nu\text{)} = 0.3$$

The boundary conditions are as follows:

$$u_y = 0 \quad \text{along line ab.}$$

$$u_x = 0 \quad \text{along line ad.}$$

The cylindrical punch is subjected to a constant compressive stress of 2.8128×10^4 N/mm² on the top boundary element in the y-direction. This high stress is used to make the contact surface and creep strains not too small since the creep constant B is very small. This test is the plane strain and secondary creep problem based on time hardening law. The test is conducted for creep for 1 hour after solving the BE frictionless contact solutions. The initial time step of 10^{-6} hour and Gaussian integration points of 6 are used. The automatic time step control (criterion 4) with the maximum and minimum stress tolerances of 0.1 and 0.01 is employed. In this test, the actual contact area is unknown in advance. After solving the BE contact solutions, there are four pairs of elements in contact. The normal stresses of the cylindrical punch at the final time are plotted along the contact interface and compared with corresponding finite element solutions using ABAQUS [1997] and shown in Figure 8.5. It can be seen that the BE elastic solutions agree well with the FE solutions except

the node at the end of contact. This might be because the BE solutions use the average values of stress at common nodes. The actual elastic contact area is around 0.18 mm. From Figure 8.5 (b), the BE creep stresses along the contact interface agree well with the FE solutions up to a distance of around 0.1 mm. After this point, large differences occur. This is because the BE program keeps the contact area constant during the creep process while the FE program adjusts the contact area during the creep process. For the FE solutions, the new contact area expands to around 0.29 mm.

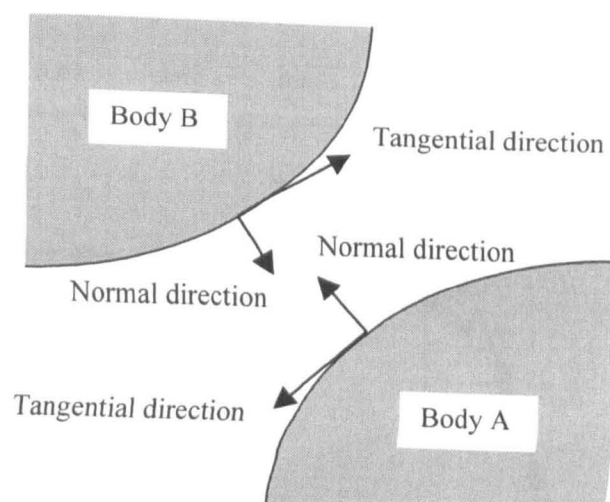


Figure 8.1 Normal and tangential directions in contact problems.

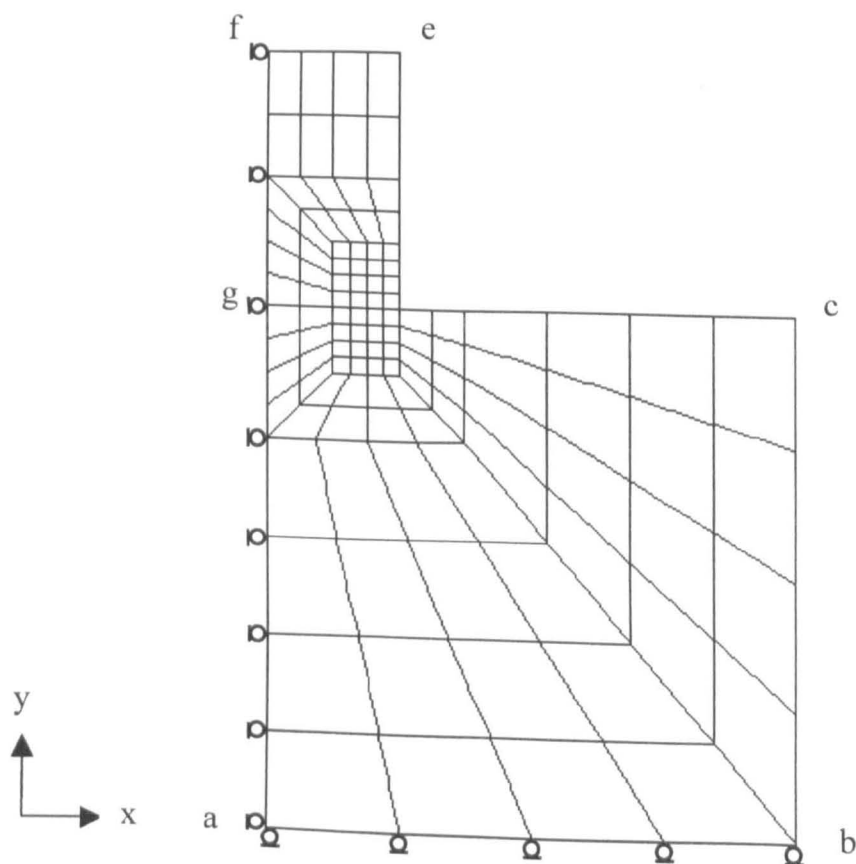
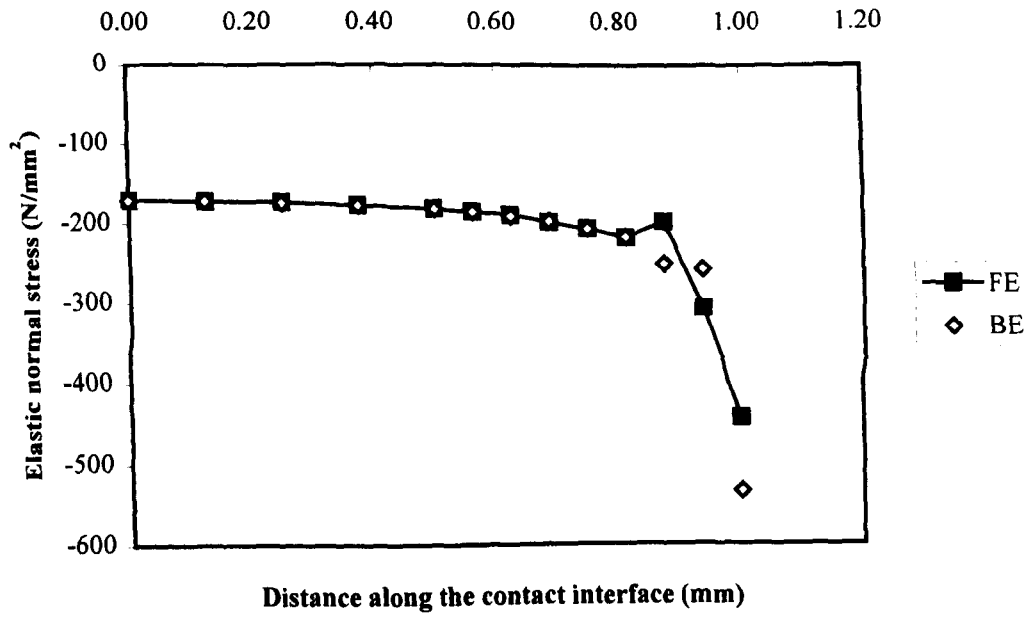
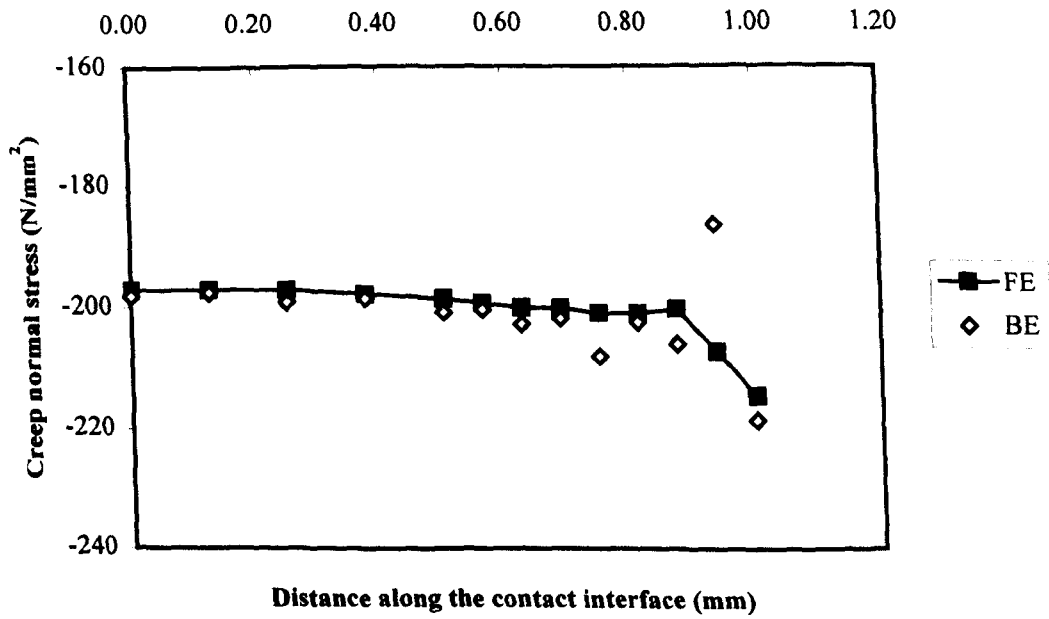


Figure 8.2 The BE and FE meshes of the punch on the foundation.



(a)



(b)

Figure 8.3 Normal stress distributions along the contact interface,
 (a) elastic contact solutions, (b) creep contact solutions.

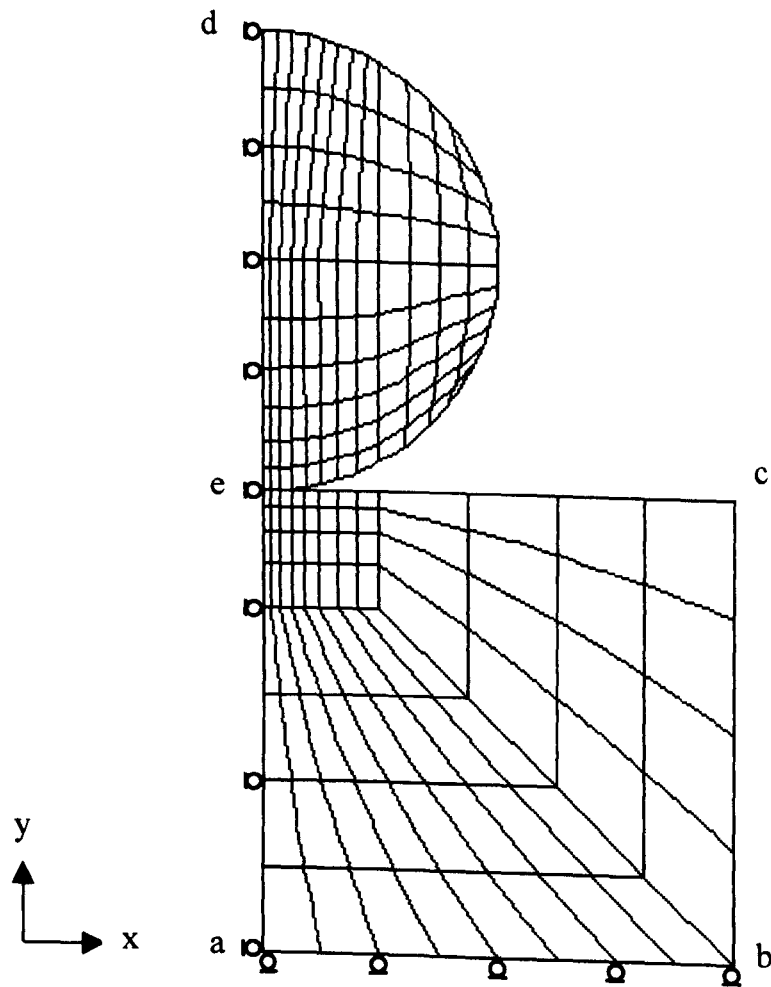
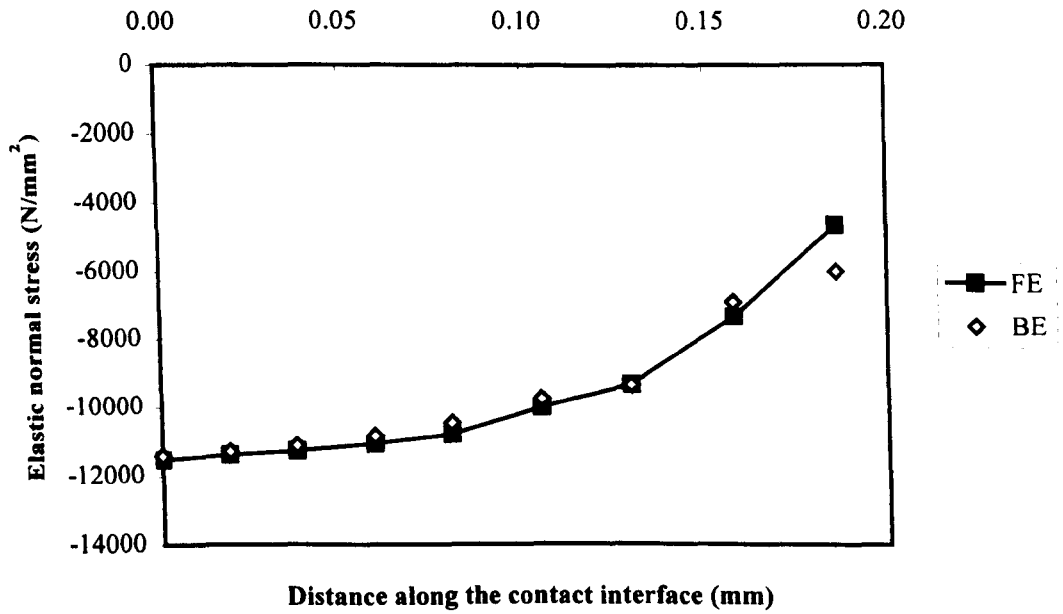
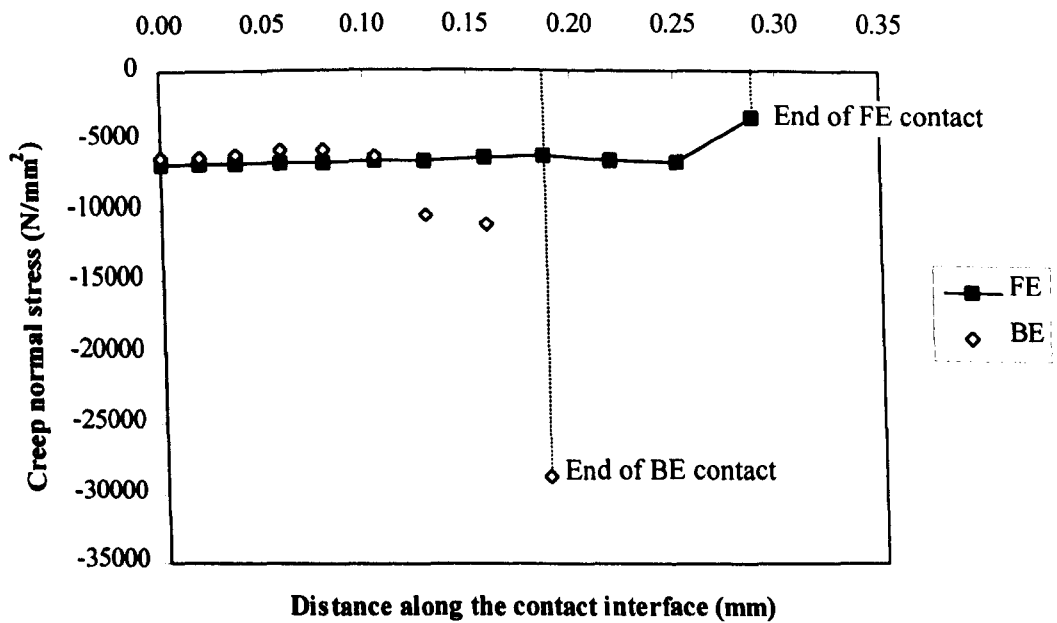


Figure 8.4 The BE and FE meshes of the cylindrical punch on the foundation.



(a)



(b)

Figure 8.5 Normal stress distributions along the contact interface,
 (a) elastic contact solutions, (b) creep contact solutions.

Chapter 9

Conclusions and Further Studies

9.1 Conclusions

The 2-D boundary element program for creep problems based on an initial strain approach has been successfully established. The boundary integral equations for creep have the same form as those for elastoplasticity except the plastic strain rates are replaced by the creep strain rates. The main difference between the BE for elastoplasticity and the BE for creep is that the BE for elastoplasticity is written in an incremental form (time-independent form) while the BE for creep is written in the rate form (time-dependent form).

The BE program for creep is tested for the problems of a square plate, a plate with a circular hole and a plate with a semicircular notch. The tests include primary and secondary creep and plane stress and plane strain cases. Both creep laws, time hardening and strain hardening, have been applied. The results are compared with the corresponding finite element solutions using ABAQUS and analytical solutions where available. The results agree very well with both the finite element solutions and the analytical solutions.

The size of the initial time step is very crucial for accurate solutions. If it is too large, the final solutions will not be accurate. If it is too small, the final solutions will be more accurate but it will take longer CPU time and the computational cost will be very high. The prescribed tolerances also give the same effect as the initial time step. Therefore,

the initial time step and the prescribed tolerances must be chosen as a compromise between accuracy and computational cost.

The 2-D BE program for creep damage has been written as well. The procedure of BE for creep damage is the same as that of BE for creep with an addition of a damage evolution equation. The problems of a rectangular plate and a plate with a hole are tested and compared with the 2-D finite element solutions using ABAQUS UMAT. The results agree well for the rectangular plate while, for the plate with a hole, the results are slightly different in values but the trend is the same.

The 2-D BE program for combined plasticity and creep has also been established. It is assumed that the plasticity process and the creep process are separable. Superposition is then used to combine plastic and creep strains. Two approaches have been investigated for the problems of a square plate, a plate with a circular hole and a plate with a semicircular notch. The first approach called "full load" approach is that the plastic part is calculated for the full applied load and then the creep part is calculated until the total time is reached. The second approach called "part-load" approach is that the plastic part is calculated for an incremental applied load and then the creep part is calculated for a certain time. The procedure is repeated until the full applied load and the total time are reached. The results are compared with the corresponding finite element solutions using ABAQUS and are shown to be in very good agreement.

The 2-D BE program for creep contact problems without friction has been established as well. The procedure is similar to that of combined plasticity and creep. The problems of a punch and a cylindrical punch on foundations are investigated and

compared with the corresponding finite element solutions using ABAQUS. The program works well with the problems of fixed contact area because the BE program has been written such that the contact area is held constant during the creep process.

9.2 Further Studies

The 2-D BE formulation for creep can be extended to three dimensional applications by including the z-components in the program. The kernels U_{ij} , T_{ij} , and W_{kij} used in the 2-D boundary integral equations must be changed. These kernels would be the same as those of the 3-D BE for elastoplasticity. The domain must be divided into surface elements and volume cells. The surface elements and volume cells can be eight-node quadrilateral elements and twenty-node cubic cells, respectively. The numerical creep algorithm would be similar to that of 2-D BE for creep.

The 2-D axisymmetric BE formulation for creep is another possibility for further work. The transformation from 2-D to axisymmetric BE creep formulation is not straightforward to apply. All the 2-D kernels as well as creep laws have to change from cartesian to cylindrical coordinate system.

In the frictionless contact problems, the BE for creep contact can be rewritten to check contact conditions and update the contact area after each time step of the creep procedure. This might improve the solutions of creep contact problems in which the contact area changes with time. Friction contact problems can also be added in the program.

References

ABAQUS Version 5.7, [1997], HKS Inc., Rhode Island

Andersson, T., [1981], "The boundary Element Method Applied to Two-Dimensional Contact Problems with Friction," Procedures of 3rd International Seminar, California, Edited by C.A. Brebbia, Springer-Verlay, Berlin, pp. 239-258.

Andersson, T., [1982], "The Second Generation Boundary Element Contact Program," BEMs in Engineering, Procedures of 4th International Seminar, Southampton, September, pp 409-427.

Andersson, T., Fredriksson, B., and Persson, B.G.A., [1980], "The Boundary Element Method Applied to Two-Dimensional Contact Problems," New Developments in BEMs, Procedures of 2nd International Seminar on Recent Advances in BEMs, Southampton, March, pp. 247-263.

Banerjee, P.K., and Davies, T.G., [1984], "Advanced Implementation of Boundary Element Methods for Three-Dimensional Problems of Elastoplasticity and Viscoplasticity," Chapter 1 in Developments in Boundary Element Methods-3, Edited by P. K. Banerjee and S. Mukherjee, Elsevier Applied Science Publishers Ltd, London, pp. 1-26.

Banerjee, P.K., and Raveendra, S.T., [1986], "Advanced Boundary Element Analysis of Two- and Three-Dimensional Problems of Elasto-Plasticity," International Journal

for Numerical Methods in Engineering, Vol. 23, No. 6, pp. 985-1002.

Banthia, V., and Mukherjee, S., [1985], "BEM and FEM Analysis of Planar Moving Cracks in Creeping Solids," International Journal of Fracture, Vol. 28, No. 2, pp. 83-101.

Becker, A.A., [1992], "The Boundary Element Method in Engineering," McGraw-Hill Book Company, London.

Becker, A.A., and Hyde, T.H., [1993], "Fundamental Tests of Creep Behaviour," NAFEMS Report R0027.

Boyle, T.J., and Spence, J., [1983], "Stress Analysis for Creep," Butterworths, London.

Brebbia, C.A., Telles, J.C.F., and Wrobel, L.C., [1984], "Boundary Element Techniques: Theory and Applications in Engineering," Springer-Verlag, Berlin.

Cathie, D.N., and Banerjee, P.K., [1982], "Boundary Element Methods for Plasticity and Creep Including a Visco-Plastic Approach," Res Mechanica, Vol. 4, pp. 3-22.

Chen, G.G., and Hsu, T.R., [1987], "A Finite Element Model for Creep Fracture Analysis Using Continuum Damage Approach," Numerical Method in Fracture Mechanics, Proceedings of 4th International Conference, Texas, Edited by A.R. Luxmoore, D.R.J. Owen, Y.P.S. Rajapakse, and M.F. Kanninen, Pintridge Press, Swansea, pp. 401-410.

Dandekar, B.W., and Conant, R.J., [1992a], "Numerical Analysis of Elastic Contact Problems Using the Boundary Integral Equation Method. Part 1: Theory," *International Journal for Numerical Methods in Engineering*, Vol. 33, pp. 1513-1522.

Dandekar, B.W., and Conant, R.J., [1992b], "Numerical Analysis of Elastic Contact Problems Using the Boundary Integral Equation Method. Part 2: Results," *International Journal for Numerical Methods in Engineering*, Vol. 33, pp. 1523-1535.

Duan, Y., Webster, J.J., and Hyde, T.H., [1991], "Finite Element Prediction of Creep Damage and Creep Crack Growth," *Mechanics of Creep Brittle Materials 2*, Edited by A.C.F. Cocks and A.R.S. Porter, Elsevier Applied Science, London, pp. 37-48.

Dunne, F.P.E., Othman, A.M., Hall, F.R., and Hayhurst, D.R., [1990], "Representation of Uniaxial Creep Curves Using Continuum Damage Mechanics," *International Journal of Mechanical Sciences*, Vol. 32, No. 11, pp. 945-957.

Dyson, B.F., and Hayhurst, D.R., [1993], "A Limit on the Applicability of Skeletal Point Stress Solutions for Predicting Circumferential Notched-Bar Lifetimes," *Creep and Fracture of Engineering Materials and Structures, Procedures of 5th International Conference*, Edited by B. Wilshire and R.W. Evans, London, pp. 159-166.

El-Zafrany, A., [1993], "Techniques of the Boundary Element Method," Ellis Horwood Limited, London.

Garrido, J.A., Foces, A., and Paris, F., [1994], "An Incremental Procedure for Three-

Dimensional Contact Problems With Friction,” *Computer & Structures*, Vol. 50, No. 2, pp. 201-215.

Gun, H., [1997], “Boundary Element Formulations for Elastoplastic Stress Analysis Problems,” PhD Thesis, University of Nottingham.

Hart, E.W., [1976], “Constitutive Relations for the Nonelastic Deformation of Metals,” *ASME Journal of Engineering Materials and Technology*, Vol. 98, No. 3, pp. 193-202.

Hayhurst, D.R., [1973], “Stress Redistribution and Rupture Due to Creep in a Uniformly Stretched Thin Plate Containing a Circular Hole,” *Journal of Applied Mechanics*, Vol. 95, No. 1, pp. 244-250.

Hyde, T.H., Webster, J.J., and Smith, S.D., [1990], “Assessment of Continuum Damage and C^* Approaches to Predicting Creep Crack Growth,” *Proceedures of 4th International Conference on Creep and Fracture of Engineering Materials and Structures*, Swansea, pp. 715-727.

Hyde, T.H., Sun, W., and Becker, A.A., [1996a], “Analysis of the Impression Creep Test Method Using a Rectangular Indenter for Determining the Creep Properties in Welds,” *International Journal of Mechanical Sciences*, Vol. 38, No. 10, pp. 1089-1102.

Hyde, T.H., Yehia, K.A., and Becker, A.A., [1996b], “Application of the Reference Stress Method for Interpreting Impression Creep Test Data,” *Materials at High Temperatures*, Vol. 13, No. 3, pp. 133-138.

Kamimura, Y., Aizawa, T., and Kihara, J., [1996], "Elasto-plastic Contact Analysis in Rolling by Two Dimensional Boundary Element Method," *Boundary Element Methods*, Edited by M. Tanaka and Z. Yao, Elsevier Science B.V., pp. 277-285.

Kamiya, N., and Nishiki, T., [1996], "Efficient Boundary Element Analysis of Three-Dimensional Elastic Contact Problem," *Boundary Element Methods*, Edited by M. Tanaka and Z. Yao, Elsevier Science B.V., pp. 267-275.

Karami, G., and Fenner, R.T., [1987], "Application of Boundary Integral Equation (BIE) Method to Two-Dimensional Elastic Contact Problems Using Isoparametric Quadratic Element," *Iranian Journal of Science & Technology*, Vol. 11, No. 2, pp. 153-176.

Kraus, H., [1980], "Creep Analysis," John Wiley & Sons, New York.

Kumar, V., and Mukherjee, S., [1977], "A Boundary-Integral Equation Formulation for Time-Dependent Inelastic Deformation in Metals," *International Journal of Mechanical Sciences*, Vol. 19, No. 12, pp. 713-724.

Leahy, J.G., and Becker, A.A., [1999a], "The Numerical Treatment of Local Variables in Three-Dimensional Frictional Contact Problems Using the Boundary Element Method," *Computer and Structures*, Vol. 71, pp. 383-395.

Leahy, J.G., and Becker, A.A., [1999b], "A Quadratic Boundary Element Formulation for Three-Dimensional Contact Problems With Friction," *Journal of Strain Analysis*,

Vol. 34, No. 4, pp. 235-251.

Leckie, F.A., and Hayhurst, D.R., [1977], "Constitutive Equations for Creep Rupture," *ACTA Metallurgica*, Vol. 25, No. 9, pp. 1059-1070.

Lee, K.H., [1983], "A Boundary Integral Equation Method for Two Dimensional Elastoplastic Analysis," PhD Thesis, Imperial College, University of London.

Lee, K.H., and Fenner, R.T., [1986], "A Quadratic Formulation for Two-Dimensional Elastoplastic Analysis Using the Boundary Integral Equation Method," *Journal of Strain Analysis*, Vol. 21, No. 3, pp. 159-175.

Man, K.W., Aliabadi, M.H., and Rooke, D.P., [1993], "BEM Frictional Contact Analysis: Modelling Considerations," *Engineering Analysis With Boundary Elements*, Vol. 11, pp. 77-85.

Morjaria, M., and Mukherjee, S., [1980], "Improved Boundary-Integral Equation Method for Time-Dependent Inelastic Deformation in Metals," *International Journal for Numerical Methods in Engineering*, Vol. 15, pp. 97-111.

Morjaria, M., and Mukherjee, S., [1981], "Numerical Analysis of Planar, Time-Dependent Inelastic Deformation of Plates With Cracks by the Boundary Element Method," *International Journal of Solids and Structures*, Vol. 17, No. 1, pp. 127-143.

Morjaria, M., and Mukherjee, S., [1982], "Numerical Solution for Stresses Near Crack

Tip in Time-Dependent Inelastic Fracture Mechanics,” International Journal of Fracture, Vol. 18, No. 4, pp. 293-310.

Morjaria, M., Sarihan, V., and Mukherjee, S., [1980], “Comparison of Boundary Element and Finite Element Methods in Two-Dimensional Inelastic Analysis,” Res Mechanica, Vol. 1, pp. 3-20.

Mukherjee, S., [1980], “Application of the Boundary Element Method in Time-Dependent Inelastic Deformation,” Proceedings of 2nd International Symposium on Innovative Numerical Analysis in Applied Engineering Sciences, Edited by R. Shaw et al., June Montreal, Canada.

Mukherjee, S., [1982a], “Time-Dependent Inelastic Deformation of Metals by Boundary Element Method,” Chapter 5 in Developments in Boundary Element Methods-2, Applied Science Publishers, London, pp. 111-142.

Mukherjee, S., [1982b], “Boundary Element Methods in Creep and Fracture,” Applied Science Publishers Ltd, London.

Mukherjee, S., and Banthia, V., [1984], “Non-Linear Problems of Fracture Mechanics,” Chapter 4 in Development in Boundary Element Methods-3, Edited by P.K. Banerjee and S. Mukherjee, Elsevier Applied Science Publishers, London, pp. 87-114.

Mukherjee, S., and Kumar, V., [1978], “Numerical Analysis of Time-Dependent

Inelastic Deformation in Metallic Media Using the Boundary-Integral Equation Method," *Journal of Applied Mechanics*, Vol. 45, pp. 785-790.

Mukherjee, S., and Morjaria, M., [1981], "Boundary Element Analysis of Time-Dependent Inelastic Deformation of Cracked Plates Loading in Anti-Plane Shear," *International Journal of Solids and Structures*, Vol. 17, No. 8, pp. 753-763.

Mukherjee, S., Kumar, V., and Chang, K.J., [1978], "Elevated Temperature Inelastic Analysis of Metallic Media Under Time Varying Loads Using State Variable Theories," *International Journal of Solids and Structures*, Vol. 14, No. 8, pp. 663-679.

Murakami, S., Kawai, K., and Rong, H., [1988], "Finite Element Analysis of Creep Crack Growth by a Local Approach," *International Journal of Mechanical Sciences*, Vol. 30, No. 7, pp. 491-502.

Olukoko, O.A., Becker, A.A., and Fenner, R.T., [1993], "Three Benchmark Examples for Frictional Contact Modelling Using Finite Element and Boundary Element Methods," *Journal of Strain Analysis*, Vol. 28, No. 4, pp. 293-301.

Othman, A.M., Lin, J., Hayhurst, D.R., and Dyson, B.F., [1993], "Comparison of Creep Rupture Lifetimes of Single and Double Notched Tensile Bars," *ACTA metallurgy Materials*, Vol. 41, No. 4, pp. 1251-1222.

Paris, F., and Garrido, J.A., [1990], "An Incremental Procedure for Friction Contact Problems With the Boundary Element Method," *Engineering Analysis With Boundary*

Elements, Vol. 6, No. 4, pp. 202-213.

Paris, F., Foces, A., and Garrido, J.A., [1992], "Application of Boundary Element Method to Solve Three-Dimensional Elastic Contact Problems Without Friction," *Computers & Structures*, Vol. 43, No. 1, pp. 19-30.

Sarihan, V., and Mukherjee, S., [1982], "Axisymmetric Viscoplastic Deformation by the Boundary Element Method," *International Journal of Solids and Structures*, Vol. 18, No. 12, pp. 1113-1128.

Smith, S.D., Webster, J.J., and Hyde, T.H., [1989], "Three-Dimensional Damage Calculations for Creep Crack Growth in 316 Stainless Steel," *Applied Mechanics-3*, Edited by I.M. Allison and C. Ruiz, Elsevier Applied Science, London, pp. 363-378.

Spencer, G.C., [1968], "An Introduction to Plasticity," Chapman & Hall Ltd., London.

Sun, W., Becker, A.A., and Hyde, T.H., [1999], "2D Functions of ABAQUS UMAT Damage Code for Creep Continuum Damage Mechanics Analysis," Internal Report, University of Nottingham, 1999.

Swedlow, J.L., and Cruse, T.A., [1971], "Formulation of Boundary Integral Equations for Three-Dimensional Elasto-Plastic Flow," *International Journal of Solids and Structures*, Vol. 7, pp. 1673-1683.

Telles, J.C.F., and Brebbia, C.A., [1981], "The Boundary Element Method in

Plasticity,” *Applied Mathematical Modelling*, Vol. 5, No. 4, pp. 275-281.

Telles, J.C.F., and Brebbia, C.A., [1983], “Viscoplasticity and Creep Using Boundary Elements,” Chapter 8 in *Progress in Boundary Element Methods-Volume 2*, Edited by C.A. Brebbia, Pentech Press, London, pp. 200-215.

Tsuta, T., and Yamaji, S., [1983], “Boundary Element Analysis of Contact Thermo-Elastoplastic Problems With Creep and The Numerical Technique,” *Boundary Elements, Procedures of 5th International Conference*, Hiroshima, Japan, November, Edited by C.A. Brebbia, T. Futagami and M. Tanaha, Springer-Verlay, Berlin, pp. 567-576.

Xiao, H., Aizawa, T., and Kihara, J., [1996], “Development of Three dimensional Boundary Element Simulator for Rolling,” *Boundary Element Methods*, Edited by M. Tanaka and Z. Yao, Elsevier Science B.V., pp. 287-296.

Appendix A: Differentials of the Linear Shape Functions.

$$\frac{\partial L_1(\eta_1, \eta_2)}{\partial \eta_1} = \frac{-1}{4}(1 - \eta_2)$$

$$\frac{\partial L_2(\eta_1, \eta_2)}{\partial \eta_1} = \frac{1}{4}(1 - \eta_2)$$

$$\frac{\partial L_3(\eta_1, \eta_2)}{\partial \eta_1} = \frac{1}{4}(1 + \eta_2)$$

$$\frac{\partial L_4(\eta_1, \eta_2)}{\partial \eta_1} = \frac{-1}{4}(1 + \eta_2)$$

$$\frac{\partial L_1(\eta_1, \eta_2)}{\partial \eta_2} = \frac{-1}{4}(1 - \eta_1)$$

$$\frac{\partial L_2(\eta_1, \eta_2)}{\partial \eta_2} = \frac{-1}{4}(1 + \eta_1)$$

$$\frac{\partial L_3(\eta_1, \eta_2)}{\partial \eta_2} = \frac{1}{4}(1 + \eta_1)$$

$$\frac{\partial L_4(\eta_1, \eta_2)}{\partial \eta_2} = \frac{1}{4}(1 - \eta_1)$$

Appendix B: Differentials of the Quadratic Shape Functions.

$$\frac{\partial N_1(\xi_1, \xi_2)}{\partial \xi_1} = \frac{1}{4}(1 - \xi_2)(2\xi_1 + \xi_2)$$

$$\frac{\partial N_2(\xi_1, \xi_2)}{\partial \xi_1} = -\xi_1(1 - \xi_2)$$

$$\frac{\partial N_3(\xi_1, \xi_2)}{\partial \xi_1} = \frac{1}{4}(1 - \xi_2)(2\xi_1 - \xi_2)$$

$$\frac{\partial N_4(\xi_1, \xi_2)}{\partial \xi_1} = \frac{1}{2}(1 - \xi_2^2)$$

$$\frac{\partial N_5(\xi_1, \xi_2)}{\partial \xi_1} = \frac{1}{4}(1 + \xi_2)(2\xi_1 + \xi_2)$$

$$\frac{\partial N_6(\xi_1, \xi_2)}{\partial \xi_1} = -\xi_1(1 + \xi_2)$$

$$\frac{\partial N_7(\xi_1, \xi_2)}{\partial \xi_1} = \frac{1}{4}(1 + \xi_2)(2\xi_1 - \xi_2)$$

$$\frac{\partial N_8(\xi_1, \xi_2)}{\partial \xi_1} = \frac{-1}{2}(1 - \xi_2^2)$$

$$\frac{\partial N_1(\xi_1, \xi_2)}{\partial \xi_2} = \frac{1}{4}(1 - \xi_1)(2\xi_2 + \xi_1)$$

$$\frac{\partial N_2(\xi_1, \xi_2)}{\partial \xi_2} = \frac{-1}{2}(1 - \xi_1^2)$$

$$\frac{\partial N_3(\xi_1, \xi_2)}{\partial \xi_2} = \frac{1}{4}(1 + \xi_1)(2\xi_2 - \xi_1)$$

$$\frac{\partial N_4(\xi_1, \xi_2)}{\partial \xi_2} = -\xi_2(1 + \xi_1)$$

$$\frac{\partial N_5(\xi_1, \xi_2)}{\partial \xi_2} = \frac{1}{4}(1 + \xi_1)(2\xi_2 + \xi_1)$$

$$\frac{\partial N_6(\xi_1, \xi_2)}{\partial \xi_2} = \frac{1}{2}(1 - \xi_1^2)$$

$$\frac{\partial N_7(\xi_1, \xi_2)}{\partial \xi_2} = \frac{1}{4}(1 - \xi_1)(2\xi_2 - \xi_1)$$

$$\frac{\partial N_8(\xi_1, \xi_2)}{\partial \xi_2} = -\xi_2(1 - \xi_1)$$

Appendix C: Analytical Solutions of Plasticity of a Plate under Uniaxial Load in Plane Stress Problems.

A plate is subjected to uniaxial stress in the x direction as follows:

$$\sigma_{xx} = 300 \text{ N/mm}^2; \quad \sigma_{yy} = 0 \text{ N/mm}^2$$

The material properties of the plate are as follows:

$$E = 207 \times 10^3 \text{ N/mm}^2$$

$$\nu = 0.3$$

$$\sigma_y = 250 \text{ N/mm}^2$$

$$H = 4223.8267 \text{ N/mm}^2$$

$$\mu = E/2(1 - \nu) = 147857.14 \text{ N/mm}^2$$

The plastic strain increments can be defined as follows:

$$\dot{\varepsilon}_{ij}^p = \frac{3}{2} \left(\frac{\dot{S}_{kl} \dot{\varepsilon}_{kl}}{1 + H/3\mu} \right) \frac{\dot{S}_{ij}}{(\dot{\sigma}_{eff})^2} \quad (c1)$$

To calculate plastic strains using the above equation, the incremental applied stress after yielding must be used. Firstly, the effective stress resulting from the applied stress must be calculated using equation (2.23) in order to find the incremental applied load.

For plane stress, $\sigma_{zz} = 0$.

$$\sigma_{eff} = \sqrt{\{(300-0)^2 + (0-0)^2 + (300-0)^2 + 6(0^2 + 0^2 + 0^2)\}}/2 = 300 \text{ N/mm}^2$$

Therefore, the incremental applied load is equal to 50 N/mm^2 in the x direction. From equation (c1), the total strain increments can be written in terms of elastic strain increments and plastic strain increments. Therefore, equation (c1) can be rewritten and rearranged in the way that all plastic strain increments are in the left hand side as follows:

$$\begin{aligned} & \left[\dot{S}_{xx}^2 - \frac{2}{3} \left(1 + \frac{H}{3\mu} \right) (\dot{\sigma}_{eff})^2 \right] \dot{\epsilon}_{xx}^p + \dot{S}_{xx} \dot{S}_{yy} \dot{\epsilon}_{yy}^p + \dot{S}_{xx} \dot{S}_{zz} \dot{\epsilon}_{zz}^p + \dot{S}_{xx} \dot{S}_{xy} \dot{\epsilon}_{xy}^p + \dot{S}_{xx} \dot{S}_{xz} \dot{\epsilon}_{xz}^p + \dot{S}_{xx} \dot{S}_{yz} \dot{\epsilon}_{yz}^p = \\ & - \dot{S}_{xx} \left[\dot{S}_{xx} \dot{\epsilon}_{xx}^e + \dot{S}_{yy} \dot{\epsilon}_{yy}^e + \dot{S}_{zz} \dot{\epsilon}_{zz}^e + \dot{S}_{xy} \dot{\epsilon}_{xy}^e + \dot{S}_{xz} \dot{\epsilon}_{xz}^e + \dot{S}_{yz} \dot{\epsilon}_{yz}^e \right] \\ & \dot{S}_{yy} \dot{S}_{xx} \dot{\epsilon}_{xx}^p + \left[\dot{S}_{yy}^2 - \frac{2}{3} \left(1 + \frac{H}{3\mu} \right) (\dot{\sigma}_{eff})^2 \right] \dot{\epsilon}_{yy}^p + \dot{S}_{yy} \dot{S}_{zz} \dot{\epsilon}_{zz}^p + \dot{S}_{yy} \dot{S}_{xy} \dot{\epsilon}_{xy}^p + \dot{S}_{yy} \dot{S}_{xz} \dot{\epsilon}_{xz}^p + \dot{S}_{yy} \dot{S}_{yz} \dot{\epsilon}_{yz}^p = \\ & - \dot{S}_{yy} \left[\dot{S}_{xx} \dot{\epsilon}_{xx}^e + \dot{S}_{yy} \dot{\epsilon}_{yy}^e + \dot{S}_{zz} \dot{\epsilon}_{zz}^e + \dot{S}_{xy} \dot{\epsilon}_{xy}^e + \dot{S}_{xz} \dot{\epsilon}_{xz}^e + \dot{S}_{yz} \dot{\epsilon}_{yz}^e \right] \\ & \dot{S}_{zz} \dot{S}_{xx} \dot{\epsilon}_{xx}^p + \dot{S}_{zz} \dot{S}_{yy} \dot{\epsilon}_{yy}^p + \left[\dot{S}_{zz}^2 - \frac{2}{3} \left(1 + \frac{H}{3\mu} \right) (\dot{\sigma}_{eff})^2 \right] \dot{\epsilon}_{zz}^p + \dot{S}_{zz} \dot{S}_{xy} \dot{\epsilon}_{xy}^p + \dot{S}_{zz} \dot{S}_{xz} \dot{\epsilon}_{xz}^p + \dot{S}_{zz} \dot{S}_{yz} \dot{\epsilon}_{yz}^p = \\ & - \dot{S}_{zz} \left[\dot{S}_{xx} \dot{\epsilon}_{xx}^e + \dot{S}_{yy} \dot{\epsilon}_{yy}^e + \dot{S}_{zz} \dot{\epsilon}_{zz}^e + \dot{S}_{xy} \dot{\epsilon}_{xy}^e + \dot{S}_{xz} \dot{\epsilon}_{xz}^e + \dot{S}_{yz} \dot{\epsilon}_{yz}^e \right] \\ & \dot{S}_{xy} \dot{S}_{xx} \dot{\epsilon}_{xx}^p + \dot{S}_{xy} \dot{S}_{yy} \dot{\epsilon}_{yy}^p + \dot{S}_{xy} \dot{S}_{zz} \dot{\epsilon}_{zz}^p + \left[\dot{S}_{xy}^2 - \frac{2}{3} \left(1 + \frac{H}{3\mu} \right) (\dot{\sigma}_{eff})^2 \right] \dot{\epsilon}_{xy}^p + \dot{S}_{xy} \dot{S}_{xz} \dot{\epsilon}_{xz}^p + \dot{S}_{xy} \dot{S}_{yz} \dot{\epsilon}_{yz}^p = \\ & - \dot{S}_{xy} \left[\dot{S}_{xx} \dot{\epsilon}_{xx}^e + \dot{S}_{yy} \dot{\epsilon}_{yy}^e + \dot{S}_{zz} \dot{\epsilon}_{zz}^e + \dot{S}_{xy} \dot{\epsilon}_{xy}^e + \dot{S}_{xz} \dot{\epsilon}_{xz}^e + \dot{S}_{yz} \dot{\epsilon}_{yz}^e \right] \\ & \dot{S}_{xz} \dot{S}_{xx} \dot{\epsilon}_{xx}^p + \dot{S}_{xz} \dot{S}_{yy} \dot{\epsilon}_{yy}^p + \dot{S}_{xz} \dot{S}_{zz} \dot{\epsilon}_{zz}^p + \dot{S}_{xz} \dot{S}_{xy} \dot{\epsilon}_{xy}^p + \left[\dot{S}_{xz}^2 - \frac{2}{3} \left(1 + \frac{H}{3\mu} \right) (\dot{\sigma}_{eff})^2 \right] \dot{\epsilon}_{xz}^p + \dot{S}_{xz} \dot{S}_{yz} \dot{\epsilon}_{yz}^p = \\ & - \dot{S}_{xz} \left[\dot{S}_{xx} \dot{\epsilon}_{xx}^e + \dot{S}_{yy} \dot{\epsilon}_{yy}^e + \dot{S}_{zz} \dot{\epsilon}_{zz}^e + \dot{S}_{xy} \dot{\epsilon}_{xy}^e + \dot{S}_{xz} \dot{\epsilon}_{xz}^e + \dot{S}_{yz} \dot{\epsilon}_{yz}^e \right] \\ & \dot{S}_{yz} \dot{S}_{xx} \dot{\epsilon}_{xx}^p + \dot{S}_{yz} \dot{S}_{yy} \dot{\epsilon}_{yy}^p + \dot{S}_{yz} \dot{S}_{zz} \dot{\epsilon}_{zz}^p + \dot{S}_{yz} \dot{S}_{xy} \dot{\epsilon}_{xy}^p + \dot{S}_{yz} \dot{S}_{xz} \dot{\epsilon}_{xz}^p + \left[\dot{S}_{yz}^2 - \frac{2}{3} \left(1 + \frac{H}{3\mu} \right) (\dot{\sigma}_{eff})^2 \right] \dot{\epsilon}_{yz}^p = \\ & - \dot{S}_{yz} \left[\dot{S}_{xx} \dot{\epsilon}_{xx}^e + \dot{S}_{yy} \dot{\epsilon}_{yy}^e + \dot{S}_{zz} \dot{\epsilon}_{zz}^e + \dot{S}_{xy} \dot{\epsilon}_{xy}^e + \dot{S}_{xz} \dot{\epsilon}_{xz}^e + \dot{S}_{yz} \dot{\epsilon}_{yz}^e \right] \end{aligned} \tag{c2}$$

The effective stress increment ($\dot{\sigma}_{eff}$) can be calculated as follows:

$$\dot{\sigma}_{eff} = \sqrt{\{(50-0)^2 + (0-0)^2 + (50-0)^2 + 6(0^2 + 0^2 + 0^2)\}}/2 = 50 \text{ N/mm}^2$$

The deviatoric stress increments (\dot{S}_{ij}) can be calculated as follows:

$$\dot{S}_{xx} = 50 - (50 + 0 + 0)/3 = 33.33333 \text{ N/mm}^2$$

$$\dot{S}_{yy} = 0 - (50 + 0 + 0)/3 = -16.66667 \text{ N/mm}^2$$

$$\dot{S}_{zz} = 0 - (50 + 0 + 0)/3 = -16.66667 \text{ N/mm}^2$$

$$\dot{S}_{xy} = 0; \quad \dot{S}_{xz} = 0; \quad \dot{S}_{yz} = 0$$

The elastic strain increments ($\dot{\epsilon}_{ij}^e$) can be calculated from Hooke's law as follows:

$$\dot{\epsilon}_{xx}^e = (50 - 0.3(0 + 0))/207000 = 2.4155 \times 10^{-4}$$

$$\dot{\epsilon}_{yy}^e = (0 - 0.3(50 + 0))/207000 = -7.246 \times 10^{-5}$$

$$\dot{\epsilon}_{zz}^e = (0 - 0.3(50 + 0))/207000 = -7.246 \times 10^{-5}$$

$$\dot{\epsilon}_{xy}^e = 0; \quad \dot{\epsilon}_{xz}^e = 0; \quad \dot{\epsilon}_{yz}^e = 0$$

Substituting all known values to equation (c2), the equation (c2) can be reduced as follows:

$$- 585.02939 \dot{\epsilon}_{xx}^p - 555.55556 \dot{\epsilon}_{yy}^p - 555.55556 \dot{\epsilon}_{zz}^p = -0.34890$$

$$- 555.55556 \dot{\epsilon}_{xx}^p - 1418.36272 \dot{\epsilon}_{yy}^p + 277.77778 \dot{\epsilon}_{zz}^p = 0.17445$$

$$- 555.55556 \dot{\epsilon}_{xx}^p + 277.77778 \dot{\epsilon}_{yy}^p - 1418.36272 \dot{\epsilon}_{zz}^p = 0.17445$$

$$-1696.14050 \dot{\epsilon}_{xy}^p = 0$$

$$-1696.14050 \dot{\epsilon}_{xz}^p = 0$$

$$-1696.14050 \dot{\epsilon}_{yz}^p = 0$$

After solving above equations, the solutions of plastic increments can be obtained as follows:

$$\dot{\epsilon}_{xx}^p = 1.1838 \times 10^{-2}$$

$$\dot{\epsilon}_{yy}^p = -5.9188 \times 10^{-3}$$

$$\dot{\epsilon}_{zz}^p = -5.9188 \times 10^{-3}$$

$$\dot{\epsilon}_{xy}^p = 0; \dot{\epsilon}_{xz}^p = 0; \dot{\epsilon}_{yz}^p = 0$$